INVESTIGATION OF STEAM RELATED FORMATION DAMAGE AND OIL RECOVERY FACTORS FOR SANDPACKS OF VARIABLE MINERALOGY

A Dissertation

by

VIACHESLAU YURYEVICH KUDRASHOU

Submitted to the Office of Graduate and Professional Studies of
Texas A&M University
in partial fulfillment of the requirements for the degree of

DOCTOR OF PHILOSOPHY

Chair of Committee,	Hisham A. Nasr-El-Din
Committee Members,	Berna Hascakir
	Kan Wu
	Mahmoud M. El-Halwagi
Head of Department,	Jeff Spath

August 2019

Major Subject: Petroleum Engineering

ABSTRACT

Reactive nature of steam and clay minerals may lead to formation damage and flow assurance issues. This dissertation presents experimental investigation of oil recovery and changes in petrophysical properties as a function of mineralogy and amount of injected steam.

Sandpacks with fixed amounts of quartz, calcite, dolomite, kaolinite, and montmorillonite were prepared to identify mineral reactions, their conditions, and effects of these processes on porosity and permeability. Rock mixtures were aged in HP/HT cells. Sandpacks with quartz, calcite, feldspar, kaolinite, smectite, and illite were prepared for investigation of oil recovery factors in steam injection experiments. Porosity and permeability of the initial and steamed sandpacks were determined using CT scan and coreflooding respectively. Composition of the collected liquid samples was analyzed using ICP-OES. Rock morphology and pore-space configuration were studied using SEM-EDS, and mineralogy was analyzed using XRD.

Sandpacks without clay minerals were found to be the least prone to formation damage associated with steam injection. Silica dissolution/precipitation reaction resulted in 5% permeability reduction and 1-2% porosity reduction. Mixtures of quartz, kaolinite and carbonate minerals (calcite or dolomite) after steam injection lost 11-22% of permeability and 2-7% of porosity. Kaolinite fines were shown to be mobilized during steam treatment. Aging of these mixtures for 10 days at 400°F and 1,000 psi lead to formation of swelling smectite clay (Ca montmorillonite). Steam injection in montmorillonite-rich sandpacks caused up to 84% permeability loss and up to 8% porosity loss. This was explained by clay swelling and pore-bridging. Microporous network that filled the pores significantly restricted the flow.

Oil recovery factors for 100% quartz case was determined to be 65 wt%. Calcite- and feldspar-rich sandpacks produced 56 and 61 wt% of oil respectively. Sandpacks with clay fractions have shown the lowest oil recovery – 39, 29, and 28 wt% for kaolinite-, smectite-, and illite-rich samples respectively. Feldspar-rich sandpack demonstrated signs of structural destruction and fines release. Steam interaction with illite-rich sandpacks caused formation of amorphous silica.

Obtained results characterize petrophysical changes and formation damage mechanisms caused by hydrothermal alterations and identify oil recovery factors of sandpacks containing minerals with different structures and properties.

DEDICATION

I dedicate this work to my dear and beloved family – my parents, Yuri and Valentina Kudrashov, and my brother – Igor Kudrashov.

ACKNOWLEDGEMENTS

I am very thankful to my advisor Dr. Hisham A. Nasr-El-Din for the provided guidance, support, and motivation. I strongly appreciate the opportunity to be a part of this research team.

I would like to thank my committee members, Dr. Berna Hascakir, Dr. Kan Wu, and Dr. Mahmoud M. El-Halwagi, for their help and feedback on my results throughout the course of this research.

I am very grateful to my friends, colleagues, and the department faculty and staff for constant assistance and for making my time at Texas A&M University a great experience. I appreciate help from Sherif Abdelmoneim in assembling the steam generator setup, thermocouples, and LabVIEW software. I acknowledge Gia Alexander for editorial assistance in preparing the manuscript.

Finally, I am forever thankful to my family for their support and encouragement.

CONTRIBUTORS AND FUNDING SOURCES

Contributors

This work was supervised by a dissertation committee consisting of Professors Hisham Nasr-El-Din, Berna Hascakir, and Kan Wu of the Department of Petroleum Engineering and Professor Mahmoud El-Halwagi of the Department of Chemical Engineering.

The research data was obtained in the laboratories supported by Professor Hisham Nasr-El-Din and Harold Vance Department of Petroleum Engineering.

All other work conducted for the dissertation was completed by the student independently.

Funding Sources

This graduate study was supported and made possible by Research Assistant fellowship from Dr. Hisham Nasr-El-Din's research group fund at Texas A&M University.

This work was also in part supported by Cenovus Energy under Agreement between Cenovus FCCL Ltd. and Texas A&M Engineering Experiment Station (TEES) from April 9, 2015. Contents of this research work are solely responsibility of the authors and do not necessarily represent the official views of the Cenovus Energy or Texas A&M Engineering Experiment Station (TEES).

NOMENCLATURE

CT	Computed Tomography
DI	Deionized Water
ESP	Electric Submersible Pump
GLDA	Glutamic Acid N, N-Diacetic Acid
HCl	Hydrochloric Acid
HF	Hydrofluoric Acid
HT/HP	High Temperature High Pressure
ICP	Inductive Coupled Plasma
ICP-OES	Inductively Coupled Plasma-Optical Emission Spectroscopy
RLP	Residual Liquid Phase
SAGD	Steam-Assisted Gravity Drainage
SEM	Scanning Electron Microscope
SEM-EDS	Scanning Electron Microscope-Energy Dispersive X-ray Spectroscopy
XRD	X-Ray Diffraction

TABLE OF CONTENTS

Page

LIST OF FIGURES

FIGURE Page

FIGURE Page

FIGURE Page

LIST OF TABLES

1. INTRODUCTION*

This section provides overview of the research work concerning interaction of various minerals with steam and its effect on formation damage and oil recovery. The review includes the general information about formation damage, summary of early hydrothermal alteration studies, and discussion of mineral reactions applicable to thermobaric conditions of a real reservoir.

1.1 Formation Damage Associated with Steam Injection

Heavy oils and bitumen resources are more than double the amount of conventional oil in the world. Thermal methods, such as hot waterflooding, steam injection, and in-situ combustion, are often used in the production of viscous crude oil (Yakubov et al. 2017; Khaledi et al. 2018). The increase in temperature not only lowers the viscosity of crude oil, but also accelerates chemical reactions in the reservoir. Steam injection requires generation of superheated steam at the surface. It is common to inject up to 15,000 – 20,000 bbl. of steam at about 500°F per one stimulation cycle. Chemical content and properties of boiler feed water are often field-dependent because the water is taken from local ground or surface sources (Khansari and Gates 2015). Typically, about 20-30% of the feedwater is not converted to steam. It is called the residual liquid phase (RLP). Propagation of the enormous amount of hot fluid through a sandstone reservoir often leads to the onset of processes that change petrophysical properties of the reservoir (Williamson et al. 2016).

---

*Partially reprinted with permission from "Formation Damage Associated with Mineral Alteration and Formation of Swelling Clays Caused by Steam Injection in Sandpacks" by V. Kudrashou and H. Nasr-El-Din, 2019. SPE-195700-PA, *SPE Res Eval & Eng*, Preprint, Copyright 2019 by Society of Petroleum Engineers.

Overall, most stimulation techniques cause changes in the initially-balanced reservoir rock-fluid system. Some of these changes can lead to formation damage and flow assurance issues (Moore

2001; Bennion 2002). The most common damaging mechanisms associated with steam injection include tubing corrosion (Al-Nakhli et al. 2016, Kudrashou and Nasr-El-Din 2019a), scale formation (Ameur et al. 2018), liner blockage (Romanova and Ma 2013), sand production (Bennion et al. 2009; Romanova et al. 2017), wettability changes (Schembre et al. 2006; Tang et al. 2011; Cao et al. 2017), mineral dissolution/precipitation and transformation (Levinson and Vian 1966; Xiao and Jones 2006; Tang et al. 2012), clay swelling (Jain et al. 2016), fines mobilization and pore plugging (Mahmoudi et al. 2017), rock compaction and/or matrix sand redistribution (Schutjens et al. 2004; Crawford et al. 2006), formation of in-situ emulsions (Castro 2001), asphaltene precipitation (Nabzar et al. 2005), and others. These processes often reduce oil production rates.

1.2 Review of Early Hydrothermal Alteration Studies

The early history of hydrothermal studies is full of invention and discoveries; however, many times the mineral reactions were performed in a non-reproducible manner and under undefined conditions. There were no reliable quantitative data concerning mineral synthesis available before 1917. That early period was reviewed in detail by Morey and Niggli (1913).

Morey and Fenner (1917) were the first authors who published a systematic quantitative experimental work on hydrothermal systems. In that work, equilibrium relations for the system of H_2O-K_2SiO_3-SiO_2 were obtained at constant pressure with control and measurement of temperature. The hydrothermal mineral interactions were studied at a wider range of thermobaric

conditions as aging technologies developed. Smyth and Adams (1923) designed the first successful internally-heated pressure vessel. This type of vessel did not fail due to creep and oxidation of the alloys at high temperatures.

However, on a larger scale, quantitative mineral equilibrium studies were performed only after the failing externally-heated vessels and complicated internally-heated vessels were replaced by more reliable equipment (Roy and Tuttle 1956). Hawkins and Roy (1963) analyzed 240 hydrothermal runs in CO_2-saturated, saline, acid, and basic environments. These runs were performed in test-tube-type bombs and gold- and silver-lined Morey bombs. They concluded that clay minerals and zeolites form by reactions between monomeric silicate ions, aluminate ions, and metallic ions. Numerous studies reported about changes occurring with various types of pure minerals in hydrothermal systems, such as MgO-Al_2O_3-SiO (Keith and Schairer 1952), MgO-SiO_2-H_2O (Bowen and Tuttle 1949), and Na_2O-$NaAlO_2$-SiO_2-H_2O (Regis et al. 1960). Roy and Roy (1955) investigated quaternary equilibria and reported on synthesis and stability of some groups of minerals in the system MgO-Al_2O_3-SiO_2-H_2O. Zen (1959) discussed the multicomponent systems including clay minerals (chlorite and kaolinite) and carbonate minerals (calcite and dolomite). Some of the hydrothermal synthesis results were already applicable to the conditions at which petroleum reservoirs are being developed. For example, Levinson and Vian (1966) synthesized montmorillonite from naturally occurring kaolinite, quartz and dolomite. Moreover, the reported reaction proceeded at 572°F (300°C) in only two days and at 347°F (175°C) in five days. Levinson and Day (1968) also performed low temperature hydrothermal synthesis of montmorillonite and reported similar reactions.

Many researchers reported formation of mixed-layer illite-montmorillonites in hydrothermally altered (via hypogene and supergene alteration processes) cores recovered from

drillholes in the thermal areas, such as: Wairakei, New Zealand (Steiner 1968); Steamboat Springs, Nevada (Schoen and White 1965); Cochiti Mining District, New Mexico (Bundy 1958); Front Range Mineral Belt, Colorado (Bonorino 1959); Goldfield District, Nevada (Harvey and Vitaliano 1964); and Central City-Idaho Springs Region, Colorado (Tooker 1955); Tsutsumizawa epithermal ore deposit, Japan (Sudo et al. 1962). It appears that montmorillonite and mixed-layer illite-montmorillonite minerals are common alteration products in silicate rocks influenced by hydrothermal processes.

Rieke (1972) summarized terms and definitions used to describe mineral changes. He pointed out that term "transformation" should not be confused with the term "diagenesis". For example, to describe the case of generation and disappearance of montmorillonite three processes can be suggested – detrital inheritance (genesis from weathered sediments), transformation (aggradation, degradation, and intercrystallite modification), and neoformation (structural change or crystallization out of chemically-active environment). Transformation changes do not involve solution stage but describe alteration from one clay mineral to another by ionic exchange in the silicate layer and/or the interlayer space.

At about same time, in 1970s, Butler et al. (1981) developed the concept of steam stimulation using horizontal pairs of wells, known as steam-assisted gravity drainage (SAGD). The techniques of hot fluid injection, steamflooding, and in-situ combustion were known and used even before that (Marx and Langenheim 1959; El-Saleh and Ali 1968; Howard 1923). As the use of thermal methods were becoming more widespread the need for understanding of hydrothermal mineral alteration in reservoir rocks became apparent for petroleum engineers.

1.3 Mineral Reactions in Oil Reservoirs

The following experimental works and field cases report mineral changes that happened at temperatures and pressures normally encountered in sandstone oil reservoirs during production using thermal stimulation. Bennion et al. (1992) named four common mechanisms of thermally induced formation damage. Okoye et al. (1992) related experimental data to field work and reported screening procedure for estimation of potential formation damage due to steam injection. Somerton and Boozer (1960) and Somerton and Selim (1961) observed thermal "anomalies" during measurement of thermal diffusivities of oven-dried cores at atmospheric pressure. They correlated these effects with mineral reactions, in particular: α-β quartz inversion, loss of carbon dioxide from calcite (carbonate mineral), and loss of hydroxyl water from kaolinite (phyllosilicate clay mineral).

Montgomery et al. (2014) investigated aquathermolysis experiments on heavy oils and concluded that matrix minerals affect generation of H_2S. Nengkoda (2012) analyzed CO_2 increase during cyclic steam injection in sandstone heavy oil reservoir. He concluded that the root cause of CO_2 vaporation is thermal reaction of $CaCO_3$. Kumar et al. (2005) and Nghiem et al. (2009) analyzed conversion of CO_2 into carbonate minerals in saline aquifers. They reported that this process is possible if source of Ca^{2+}, Mg^{2+}, Fe^{2+} exists. However, they stated that this mineralization process takes hundreds to thousands of years.

Day and Huitt (1967) investigated hydrothermal softening of sandstones caused by destruction and dissolution of dolomite (carbonate mineral) and kaolinite. They also investigated formation of montmorillonite (phyllosilicate clay mineral, dioctahedral smectite) and discussed fracture "healing" caused by excessive embedment of propping materials in the softened reservoir rock. Bayliss and Levinson (1971) performed 140 hydrothermal synthesis runs and reported

theoretical chemical equations responsible for formation of talk (phyllosilicate clay mineral), montmorillonite, anorthite (tectosilicate feldspar mineral), garronite (tectosilicate zeolite mineral). Hutcheon et al. (1980) investigated thermochemical data of the Kootenay Formation and reported equilibrium reaction that explains disappearance of kaolinite by formation of Mg-chlorite (phyllosilicate mineral).

Boon et al. (1983) investigated formation of montmorillonite and analcime (tectosilicate zeolite mineral) in static autoclave experiments. Additionally, based on the dynamic experiments they observed and pointed out effect of flow rate on the degree of mineral dissolution. Lefebvre and Hutcheon (1986) performed analysis of pre- and post-thermal recovery cores and concluded that steamflooding lead to formation of chlorite and illite (phyllosilicate clay mineral), while fireflooding caused formation of illite in the cooked zones, and K-feldspar (tectosilicate mineral) with hematite (iron oxide mineral) in burned zones. Kirk et al. (1987) used EDS analysis to determine reactions for beidellite (phyllosilicate smectite mineral) and montmorillonite assuming single type of interlayer cation. Oldershaw et al. (1981) reported that porosity of oil sands is generally lower in the steamed intervals and correlated it to formation of smectites.

Mohnot et al. (1987) and Mohnot and Bae (1989) investigated mineral reactions in alkaline environment. They reported the highest amount of alkalinity consumption for kaolinite and gypsum (calcium sulfate mineral), and the lowest for quartz (tectosilicate mineral, silicon oxide). Gunter et al. (1994) modeled formation damage caused by kaolinite. They concluded that at low temperature the dominant formation damage mechanism is associated with mobilization, transport, and deposition of kaolinite fines, but at high temperatures main issues are mineral reactions leading to formation of smectites. Romanova et al. (2015) also discussed kaolinite migration during

steamflooding. Another commonly reported issue caused by kaolinite is emulsion stabilization (Sztukowski and Yarranton 2005).

Keith et al. (1998) reported that smectite precipitation is found to be extremely damaging for most of the steamflooding environments. They clarified that smectites are prone to migrate and block pore throats because of its small particle size, pore-lining texture, and electrochemical properties of the surface. Smectite precipitation severely restricts pore throats and decreases permeability. Hui et al. (2006) analyzed changes in composition of injected water used for steam stimulation of viscous crude oil reservoir. They reported that the amount of hydrothermally dissolved/precipitated minerals is very significant. For example, for every 10,000 m^3 (62,898 bbl.) of injected water amount of dissolved kaolinite and quartz are 18.7 tons (41,226 lbs.) and 9.9 (21,826 lbs.) tons, respectively. This dissolution is expected to lead to precipitation of 41.2 tons (90,830 lbs.) of analcime that has swelling tendencies. Tang et al. (2012) investigated wettability alteration caused by dissolution of carbonate minerals during steam and hot water injection. They also discussed injectivity loss associated with carbonates dissolution/precipitation. Yongbin et al. (2017) performed numerical simulation of electrical-heating assisted SAGD and reported mineral changes such as montmorillonite conversion to illite and decomposition of kaolinite. Huang and Longo (1994a; 1994b) experimentally simulated reactions between silicates and carbonates that are known to lead to formation of smectites. They investigated effect of CO_2 on these reactions and observed that analcime forms instead of smectites in fluids that have higher pH or concentration of Na^+. Kudrashou and Nasr-El-Din (2019b) studied mineral transformation reactions and demonstrated how formation of swelling clay can alter porosity and permeability of a sandpack. More data about decomposition of carbonate minerals can be found in the studies of Matvienko et al. (2013), and Subagjo et al. (2017).

Table 1 presents a summary of studies that reported mineral reactions for thermobaric conditions normally observed in petroleum reservoirs. Reactions were selected for minerals that are commonly found in sandstone reservoirs.

Interactions in the system of rock-oil-steam-aqueous phase are crucial in prediction of the performance of steam flooding. Jain et al. (2015) explained importance of water analysis for identification of the problems associated with steam-rock interaction. The provided examples demonstrated how to predict and analyze mineralogical changes associated with steam injection. Kar et al. (2015) investigated effect of interaction of bitumen and clays on asphaltene deposition during steam injection. Kar and Hascakir (2016) reported formation damage mechanisms associated with interaction of water, clay, asphaltene, and aromatic oil fractions. Ameur et al. (2018) demonstrated a field case in which carbonate and silicon-based scales were removed from the wells operating under steam assisted gravity drainage. Kar and Hascakir (2017) discovered that presence of illite and kaolinite clay resulted in 15 wt% reduction in oil recovery in comparison with kaolinite only case.

Table 1: Summary of Published Mineral Reactions

Reference	Mineral Reactions
Zen (1959) (without balancing)	$\underset{(dolomite)}{CaMg(CO_3)_2} + \underset{(kaolinite)}{Al_2Si_2O_5(OH)_4} + \underset{(quartz)}{SiO_2} + \underset{(water)}{H_2O} \rightarrow \underset{(montmorillonite)}{(Ca;Mg)_2(Si;Al)_4O_{10}(OH)_2} + \underset{(calcite)}{CaCO_3} + \underset{(carbon\ dioxide)}{CO_2}$ $\underset{(dolomite)}{CaMg(CO_3)_2} + \underset{(kaolinite)}{Al_2Si_2O_5(OH)_4} + \underset{(quartz)}{SiO_2} + \underset{(water)}{H_2O} \rightarrow \underset{(chlorite)}{(Ca;Mg)_5Al_2Si_3O_{10}(OH)_8} + \underset{(calcite)}{CaCO_3} + \underset{(carbon\ dioxide)}{CO_2}$
Day and Huitt (1967) (without balancing)	$\underset{(dolomite)}{CaMg(CO_3)_2} + \underset{(kaolinite)}{Al_2Si_2O_5(OH)_4} + \underset{(quartz)}{SiO_2} + \underset{(water)}{H_2O} \rightarrow$ $\underset{(dolomite)}{CaMg(CO_3)_2} + \underset{(illite)}{K\ Al_4Si_2O_{12}} + \underset{(quartz)}{SiO_2} + \underset{(water)}{H_2O} \rightarrow$ $\underset{(dolomite)}{CaMg(CO_3)_2} + \underset{(quartz)}{SiO_2} + \underset{(water)}{H_2O} \rightarrow$ $\underset{(dolomite)}{CaMg(CO_3)_2} + \underset{(illite)}{K\ Al_4Si_2O_{12}} + \underset{(water)}{H_2O} \rightarrow$ $\underset{(illite)}{K\ Al_4Si_2O_{12}} + \underset{(quartz)}{SiO_2} + \underset{(water)}{H_2O} \rightarrow$ $\underset{(plagioclase)}{NaAlSi_3O_8} + \underset{(dolomite)}{CaMg(CO_3)_2} + \underset{(water)}{H_2O} \rightarrow$ $\underset{(microcline)}{KAlSi_3O_8} + \underset{(dolomite)}{CaMg(CO_3)_2} + \underset{(quartz)}{SiO_2} + \underset{(water)}{H_2O} \rightarrow$ All the reactions in the left column were reported to produce montmorillonite: $\rightarrow \underset{(montmorillonite)}{(Ca;Mg)_2(Si;Al)_4O_{10}(OH)_2}$
Bayliss and Levinson (1971)	$\underset{(dolomite)}{3CaMg(CO_3)_2} + \underset{(quartz)}{4SiO_2} + \underset{(water)}{H_2O} \rightarrow \underset{(talc)}{Mg_3Si_4O_{10}(OH)_2} + \underset{(calcite)}{3CaCO_3} + \underset{(carbon\ dioxide)}{3CO_2}$ $\underset{(dolomite)}{24CaMg(CO_3)_2} + \underset{(quartz)}{28SiO_2} + \underset{(kaolinite)}{Al_2Si_2O_5(OH)_4} + \underset{(water)}{6H_2O} \rightarrow \underset{(montmorillonite)}{8Ca_{1/8}Mg_3Si_{3\ 3/4}Al_{1/4}O_{10}(OH)_2} + \underset{(calcite)}{23CaCO_3} + \underset{(carbon\ dioxide)}{25CO_2}$ $\underset{(dolomite)}{CaMg(CO_3)_2} + \underset{(kaolinite)}{Al_2Si_2O_5(OH)_4} \rightarrow \underset{(anorthite)}{CaAl_2Si_2O_8} + \underset{(carbon\ dioxide)}{2CO_2} + \underset{(magnesium\ cation)}{Mg^{2+}_{aq}} + \underset{(hydroxide\ anion)}{2(OH)^-}$ $\underset{(calcite)}{CaCO_3} + \underset{(quartz)}{8SiO_2} + \underset{(kaolinite)}{7Al_2Si_2O_5(OH)_4} \rightarrow \underset{(montmorillonite)}{6Ca_{1/6}Al_2(Si_{3\ 2/3}Al_{1/3}O_{10}(OH)_2} + \underset{(carbon\ dioxide)}{CO_2} + \underset{(water)}{8H_2O}$ $\underset{(calcite)}{CaCO_3} + \underset{(kaolinite)}{Al_2Si_2O_5(OH)_4} \rightarrow \underset{(anorthite)}{CaAl_2Si_2O_8} + \underset{(carbon\ dioxide)}{CO_2} + \underset{(water)}{2H_2O}$ $\underset{(calcite)}{CaCO_3} + \underset{(quartz)}{4SiO_2} + \underset{(kaolinite)}{Al_2Si_2O_5(OH)_4} + \underset{(water)}{4H_2O} \rightarrow \underset{(garronite)}{CaAl_2Si_6O_{16}{\cdot}6H_2O} + \underset{(carbon\ dioxide)}{CO_2}$
Hutcheon et al. (1980)	$\underset{(dolomite)}{5CaMg(CO_3)_2} + \underset{(quartz)}{SiO_2} + \underset{(kaolinite)}{Al_2Si_2O_5(OH)_4} + \underset{(water)}{H_2O} \rightarrow \underset{(Mg-chlorite)}{Mg_5Si_3Al_2O_{10}(OH)_8} + \underset{(calcite)}{5CaCO_3} + \underset{(carbon\ dioxide)}{5CO_2}$

Table 1 Continued

Reference	Mineral Reactions
Oldershaw et al. (1981)	$\underset{(quartz)}{8SiO_2} + \underset{(kaolinite)}{7Al_2Si_2O_5(OH)_4} + \underset{(sodium\ cation)}{2Na^+} \rightarrow \underset{(smectite)}{2NaSi_{11}Al_7O_{30}(OH)_6} + \underset{(water)}{7H_2O} + \underset{(hydrogen\ cation)}{2H^+}$ $\underset{(quartz)}{4SiO_2} + \underset{(kaolinite)}{Al_2Si_2O_5(OH)_4} + \underset{(sodium\ cation)}{2Na^+} \rightarrow \underset{(albite)}{2NaSi_3AlO_8} + \underset{(water)}{H_2O} + \underset{(hydrogen\ cation)}{2H^+}$ $\underset{(quartz)}{10SiO_2} + \underset{(smectite)}{NaSi_{11}Al_7O_{30}(OH)_6} + \underset{(sodium\ cation)}{6Na^+} \rightarrow \underset{(albite)}{7NaSi_3AlO_8} + \underset{(hydrogen\ cation)}{6H^+}$ $\underset{(quartz)}{SiO_2} + \underset{(analcime)}{NaSi_2AlO_6H_2O} \rightarrow \underset{(albite)}{NaSi_3AlO_8} + \underset{(water)}{H_2O}$
Boon et al. (1983)	$\underset{(kaolinite)}{Al_2Si_2O_5(OH)_4} + \underset{(sodium\ cation)}{2Na^+} + \underset{(silicic\ acid)}{2H_4SiO_4} \rightarrow \underset{(analcime)}{2NaAlSi_2O_6\cdot(H_2O)} + \underset{(water)}{3H_2O} + \underset{(hydrogen\ cation)}{2H^+}$ $\underset{(dolomite)}{CaMg(CO_3)_2} + \underset{(kaolinite)}{7Al_2Si_2O_5(OH)_4} + \underset{(silicic\ acid)}{8H_4SiO_4} \rightarrow \underset{(calcite)}{CaCO_3} + \underset{(montmorillonite)}{6Mg_2(Si;Al)_4O_{10}(OH)_2} + \underset{(water)}{23H_2O} + \underset{(hydrogen\ cation)}{H^+} + \underset{(bicarbonate\ ion)}{6HCO_3^-}$ $\underset{(dolomite)}{5CaMg(CO_3)_2} + \underset{(kaolinite)}{Al_2Si_2O_5(OH)_4} + \underset{(silicic\ acid)}{H_4SiO_4} + \underset{(water)}{5H_2O} \rightarrow \underset{(calcite)}{5CaCO_3} + \underset{(Mg-chlorite)}{Mg_5Si_3Al_2O_{10}(OH)_8} + \underset{(hydrogen\ cation)}{5H^+} + \underset{(bicarbonate\ ion)}{5HCO_3^-}$
Garrels (1984)	$\underset{(montmorillonite)}{K^+_{0.33}(Al_{1.5}Fe^{3+}_{0.23}Mg^{2+}_{0.27})(Si_{3.94}Al_{0.06}O_{10}(OH)_2} + \underset{(feldspar)}{0.47KAlSi_3O_8} \rightarrow \underset{(illite)}{K^+_{0.8}(Al_{1.5}Fe^{3+}_{0.23}Mg^{2+}_{0.27})(Si_{3.47}Al_{0.53})O_{10}(OH)_2} + \underset{(quartz)}{1.88SiO_2}$
Kirk et al. (1987)	$\underset{(dolomite)}{2.5CaMg(CO_3)_2} + \underset{(silicic\ acid)}{32H_4SiO_4} + \underset{(kaolinite)}{28Al_2Si_2O_5(OH)_4} + \underset{(sodium\ cation)}{Na^+} \rightarrow \underset{(beidellite)}{24Na_{1/24}Ca_{1/24}Mg_{5/48}Si_{11/3}Al_{7/3}O_{10}(OH)_2} + \underset{(calcite)}{1.5CaCO_3} + \underset{(carbon\ dioxide)}{3.5CO_2} + \underset{(water)}{95.5H_2O} + \underset{(hydrogen\ cation)}{H^+}$ $\underset{(dolomite)}{4CaMg(CO_3)_2} + \underset{(silicic\ acid)}{28H_4SiO_4} + \underset{(kaolinite)}{10Al_2Si_2O_5(OH)_4} + \underset{(sodium\ cation)}{Na^+} \rightarrow \underset{(montmorillonite)}{12Na_{1/12}Ca_{1/8}Mg_{1/3}Si_4Al_{5/3}O_{10}(OH)_2} + \underset{(calcite)}{2.5CaCO_3} + \underset{(carbon\ dioxide)}{5.5CO_2} + \underset{(water)}{63.5H_2O} + \underset{(hydrogen\ cation)}{H^+}$
Xiao and Jones (2006)	$\underset{(orthoclase)}{3KAlSi_3O_8} + \underset{(hydrogen\ cation)}{2H^+} \rightarrow \underset{(illite)}{KAl_3Si_3O_{10}(OH)_2} + \underset{(potassium\ cation)}{2K^+} + \underset{(quartz)}{6SiO_2}$
Nengkoda (2012)	$\underset{(dolomite)}{5CaMg(CO_3)_2} + \underset{(kaolinite)}{Al_2Si_2O_5(OH)_4} + \underset{(quartz)}{SiO_2} + \underset{(water)}{2H_2O} \rightarrow \underset{(calcite)}{5CaCO_3} + \underset{(chlorite)}{Mg_5Si_3Al_2O_{10}(OH)_8} + \underset{(carbon\ dioxide)}{5CO_2}$ $\underset{(dolomite)}{0.25CaMg(CO_3)_2} + \underset{(quartz)}{1.2SiO_2} + \underset{(kaolinite)}{1.15Al_2Si_2O_5(OH)_4} + \underset{(potassium\ cation)}{0.6K^+} \rightarrow \underset{(illite)}{KAl_3Si_3O_{10}(OH)_2} + \underset{(calcite)}{0.25CaCO_3} + \underset{(carbon\ dioxide)}{0.25CO_2} + \underset{(water)}{H_2O} + \underset{(hydrogen\ cation)}{0.6H^+}$

Numerous researchers investigated formation damage mechanisms associated with clay-steam interaction. Mishra et al. (2018) investigated swelling and dispersion of clay minerals caused by exposure to steam. They provided description of conditions, mechanisms and reactions associated with clay minerals subjected to high temperatures. Hebner et al. (1986) concluded that some of the steam-clay interactions can be beneficial for production, for example formation of non-swelling analcime from smectite. Watkins et al. (1987) discussed fines migration mechanisms associated with high superficial velocity, wettability, reactive nature of the injected steam, and balance between attractive and repulsive forces. Li and Wong (2015) investigated thermal deformation of shale rocks and its effect on clay properties. Jain et al. (2016) determined that contact of steam and reservoir's clay fraction may induce significant permeability reduction caused by clay swelling, dispersion, and migration.

Some non-clay fine particles are known to cause issues in thermal recovery wells. Al Shizawi et al. (2018) reported that feldspar can release fines because of mineral dissolution associated with heat from steam flood. They also found that at temperatures above 200^{o}C (392^{o}F) feldspar can transform into smectite which is quite reactive and tend to swell in contact with fresh water.

2. MINERAL REACTIONS*

This section describes interactions between steam and reservoir rock. Samples of various mineralogical compositions were aged and treated with steam to characterize hydrothermal alterations and their effects on the petrophysical properties of reservoir rocks.

2.1 Materials and Methods

2.1.1 Sandpacks Preparation

Sandpacks were prepared from the following components: quartz (SiO_2, 50-70 mesh or 210-297 µm particle size), calcite (limestone $CaCO_3$, 70 mesh or particle size smaller than 212 µm), dolomite ($CaMg(CO_3)_2$, 70 mesh or particle size smaller than 212 µm), kaolinite ($Al_2Si_2O_5(OH)_4$, clay size particles), montmorillonite (Ca type, $Ca_{0.3}Al_2Si_4O_{10}(OH)_2 \bullet n(H_2O)$, clay size particles).

Weight of the pure minerals was measured to prepare the mixtures with predetermined mineralogical content. 12 mixtures were prepared (**Table 2**). Four groups of samples were prepared. Each group contains three samples. In the first group, the concentration of calcite was varied from 10 to 20 wt%; in the second group, the concentration of calcite was fixed, and the concentration of kaolinite was varied from 5 to 15 wt%. In the third group, the concentration of dolomite was fixed and the concentration of kaolinite was increased from 5 to 15 wt%; in the

---

*Partially reprinted with permission from "Formation Damage Associated with Mineral Alteration and Formation of Swelling Clays Caused by Steam Injection in Sandpacks" by V. Kudrashou and H. Nasr-El-Din, 2019. SPE-195700-PA, *SPE Res Eval & Eng*, Preprint, Copyright 2019 by Society of Petroleum Engineers.

fourth group, the concentration of montmorillonite was increased from 5 to 15 wt%.

Every prepared mixture was split in three portions – one portion was designated for XRD analysis, one for sandpacking and steam injection, and one for the aging experiments. **Fig. 1** shows the flow diagram of the conducted experimental work. XRD analysis of the initial rock mixture was performed to confirm the mineral composition of the prepared mixture. Later, the initial XRD pattern was compared to the XRD patterns obtained for the steamed and aged samples of the same rock mixture (dashed line in **Fig. 1**).

Table 2: Mineralogical Composition of the Prepared Samples

Sample #	Group #	Mineralogical Content of Mixture (wt%)
1		90% Quartz + 10% Calcite
2	1	85% Quartz + 15% Calcite
3		80% Quartz + 20% Calcite
4		85% Quartz + 10% Calcite + 5% Kaolinite
5	2	80% Quartz + 10% Calcite + 10% Kaolinite
6		75% Quartz + 10% Calcite + 15% Kaolinite
7		85% Quartz + 10% Dolomite + 5% Kaolinite
8	3	80% Quartz + 10% Dolomite + 10% Kaolinite
9		75% Quartz + 10% Dolomite + 15% Kaolinite
10		95% Quartz + 5% Montmorillonite
11	4	90% Quartz + 10% Montmorillonite
12		85% Quartz + 15% Montmorillonite

The unconsolidated mixtures were dry packed for steam injection experiments (Portion 2 in **Fig. 1**). Procedure of preparation of 6-in. long sandpacks included using a Teflon tube, which was thermally treated to have 1.5 in. diameter. Each tube was closed with 0.5-in.-long limestone plugs (**Fig. 2**). The obtained sandpack was heated with fan to shrink Teflon sleeve and then it was placed in a rubber sleeve of a coreflooding setup for further tightening of the Teflon. 800 psi and 400°F were applied to finalize the mixture compaction and shrinking of Teflon.

Porosity of sandpacks was determined using CT scan. This technique relies on the comparison of matrix attenuation density obtained for dry and brine-saturated sandpacks. It allows to obtain effective porosity values for each slice of the sandpack. This feature was used to plot the porosity values for each sandpack as a function of length.

CT scans of dry sandpacks were collected. Next, sandpacks were saturated with 5 wt% KCl and CT-scan of saturated sandpack was collected for determination of the initial porosity at any point in the sandpack (**Fig. 1**). Obtained CT values were imported using ImageJ software. Circular slice shape (yellow line, **Fig. 3**) was used to match the cross section of the scanned sandpacks. The average scan resolution was about 570 images per 6-in. sandpack. Based on the obtained CT values, the porosity was calculated using **Equation 1**:

$$\emptyset = \frac{CT\_number_{(saturated\ core)} - CT\_number_{(dry\ core)}}{CT\_number_{(brine)} - CT\_number_{(air)}} \qquad \text{(Equation 1)}$$

where $\emptyset$ is the porosity of the sandpack slice; CT_number corresponds to matrix attenuation density measured for saturated and dry sandpacks, as well as for brine and air. Reference CT_numbers for 5 wt% KCl brine and air were measured and found to be 48 and -1,000, respectively. These values were assumed to be constant for all samples.

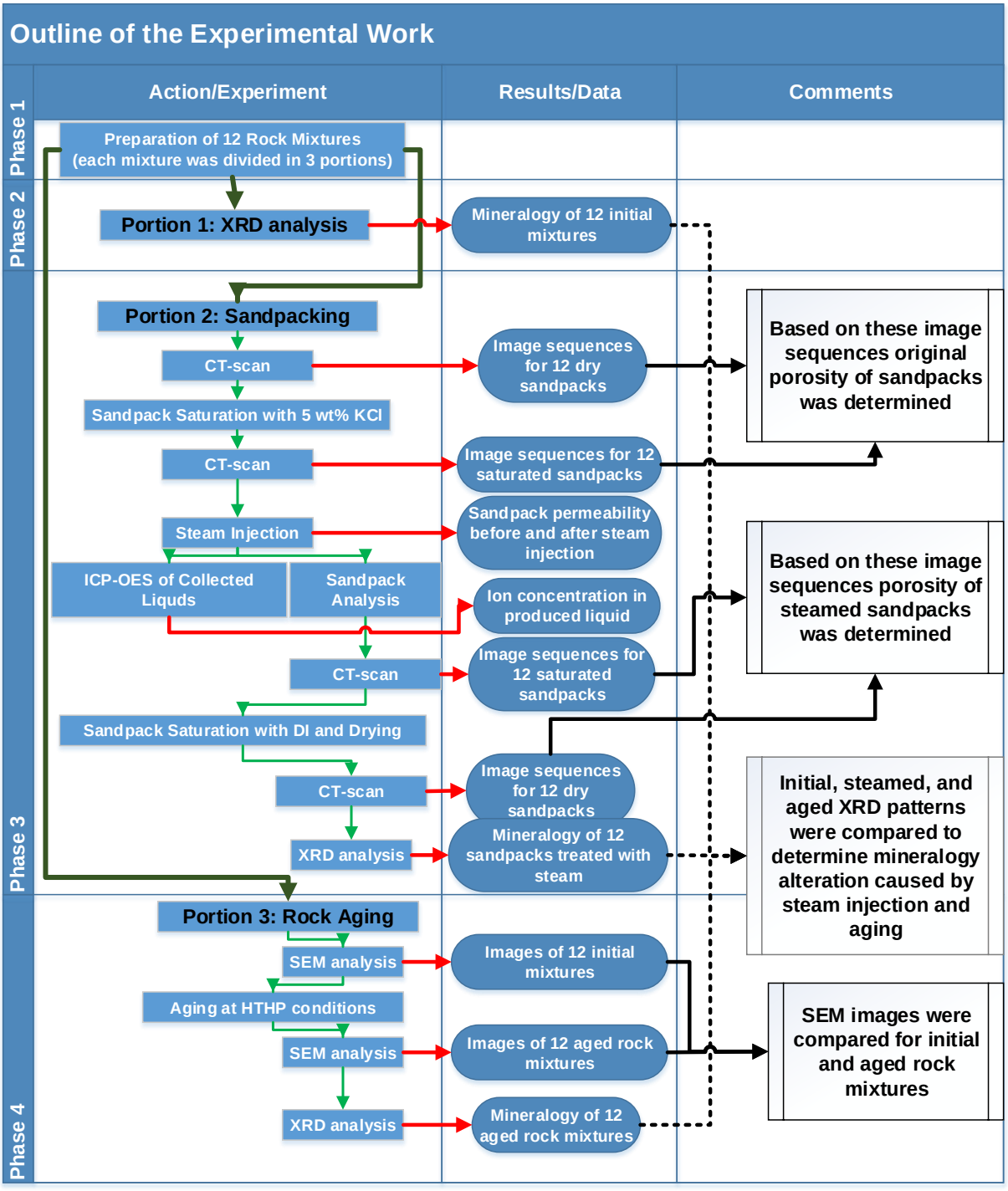

Figure 1 – Outline of the Experimental Work

Sandpacks were CT scanned at ambient conditions (no overburden pressure), so the reported porosity values are most probably higher than those at reservoir conditions. However, the objective of this study is to illustrate the relative change of the porosity for initial and steamed sandpacks.

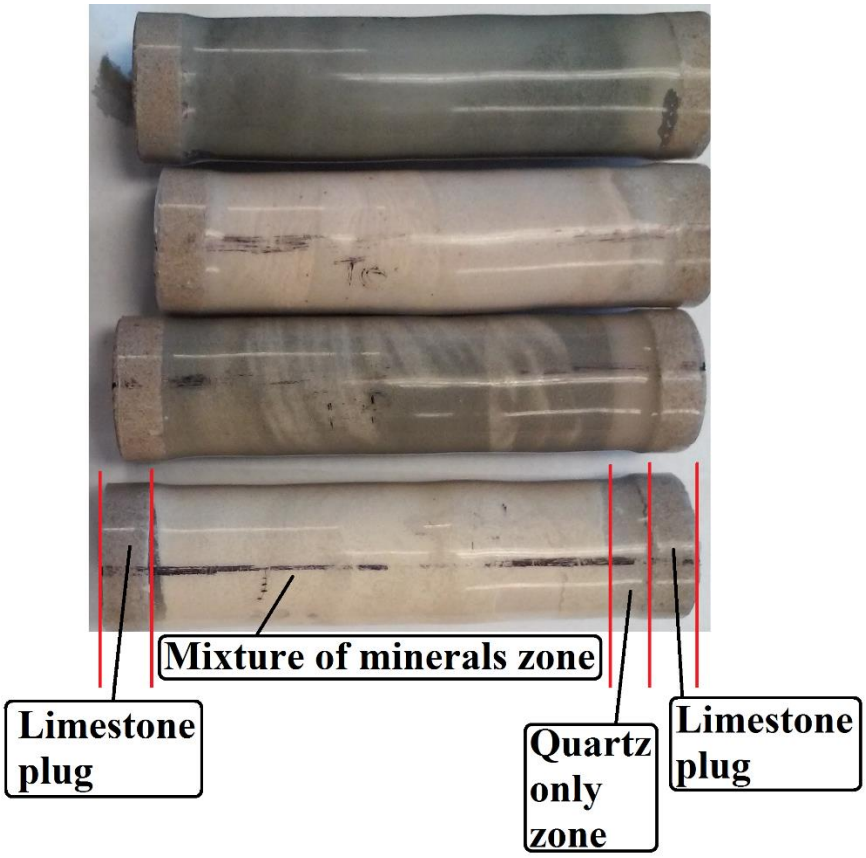

Figure 2 – Prepared Sandpacks

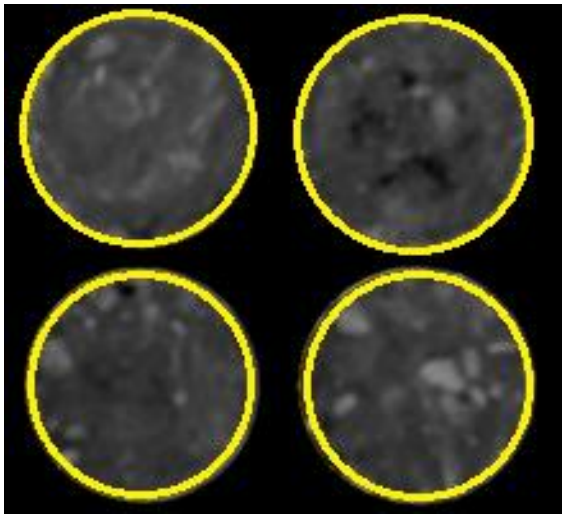

Figure 3 – Porosity Measurement using CT-Scan

2.1.2 Steam Injection Experiments

The steam generator used in this study was assembled in-house (**Fig. 4**). It contains two heaters (120V, 600 watt each) and can operate at pressures up to 3,000 psi. The controller system works with type K thermocouples to set the temperature on the heaters. Additional thermocouples were installed to monitor steam temperature at the outlet and in the insulated flowlines. The steam generator was connected to a regular coreflood setup. This configuration allows measurement of the permeability of a sandpack before, during, and after the steam injection. Measurements of initial and final permeability for all sandpacks were conducted using 5 wt% KCl brine at 800 psi overburden pressure and 400°F oven temperature. During the steam treatment phase, deionized water (DI) was used as boiler feed water. The amount of injected steam was normalized based on the initial pore volume of each sandpack. The volume of deionized water used for steam generation was equal to 15 pore volumes of the sandpack.

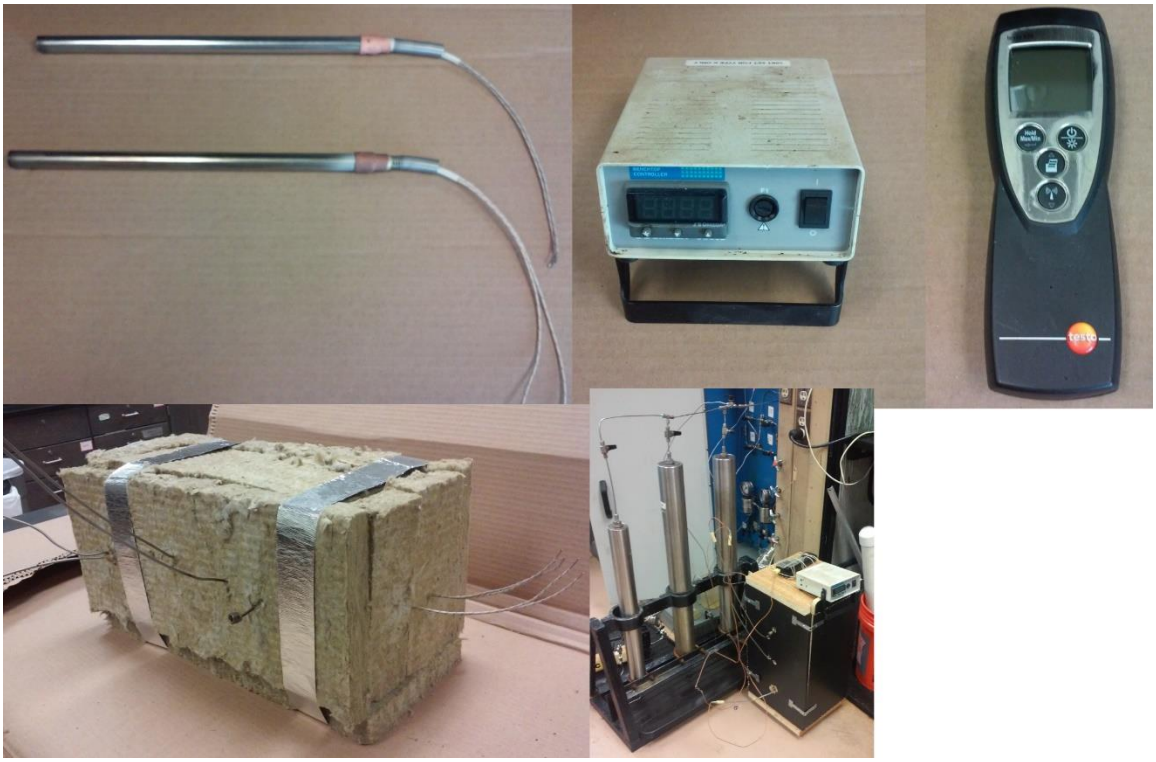

Figure 4 – Steam Generator Components

Sandpacks saturated with 5 wt% KCl brine were placed inside the core holder of the steamflooding setup. First, the oven was turned on at 400°F but the steam generator was turned off. Once the temperature of the sandpack increased to 400°F then 5 wt% KCl was circulated at 3 different flow rates until stabilization of the measured pressure drop was achieved. This data was used to determine the initial permeability of the sandpack. After that, 1 pore volume of deionized water was injected to displace KCl brine. Next, the steam generator heaters were turned on and steam was continuously injected in the sandpack at a constant flow rate of 2 cm^3/min. Steam was generated from deionized water. The injected steam was kept in superheated condition. This was

done by controlling the heater temperature depending on the changes in the injection pressure. Since the injection was conducted at a constant flow rate and constant outlet pressure then changes in pump injection pressure was constantly monitored. For example, if initial sandpack permeability was relatively high, then pressure drop across the sandpack was low and to inject constant flow of 2 cm^3/min pump pressure was only 500 psi, then the heater temperature would be set at only about 480°F. Once the operator observed that the injection pressure is increasing to 700 psi then the temperature was immediately set to 520°F. The temperature of the injected steam was monitored using thermocouples. During the steam injection phase, hot liquid samples flowing out of the outlet of the sandpack were collected every 10 minutes. After injection of steam the heaters were turned off but the oven remained on at 400°F. After cooling of the sandpack to 400°F permeability measurement was repeated using 5 wt% KCl. The brine was circulated at 3 different flow rates until stabilization of the measured pressure drop to determine the final permeability of the sandpack that was treated with steam. The permeability was determined using Darcy's law represented by **Equation 2**:

$$Q = \frac{kA(p_{inlet} - p_{outlet})}{\mu L} \quad \text{(Equation 2)}$$

The units in this equation are: Q is the flow rate (units of volume per time, m^3/s); k is the permeability of the porous medium (units of area, m^2); A is the cross-sectional area of the sandpack (units of area, m^2); μ is the dynamic viscosity (units is Pa·s); L is the length of the sandpack (units of length, m); total pressure drop is defined as difference between pressure at the inlet (p_{inlet}) and pressure at the outlet (p_{outlet}) of the sandpack (units of pressure, Pa).

After the steam injection, the system was cooled down for about 4 hours. Next, the sandpack was extracted from the core holder, and, while it was still saturated with 5 wt% KCl, it was CT-scanned. Then, the sandpack was saturated with DI water to prevent precipitation of KCl

salt inside the pores during drying. Finally, the treated sandpack was dried in a static oven at 14.7 psi and 140°F for 12 hours. Dried sandpacks were CT-scanned and based on the collected CT-numbers the final porosity of the sandpack was determined using the same procedure and software as explained above.

The Teflon wrap was then cut open and removed to extract the sandpack mixture for further analysis. The final mineralogy was determined using XRD. Chemical composition of the collected liquid samples was analyzed using ICP-OES. In cases when solids were observed in the collected samples, they were separated, dried, and analyzed using XRD.

2.1.3 Rock Aging Experiments

The objectives of the aging experiments were to mimic the conditions common for thermal recovery projects, and to investigate silicon-carbonate reactions that can lead to neoformation of swelling clays. The advantage of the aging experiments is that they can be performed for much longer time compared to steam injection experiments. This allows more time to form reaction products and to observe the mineral alteration.

As mentioned above (**Fig. 1**) one portion (40 g) of each rock mixture was used for aging. Each sample was analyzed using SEM before being aged. Next, the rock mixture was added to deionized water in ratio 1:10 (solid to liquid) and placed inside the aging cell. The aging cell was pressurized with nitrogen up to 1,000 psi (at room temperature). The pressurized cell was then placed in a static oven preheated to 400°F. Aging was conducted for 10 days.

After the aging samples were retrieved from the cells, they were separated into liquid and solid phases. Solids were analyzed using SEM-EDS and XRD. SEM images allowed for comparison of the characteristic morphology, pore-space configuration, and rock composition. EDS analysis was used to confirm element intensities ratios. XRD analysis was used to identify

mineralogy changes caused by aging. Observations made during these experiments provided data about changes in mineralogy and structure of pore-space caused by thermal alteration of aged rock.

2.2 Results and Discussion

The results of permeability measurements for sandpacks #1-12 before and after steam injection are presented in **Table 3**. Effective porosity values are illustrated in **Fig. 5**. These values are averages determined based on the porosity profiles across the length of the sandpack (**Figs. 6-8, 11-16, 20-22**).

The following subsections are made for each group of samples.

2.2.1 Group 1

2.2.1.1 Steam Injection Experiments. For the sandpacks from the Group 1, quartz and calcite mixtures were used. This group was created to investigate petrophysical changes that can be expected due to steam injection into sandstone without clay minerals but with high concentration of carbonate cementing material.

Table 3: Permeability of the Sandpacks Before and After the Injection of Superheated Steam

Sample #	Group #	Sandpack content (wt%)	Permeability (md)		Permeability decrease (%)
			before steam injection	after steam injection	
1		Quartz 90%, Calcite 10%	211.7	202.2	4.5
2	1	Quartz 85%, Calcite 15%	232.6	227.3	2.3
3		Quartz 80%, Calcite 20%	205.7	195.6	4.9
4		Quartz 85%, Calcite 10%, Kaolinite 5%	178.2	158.1	11.3
5	2	Quartz 80%, Calcite 10%, Kaolinite 10%	192.0	156.7	18.4
6		Quartz 75%, Calcite 10%, Kaolinite 15%	154.6	120.6	22.0
7		Quartz 85%, Dolomite 10%, Kaolinite 5%	184.3	159.6	13.4
8	3	Quartz 80%, Dolomite 10%, Kaolinite 10%	180.2	150.6	16.4
9		Quartz 75%, Dolomite 10%, Kaolinite 15%	167.3	132.7	20.7
10		Quartz 95%, Montmorillonite 5%	5.2	1.2	76.9
11	4	Quartz 90%, Montmorillonite 10%	4.9	1.1	77.6
12		Quartz 85%, Montmorillonite 15%	4.3	0.7	83.7

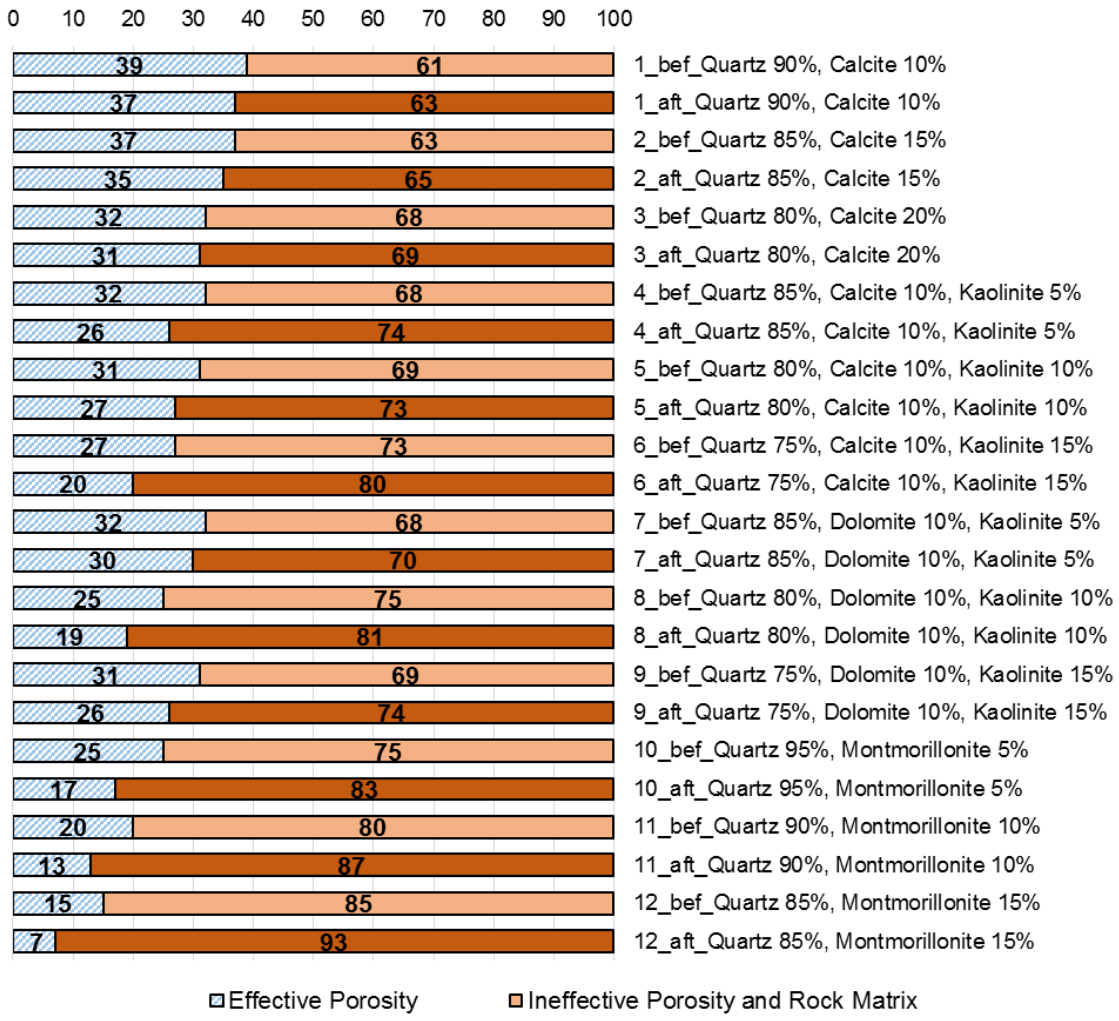

Figure 5 –Porosity Changes for Samples #1-12 ("bef" and "aft" – Before and After Steam Injection)

Initial permeability and porosity of these sandpacks were very high (206-233 md, 32-39%) and they did not change significantly during steam injection (196-227 md, 31-37%). Increase in calcite concentration does not directly correlate with permeability change because the lowest permeability drop in this group was observed for the sample with medium amount of calcite (sample #2). However, the amount of calcite does affect the effective porosity of the sandpacks.

Higher calcite concentration allows tighter packing of the rock and leaves less space for the open pores. In a real reservoir, higher calcite concentration usually means that cementation is massive and firm, which also decreases effective porosity. XRD analysis of initial and treated rock mixtures #1-3 revealed that there was no mineralogical alteration caused by steaming. Sandpacks after steam injection remained unconsolidated.

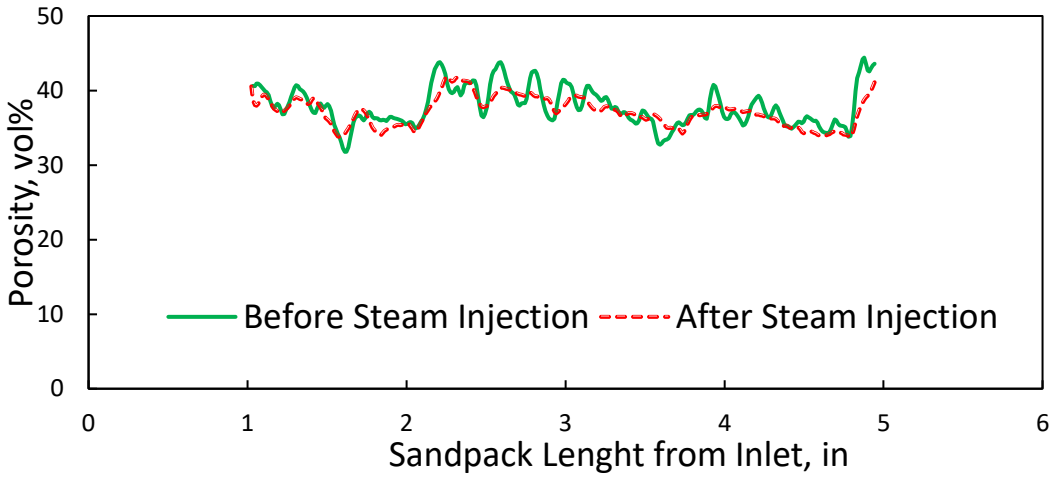

Figure 6 – Porosity of the Sample #1: 90% Quartz + 10% Calcite

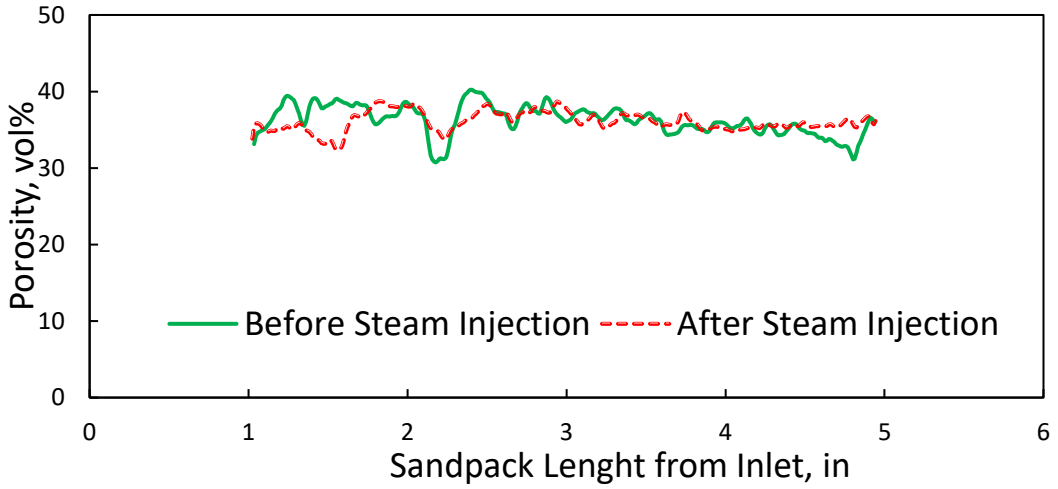

Figure 7 – Porosity of the Sample #2: 85% Quartz + 15% Calcite

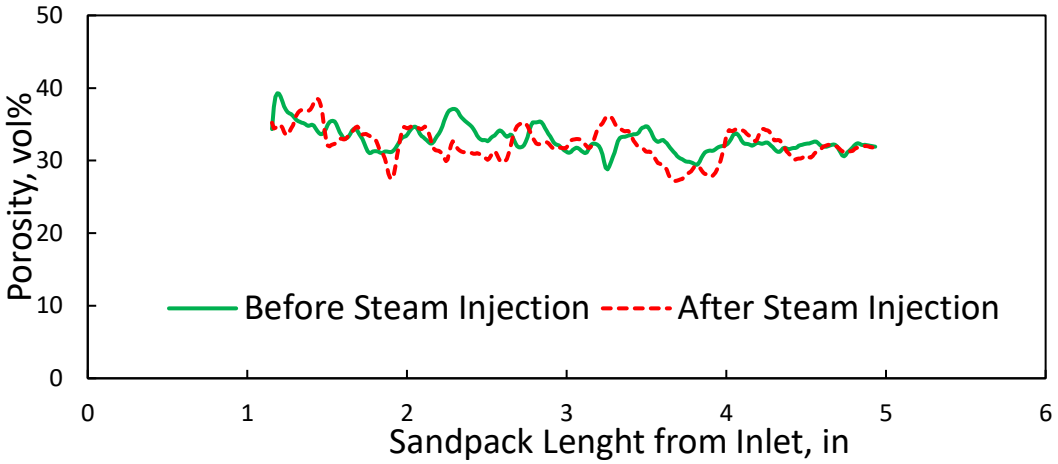

Figure 8 – Porosity of the Sample #3: 80% Quartz + 20% Calcite

Collected liquid samples did not contain any solid phase. ICP results for all three samples in this group exhibit similar trends. Concentration of Si^{4+} grows from 3 to 74 mg/L during injection of the first 2-3 pore volumes, and then it stays almost constant at this level for the rest of the steam

injection. This consistency shows that the whole sandpack was warmed up during the injection of the first 2-3 pore volumes (within about 1.5 hours). At the beginning, silica dissolution was mostly happening at the inlet and after this warm-up phase the dissolution was more uniform over the whole sandpack matrix. The injection was performed at a constant rate. Pressure drop increased slowly during injection of the first 2.3-2.7 pore volumes and then flattened and fluctuated insignificantly around the same value. This correlation of silicon ion concentration and differential pressure increase suggests that most of the formation damage happened during the warm-up phase. The observed 2.3-4.5% decrease in permeability and 1-2% decrease in effective porosity can be explained by silica dissolution followed by deposition of molecular SiO_2. It can be summarized by **Equation 3**:

$$SiO_2 + 2H_2O \rightleftharpoons H_4SiO_4 \qquad \text{(Equation 3)}$$

The mechanism of molecular deposition of silica from silicic acid is reverse of dissolution of solid silica. Iler (1979) reported that this process follows the sequence of condensation, dehydration and deposition. This only happens at a certain degree of supersaturation – it should be high enough to form deposits, but not too high as to allow the formation of colloidal silica. It was also reported that even a monomolecular silica deposit is nonporous and quite impermeable.

Equilibrium concentration of aqueous silica is temperature dependent. At the beginning of steam injection, hot condensate dissolves quartz matrix at the inlet of the sandpack and becomes saturated with silica; it then flows further in the sandpack, cools down and becomes oversaturated. This causes precipitation and redistribution of quartz matrix. Porosity profiles demonstrate that sandpacks gain porosity in some slices and lose it where silica precipitates (**Figs. 6-8**). Based on the plots of porosity versus sandpacks' length (**Figs. 6-8**) it can be observed that the initial trends for appear to be erratic and abrupt. After steam injection, these profiles follow the overall trend

but become smoother. This demonstrates the “flattening” effect of steam treatment on porosity of sandstone with carbonate cementation. Thermal treatment of these sandpacks made the range of porosity values to be smaller and more uniform.

Only one cycle (about 9-10 hours) of steam injection was performed in this study. The overall petrophysical effect for this case is negative, but not very significant because these sandpacks have high initial permeability and porosity. In a real reservoir, this effect may lead to higher formation damage. For example, Koh et al. (1996) demonstrated that water injectivity of hot diatomite wells can reduce by more than 50% after 100 days of operation. In-situ silica dissolution/precipitation have a significant effect in reservoirs with inherently low permeability.

For field application of these observations, it would also be reasonable to account for pH and water impurities effects on condensate capacity to dissolve silica. In the current study steam was generated using deionized water (pH=6.89), which has reduced capacity to dissolve silica in comparison to higher pH fluids. Collected condensate samples had pH of about 7.2. Iler (1979) discussed that condensation reaction is catalyzed by hydroxyl ions and monovalent electrolyte salts. This means that silica deposition will be accelerated in pH range of 7-11. At pH higher than 11 silica dissolves as silicate ion. Watkins et al. (1986) discussed the increase of silica dissolution with increase of bicarbonate content, and Reed (1980) reported that steam generator effluents are usually quite alkaline and have high capacity to dissolve siliceous material. However, Duanzong et al. (2000) investigated decomposition conditions of bicarbonate ion (HCO_3^-) and argued that downhole steam condensate samples at HP/HT conditions are close (in composition and pH) to boiler feed water samples. Investigation of pH effect on changes in petrophysical properties is recommended for future work.

2.2.1.2 Aging Experiments. Aging of mixtures #1-3 for 10 days at static conditions and XRD analysis of the aged samples revealed that there were no changes in mineralogical composition. SEM images (**Fig. 9**) show limited surface dissolution (some surfaces of angular quartz grains became slightly more round and smooth). There is no significant pitting or scalloping of fabric grains observed.

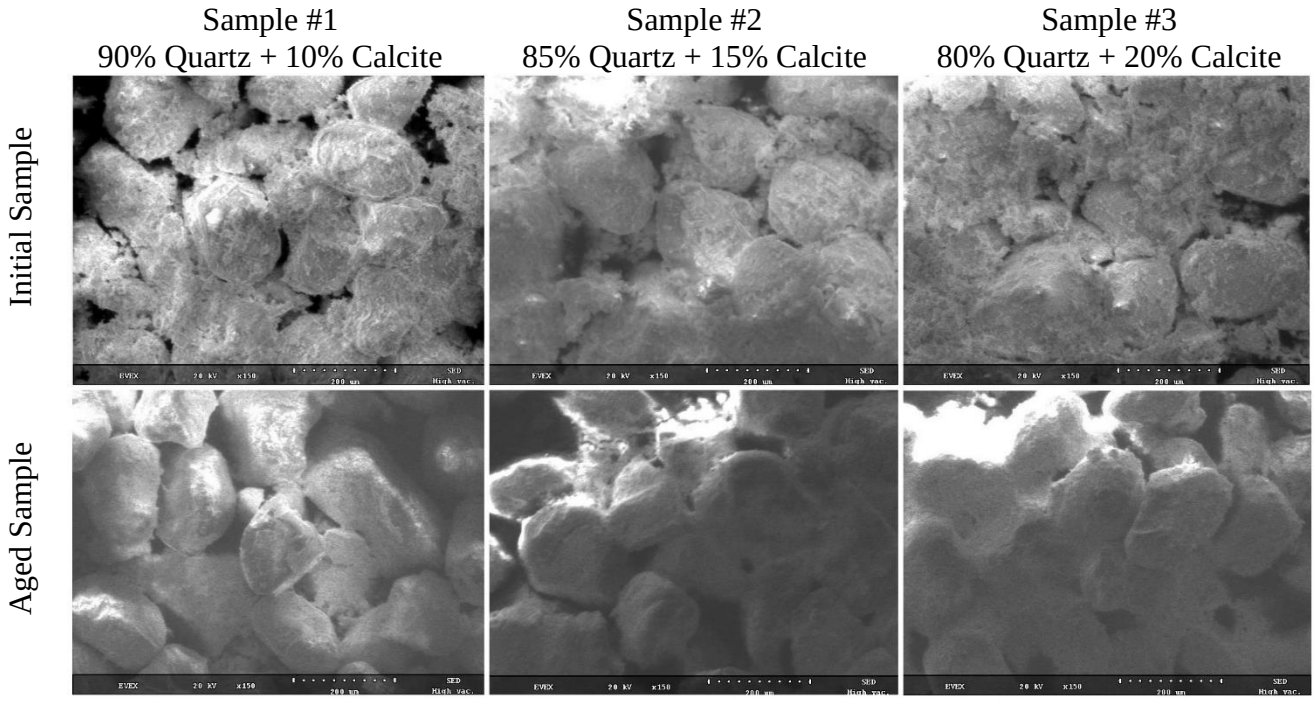

Figure 9 – SEM Images for Initial (Top Row) and Aged (Bottom Row) Samples #1-3 (Aged at 400°F and 1,000 psi for 10 Days). No Changes in Mineralogy Observed. Change in Distribution of Calcite – From Being Isolated Crystals in the Porous Space to Formation of Lining on the Quartz Grains (Cementation Effect)

Calcite distribution appears to be changed. After aging, carbonate phase lines the walls matrix rock. It also fills some of the cavities formed between the quartz grains. The lining is thin and irregular for sample #1 (contains 10 wt% calcite), but it becomes more prevalent and abundant for the sample #3 (20 wt% calcite). This morphology contributes to improvement of consolidation of framework quartz grains. Pore-space texture has changed from being filled with isolated rhombic crystals of calcite to being outlined with calcite clusters and elongated crystals.

2.2.2 Group 2 and 3

2.2.2.1 Steam Injection Experiments. The objective for these groups was to investigate the effect of steam on sand with carbonate and clay minerals. Many authors reported that kaolinite can undergo thermal alteration to montmorillonite in the presence of quartz and carbonate minerals (**Table 1**). Mixtures in Groups 2 and 3 were designed to investigate permeability and porosity changes for rocks influenced by this reaction. Sandpacks were prepared with varying amounts of kaolinite. Different carbonate minerals were used in Groups 2 and 3 (calcite and dolomite, respectively).

Permeability measurements show that increased kaolinite content is directly correlated to the permeability loss (**Table 3**). Permeability decrease ranges between 11.3-22.0% for sandpacks with calcite and 13.4-20.7% for dolomite sandpacks. Porosity decrease was observed for all of the sandpacks in both Group #2 (in a range of 4-7%) and Group #3 (in a range of 2-6%). Unlike sandpacks #1-3, none of the porosity profiles for samples #4-9 exhibit porosity increase (**Figs. 10-15**).

XRD analysis of the sandpacks treated with steam revealed that there was no mineral alteration. At the same time it was observed for sandpacks #4-9 that the relative amount of kaolinite

significantly decreased after they were exposed to steam injection (**Fig. 16**). Collected liquid samples contained solids, which were found to be fine particles of kaolinite. After steam injection sandpacks #4-9 remained unconsolidated.

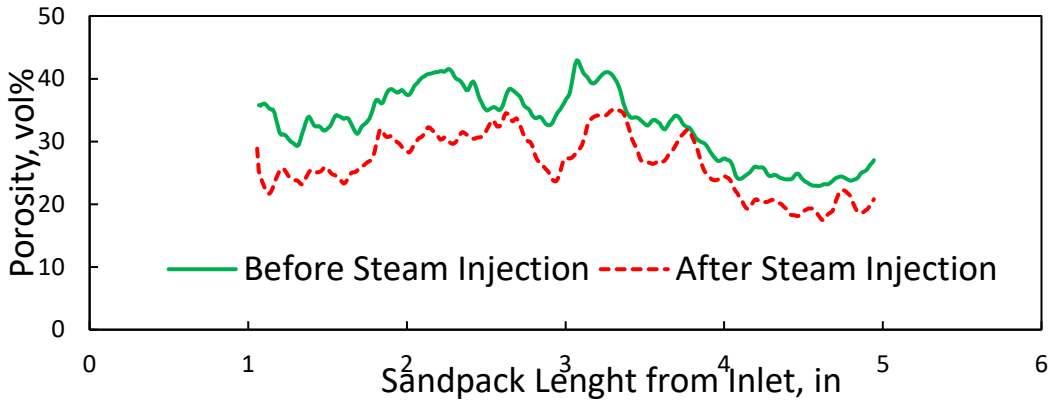

Figure 10 – Porosity of the Sample #4: 85% Quartz + 10% Calcite + 5% Kaolinite

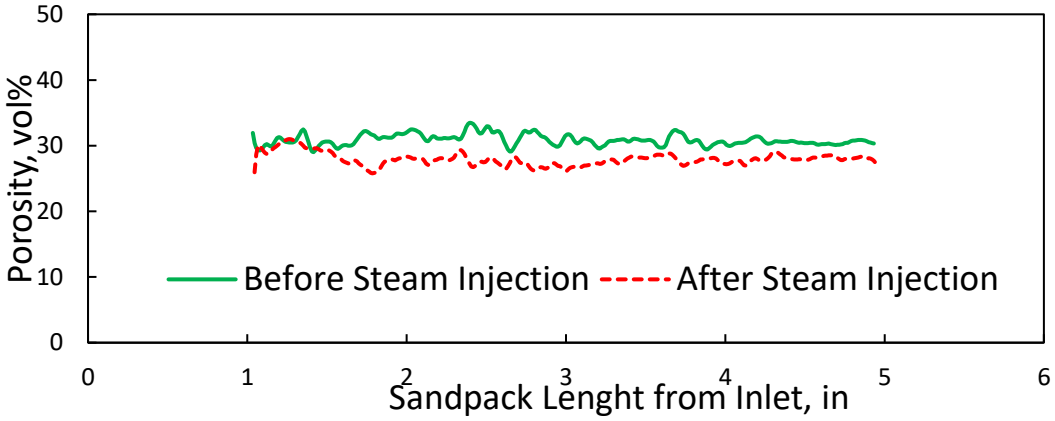

Figure 11 – Porosity of the Sample #5: 80% Quartz + 10% Calcite + 10% Kaolinite

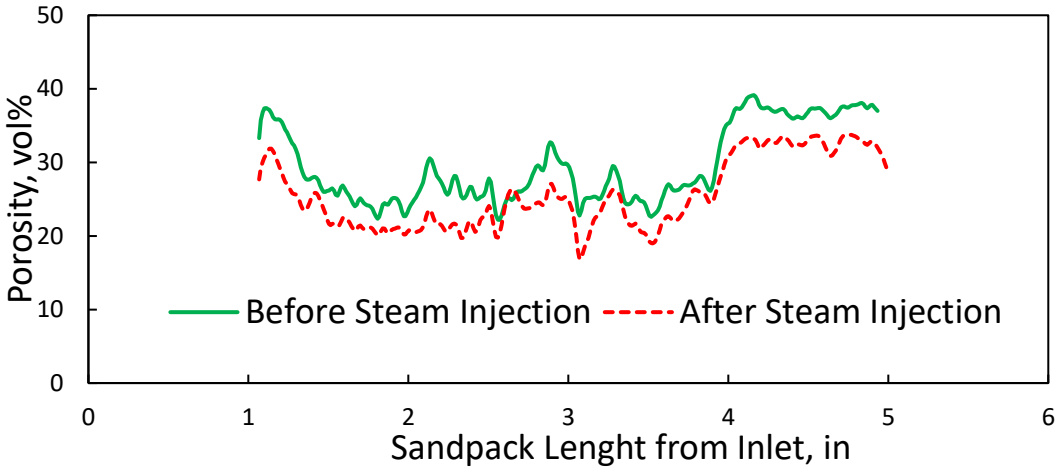

Figure 12 – Porosity of the Sample #6: 75% Quartz + 10% Calcite + 15% Kaolinite

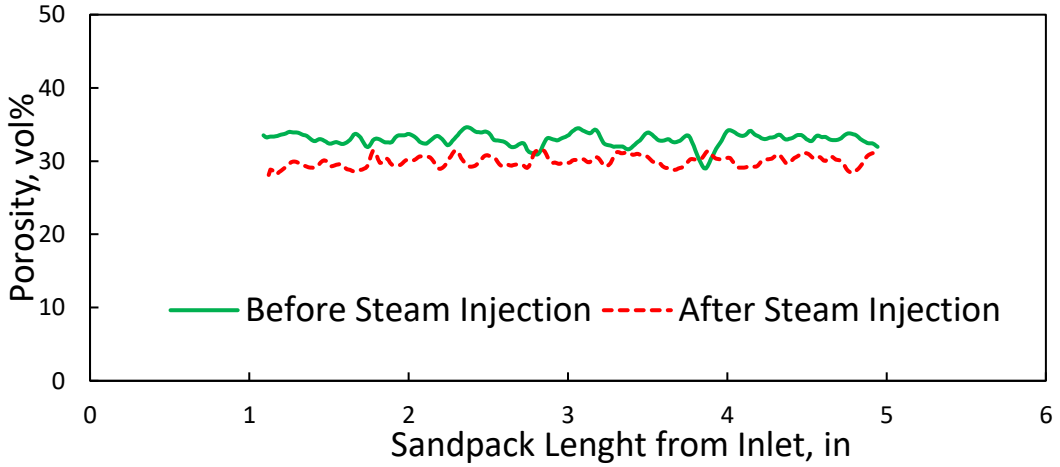

Figure 13 – Porosity of the Sample #7: 85% Quartz + 10% Dolomite + 5% Kaolinite

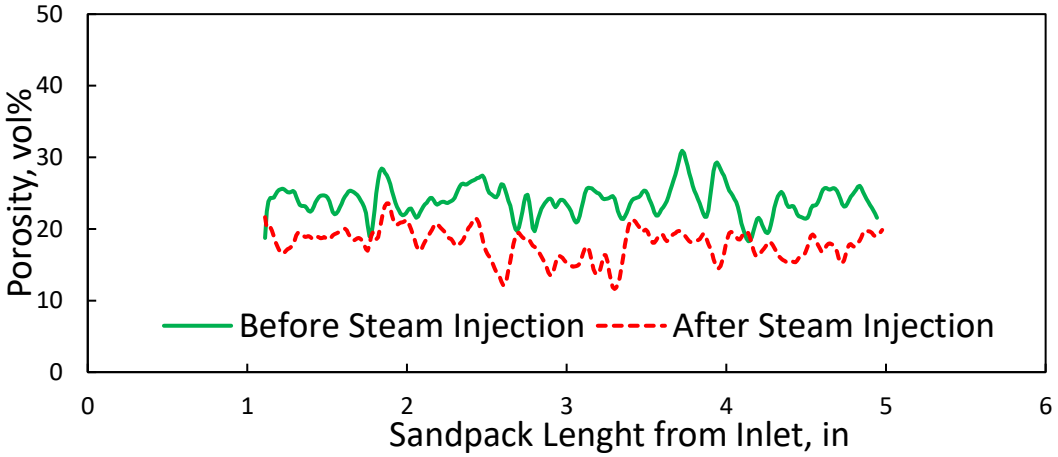

Figure 14 – Porosity of the Sample #8: 80% Quartz + 10% Dolomite + 10% Kaolinite

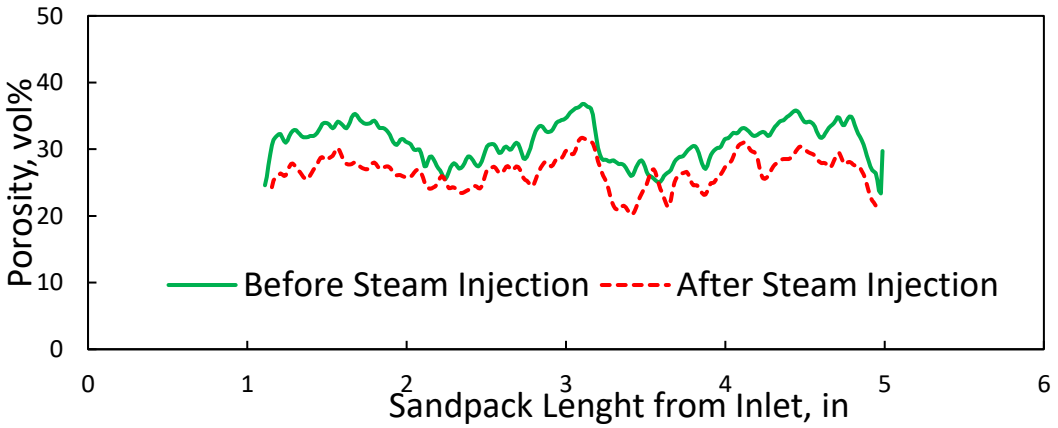

Figure 15 – Porosity of the Sample #9: 75% Quartz + 10% Dolomite + 15% Kaolinite

The obtained results prove that kaolinite is very mobile mineral that can be mobilized by injected steam and condensate. Reduction in permeability and effective porosity for these sandpacks can be explained by pore blockage caused by kaolinite fines migration. Analysis of

porosity profiles also suggests that there was redistribution and blockage of flowing channels. Some parts of the sandpacks have significant drops in effective porosity. This effect appears to be more important with increase of initial amount of kaolinite. Further analysis of hydrodynamic and colloidal forces responsible for mobilization of kaolinite is needed to model pore plugging associated with steam injection.

ICP analysis revealed that maximum concentrations of Ca^{2+} and Mg^{2+} ions reached 49 and 27 ppm, respectively. These values confirm that dissolution of calcite and dolomite occurred during steamflooding. This process can have negative effect on quartz matrix cementation. Also, similar to silica, carbonates can cause permeability reduction due to precipitation from the solution when pressure is reduced (Kubacki et al. 1984; Tang et al. 2012).

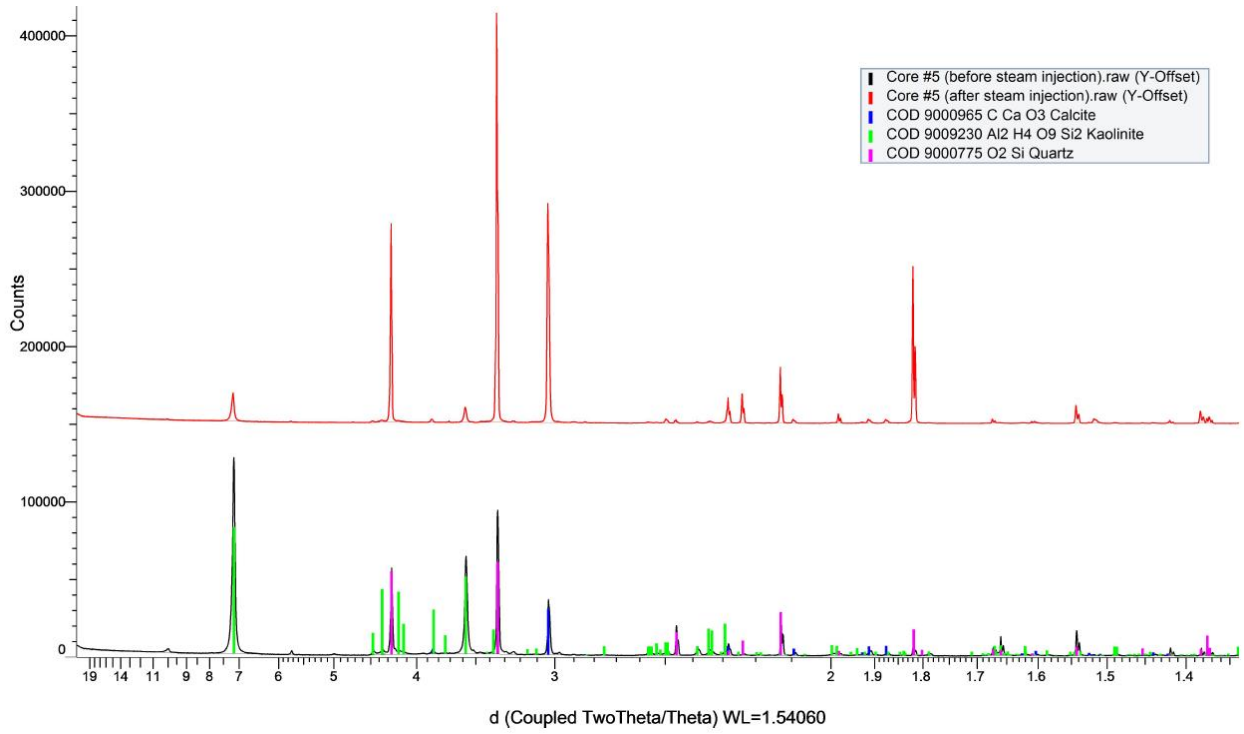

Figure 16 – Comparison of XRD Results for Sample #5 (80% Quartz + 10% Calcite + 10% Kaolinite) Before (Bottom Pattern) and After (Top Pattern) Steam Injection

2.2.2.2 Aging Experiments. Both thermal decomposition and dissolution of carbonate minerals (such as calcite $CaCO_3$, dolomite $CaMg(CO_3)_2$ or siderite $FeCO_3$) could produce CO_2. The reaction for the calcite case is given in **Equation 4**:

$$CaCO_3 + 2H^+ \rightleftharpoons Ca^{2+} + CO_2 + H_2O \qquad \text{(Equation 4)}$$

As the forward reaction progresses Ca^{2+} ions become available for formation of Ca montmorillonite but at the same time more CO_2 forms.

During aging in a constantly-closed cell with increase of partial pressure of CO_2, the forward reaction stops rather early. In these experiments formation of montmorillonite was not

identified after 10 days of aging. However, in the reservoir setting CO_2 is likely to escape or being produced and the reaction can go forward.

These observations led to a change in the design of the aging experiments. Static aging was performed at 1,000 psi and 400°F, but CO_2 was released every 10 hours. The CO_2 release was followed by immediate pressurizing of the cell with nitrogen back to 1,000 psi for the next 10 hours. For this set of aging experiments, formation of Ca montmorillonite was observed for samples #4-9.

Partial alteration of kaolinite to montmorillonite was confirmed by XRD analysis (**Fig. 17**). Small illite peak (d-spacing is 10 Å) is coming from impurity found in the initial kaolinite sample. It is not from a common conversion of montmorillonite layers to illite layers as it was reported by Garrels (1984). Peaks around d-spacing of 12 Å identify Ca montmorillonite. Also, samples with dolomite (#7-9) were able to form more montmorillonite than samples with calcite (#4-6). XRD results for samples # 5 and 8 illustrate this observation. Comparison of montmorillonite peaks (d-spacing is 12-15 Å) for these samples shows that amount of montmorillonite formed in dolomite case is about twice that formed in the case of calcite (**Fig. 17**). These differences between calcite and dolomite cases can be explained based on stability of calcite and dolomite calculated as a function of temperature and CO_2 pressure. At the same CO_2 pressure dolomite decomposes at lower temperature than calcite (Oldershaw et al. 1981). That is why dolomite ends up providing more Ca^{2+}, and samples that contained dolomite were more likely to alter to Ca montmorillonite.

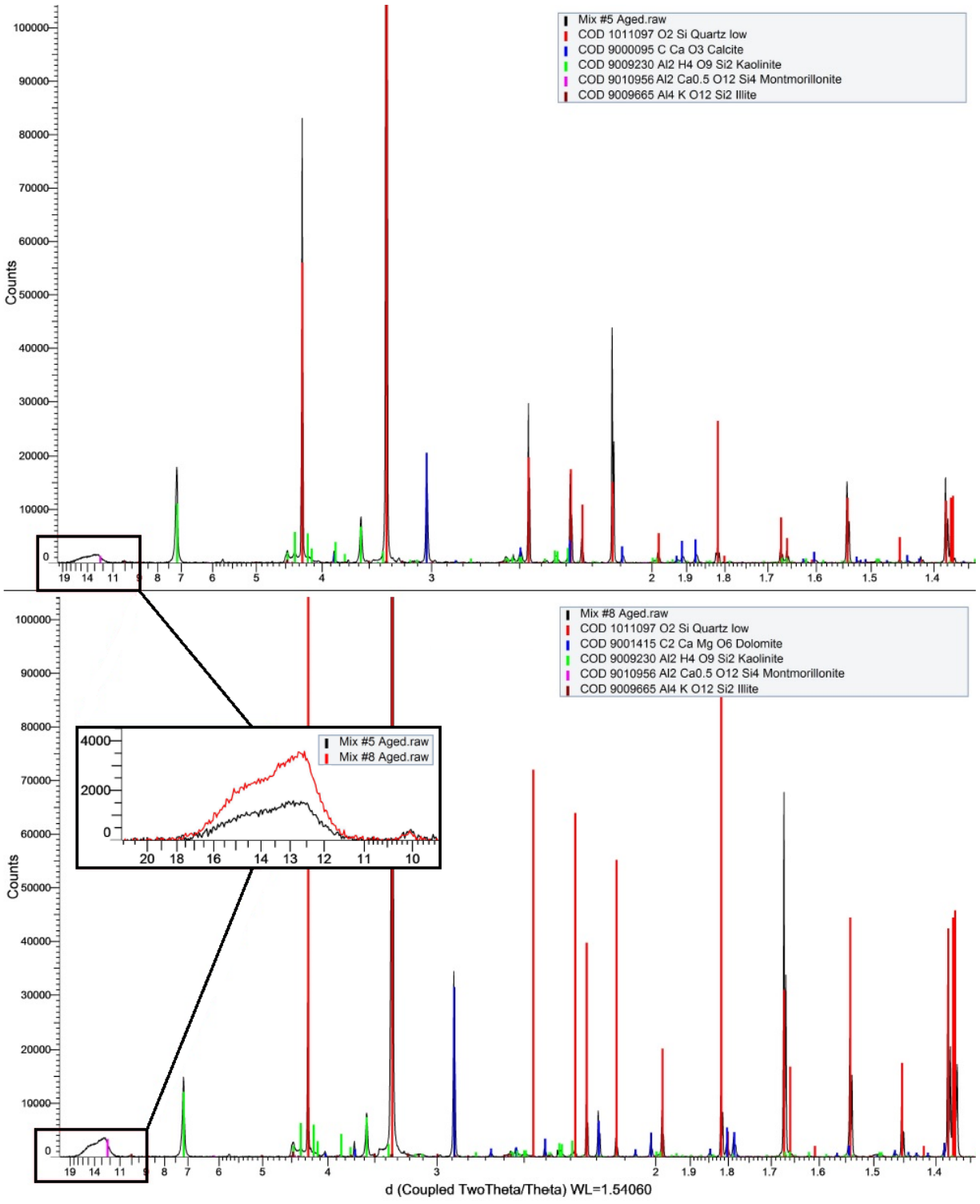

Figure 17 – Comparison of XRD Results for Samples #5 (80% Quartz + 10% Calcite + 10% Kaolinite) and #8 (80% Quartz + 10% Dolomite + 10% Kaolinite). Amount of Formed Montmorillonite is Higher for Dolomite Case (Sample #8)

SEM images for samples #4-9 (**Figs. 18 and 19**) present the changes in rock mixtures during aging. Differences in the type of carbonate rock did not have an impact on the structure of the mixtures. The initial rock is disaggregated and has visible openings between matrix grains and pore filling clay mixed with carbonate rock. However, after aging, these same samples appear to be conglomerates of quartz, lined out with thick uniform layers of cement formed by carbonate minerals, remained kaolinite, and neoformed montmorillonite. SEM results for aged samples from both groups show many similarities, even though samples with dolomite produced more montmorillonite. Kaolinite particles are very small and are not visible as a discrete phase. They are normally confined to other lithoclasts, which presented by quartz grains and calcite/dolomite clasts. After aging kaolinite maintained internal consistency of its grains.

Due to availability of water, montmorillonite has grown in an expanded form. Synthesized montmorillonite has a scale- or plate-like structure and, due to its small particle size, it is distributed through the sample as irregular blocks that coat the surface of framework grains and as elongated clay-mineral bridges across the pores. Growth of montmorillonite increases the overall surface area of mineral conglomerates in pores. This makes the rock more reactive. These results illustrate one of the mechanisms of how authigenic kaolinite located in pore-spaces can, with time, significantly modify petrophysical properties of a reservoir, depending on the chemical and physical properties of the environment. Growth of expanded montmorillonite and precipitation of silica offset the porosity increase caused by etching and dissolution of minerals. It also causes blockages of pores, and thus the effective porosity decreases due to increase in microporosity. For example, Nadeau (1998) observed carbonate-silicate reaction that produced Mg-rich saponite (smectite clay). He reported that growth of less than 5% of this smectite caused 98% permeability reduction.

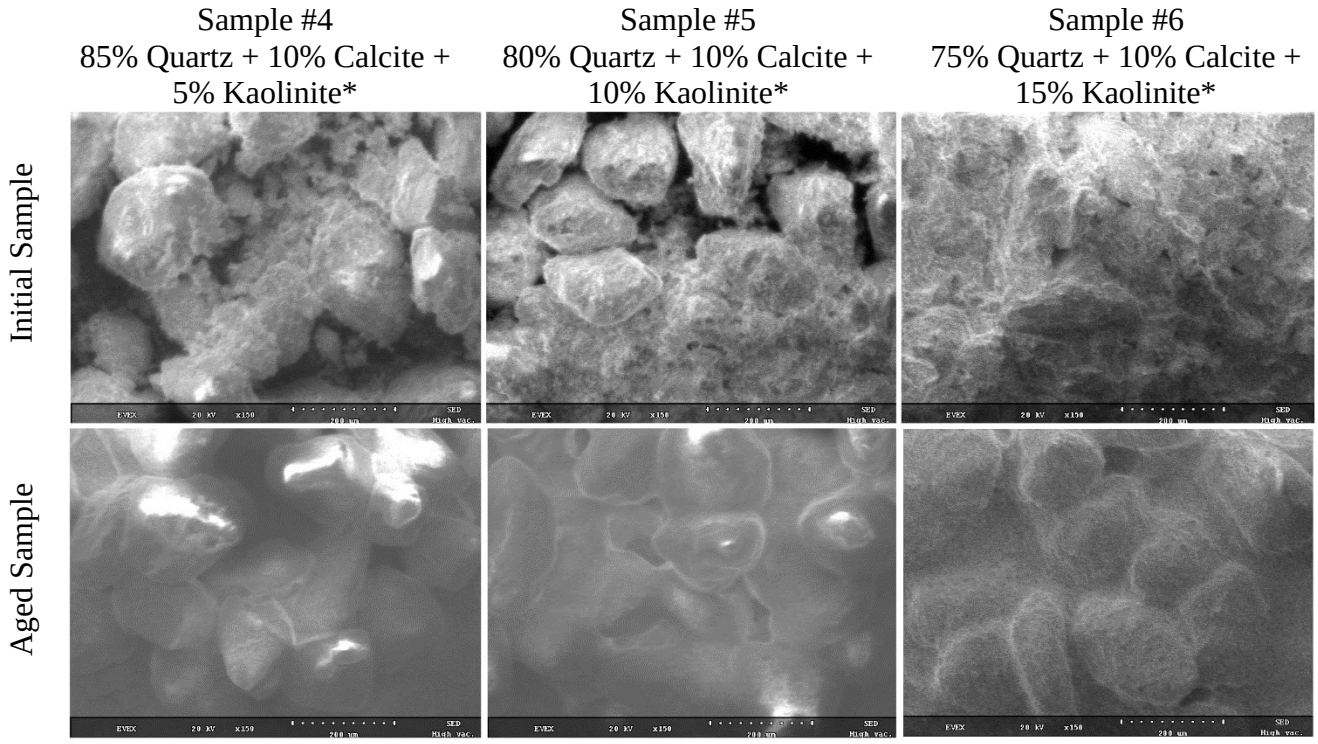

Figure 18 – SEM Images for Initial (Top Row) and Aged (Bottom Row) Samples #4-6 (*Aged Mixtures Contain Montmorillonite; Aged at 400°F and 1,000 psi for 10 Days, CO_2 Release Every 10 Hours). Conglomerates of Quartz Became Covered with a Thick Uniform Layer of Neoformed Montmorillonite and Remained Kaolinite and Calcite

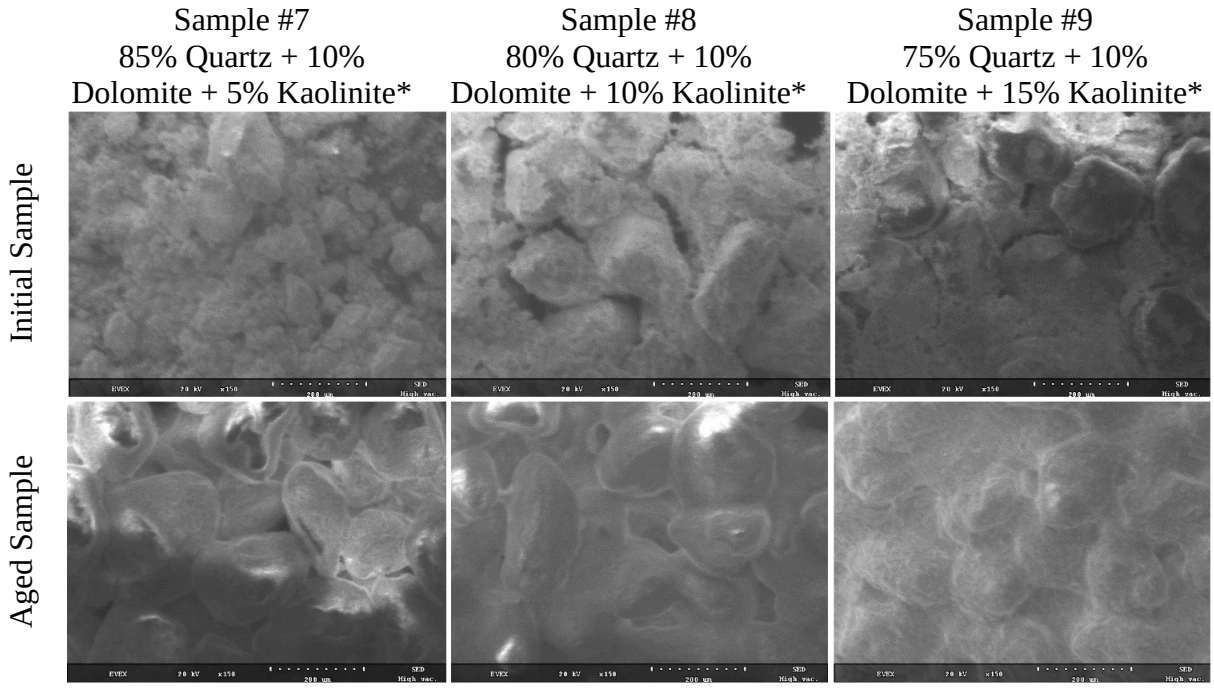

Figure 19 – SEM Images for Initial (Top Row) and Aged (Bottom Row) Samples #7-9 (* Aged Mixtures Contain Montmorillonite; Aged at 400°F and 1,000 psi for 10 Days, CO_2 Release Every 10 Hours). Aged Samples Demonstrate Montmorillonite-Based Coating and Bridges Across the Pores

2.2.3 Group 4

2.2.3.1 Steam Injection Experiments. Experiments were performed to investigate porosity changes caused by steam in montmorillonite-rich sandpacks. Sandpacks #10-12 contained various amounts (5-15 wt%) of Ca montmorillonite. The sandpacks #10-12 were packed slightly differently from the sandpacks #1-9. At the outlet, before the limestone plug, 0.5 in. of clean quartz was added to track the changes in pore structure caused by steam in both – quartz only zone and quartz with montmorillonite mix zone (**Fig. 23**).

Initial permeability of montmorillonite-rich sandpacks was much lower compared to all other sandpacks. Even saturation with 5 wt% KCl caused swelling of the clay. Once the steam injection was started the permeability dropped for up to 84% lower compared to the initial permeability. The main effect of this process is pore filling and bridging caused by clay swelling. The reduction in permeability is directly correlated to the increase in the amount of montmorillonite. There were no solids observed in the liquid samples collected during steamfloods.

Porosity trends are shown in **Figs. 20-22**. The overall reduction in effective porosity was found to be about 8%. It seems to be drastic with no trend to it. It most likely depends on how homogeneous montmorillonite was distributed in the mix of a particular sandpack. Increase in montmorillonite concentration caused initial effective porosity to be lower. This correlation is true for all 3 sandpacks. XRD analysis of initial and treated rock mixtures #10-12 revealed that there was no mineralogical alteration caused by steaming.

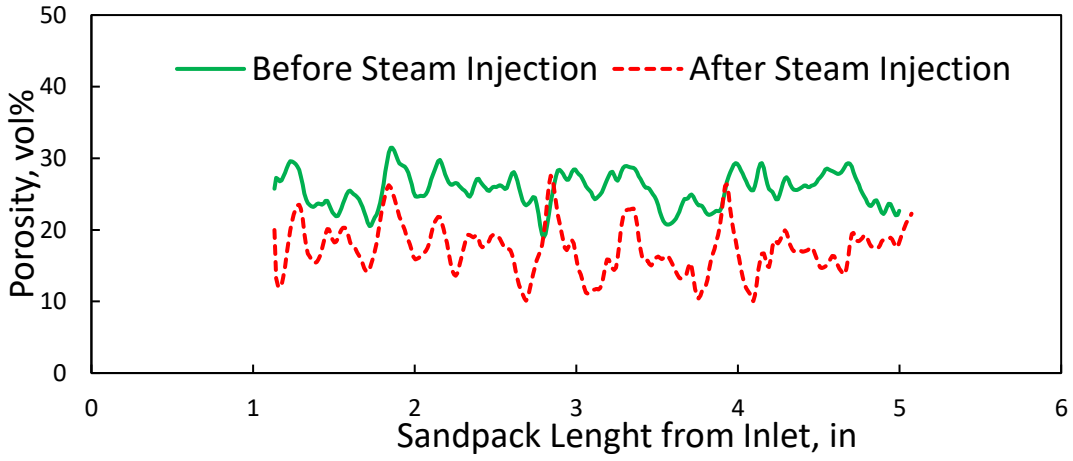

Figure 20 – Porosity of the Sample #10: 95% Quartz + 5% Montmorillonite

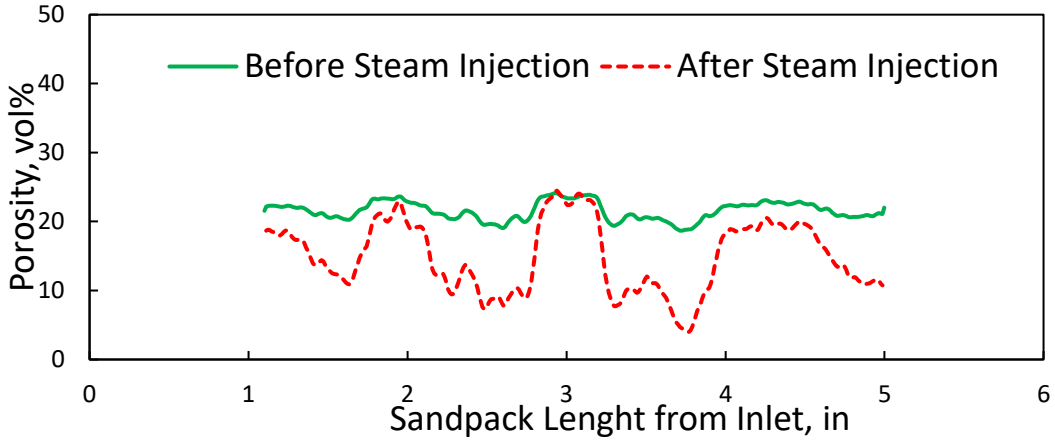

Figure 21 – Porosity of the Sample #11: 90% Quartz + 10% Montmorillonite

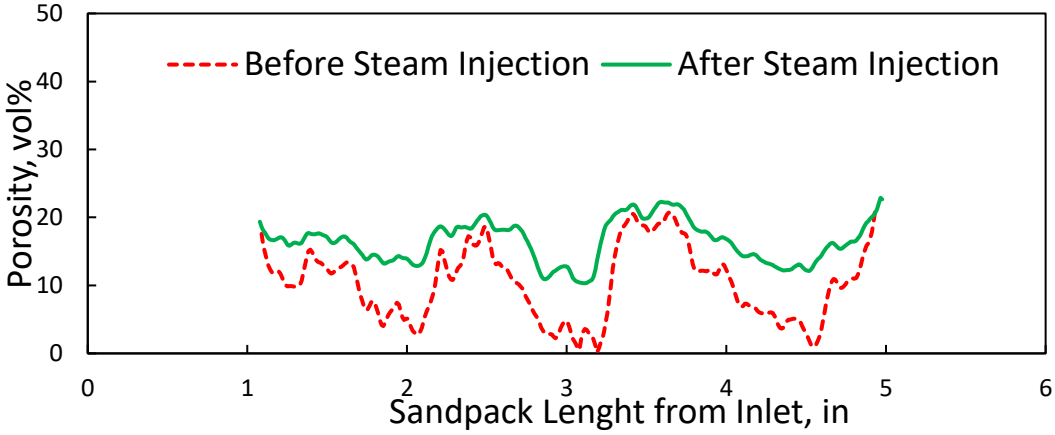

Figure 22 – Porosity of the Sample #12: 85% Quartz + 15% Montmorillonite

Additional evidence of the bridging effect of steamed montmorillonite on porous media was an observation that the sandpacks extracted from the core holder became much consolidated after steam injection. When the overburden pressure was released and the Teflon pack removed, the sandpack held its shape at points where montmorillonite was added. **Fig. 23** demonstrates that

part of sandpack #11, which contained montmorillonite and quartz mixture became consolidated, while the part with clean quartz remained unconsolidated.

Montmorillonite is known to expand considerably due to water penetration in the interlayer molecular spaces and concomitant adsorption. As previously discussed, there are numerous reports on permeability reduction caused by swelling clays. These experiments demonstrate that neutral pH steam and condensate water have similar effects on montmorillonite-rich sandpacks and can lead to formation damage.

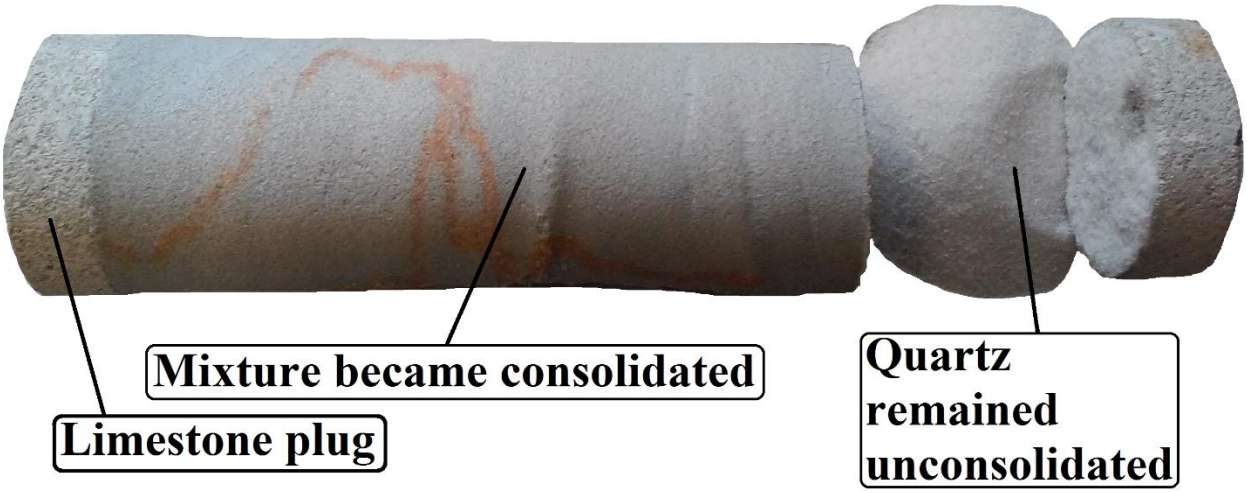

Figure 23 – Consolidation of Sandpack #11 Caused by Steam Injection – Mixture of Quartz (90%) and Montmorillonite (10%) has Consolidated, and Clean Quartz Remained Unconsolidated

2.2.3.2 Aging Experiments. No mineral changes were observed during aging of mixtures of quartz and montmorillonite. **Fig. 24** shows SEM images of the initial and aged mixtures. These images illustrate that the matrix grains did not experience dissolution, pitting, or alteration. However, the pore-space montmorillonite has changed its texture and morphology. Initially montmorillonite did not seem to bond and cover all the quartz grains completely, but after aging a uniform lining was created.

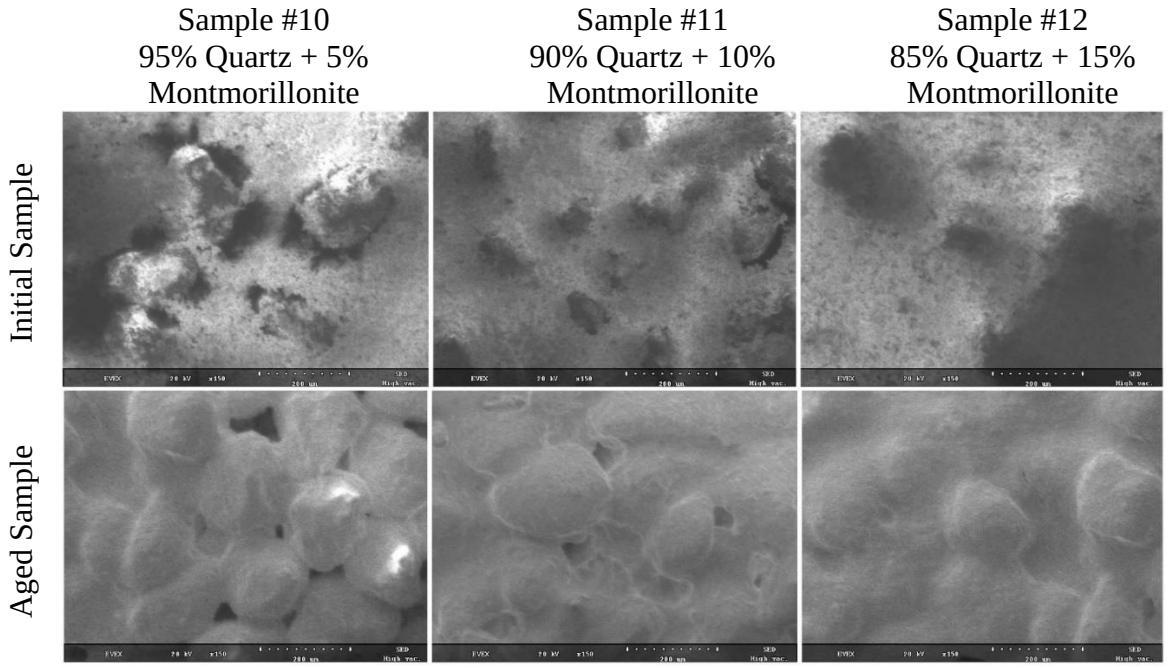

Figure 24 – SEM Images for Initial (Top Row) and Aged (Bottom Row) Samples #10-12 (Aged at 400°F and 1,000 psi for 10 Days). No Changes in Mineralogy Observed. Change in the Texture and Morphology of Pore-Space Montmorillonite – From Initially Detached Separate Particles to Thick Coating and Bonding of the Quartz Framework (Consolidation Effect)

All images were collected for dried mixtures. Aged mixtures have a thick layer of coating on the quartz framework. This layer will expand even more in a hydrated state. This means that at high concentrations montmorillonite can fill the pore spaces and create microporosity network that restricts the flow. These results demonstrate how sensitive pore-space minerals with high surface-area are to the environment they exposed to.

2.3 Conclusions

Steam treatment and aging of rock mixtures with various mineralogical content was performed in laboratory conditions. Effective porosity and permeability changes associated with steam injection were determined for each case. Mineral transformation and neoformation of swelling clay was demonstrated at physicochemical conditions of hydrothermal recovery processes. Textural relationship of pore-space mineral assemblages and framework minerals were analyzed. Dominant formation damage mechanisms were determined for each case. Overall, pore-space minerals were found to be the primary reagents that interact with the injected steam after condensation. These minerals ultimately control the petrophysical properties of treated rock. The following conclusions can be drawn from the results presented in this paper:

1. Sandstone rock with calcite cementing material exposed to steam injection can be expected to experience about 5% permeability reduction and 1-2% porosity reduction. The dominant formation damage mechanism for this case was found to be associated with silica dissolution/precipitation effects.

2. Sandpacks with quartz, kaolinite, and carbonate minerals (calcite or dolomite) after steam treatment have lost 11-22% of the initial permeability and 2-7% of the initial porosity. The principal mechanism of formation damage during steam injection experiments was shown to be associated with kaolinite fines migration. Aging of these mixtures for 10 days at 400°F and 1,000 psi led to formation of swelling smectite clay (Ca montmorillonite). Mineralogy alteration was found to only be possible when produced during the reaction CO_2 can escape from the system. Mixtures with dolomite are shown to produce more montmorillonite than mixtures with calcite.

3. Mixtures of quartz with montmorillonite exposed to steam injection experienced high permeability reduction (77-84%) and moderate porosity reduction (7-8%). Formation damage was

mainly caused by clay swelling, which lead to filling of pores with montmorillonite. Microporous network that filled the pores does not affect porosity as much as it restricts the flow. Aging of montmorillonite-rich mixtures did not reveal mineral alterations but it allowed to visualize the morphological reorganization of montmorillonite and its pore bridging effect.

3. OIL RECOVERY FACTORS

This section presents experimental study that determines oil recovery factors as a function of injected pore volume (PV) of steam for sandpacks of different mineralogy. Obtained results characterize petrophysical changes caused by steam interaction with minerals in presence of oil. This data provides insights into effects of steam on minerals with different structures and properties.

3.1 Materials and Methods

3.1.1 Samples Preparation

Mixtures of minerals were prepared from the following components: quartz (SiO_2, 50-70 mesh or 210-297 μm particle size), calcite (limestone $CaCO_3$, 70 mesh or particle size smaller than 212 μm), orthoclase (potassium feldspar $KAlSi_3O_8$, 70 mesh or particle size smaller than 212 μm), kaolinite ($Al_2Si_2O_5(OH)_4$, clay size particles), smectite (Ca montmorillonite, $Ca_{0.3}Al_2Si_4O_{10}(OH)_2 \bullet n(H_2O)$, clay size particles), illite ($K_{0.7}Al_3Si_3O_{10}(OH)_2$, clay size particles).

Five mineral mixtures were prepared. These mixtures consisted of 90 wt% of quartz and 10 wt% of one of the following additional minerals: calcite, feldspar, kaolinite, montmorillonite, or illite. Mixtures contained 180 g of quartz and 20 g of additional mineral. One more sample that consisted of 100% quartz was prepared to be used as a baseline for comparison of the results. The composition of the mineral mixtures is summarized in the **Table 4**.

Table 4: Mineralogical Composition of the Sandpacks

Sample #	Minerals		Additive Mineral		Quartz		Oil Mass, g	Mass of Sandpack with Oil, g
	Additive	Base	Mass, g	wt%	Mass, g	wt%		
1	Calcite	Quartz	20	10	180	90	20	220
2	Feldspar	Quartz	20	10	180	90	20	220
3	Kaolinite	Quartz	20	10	180	90	20	220
4	Smectite	Quartz	20	10	180	90	20	220
5	Illite	Quartz	20	10	180	90	20	220
6	NA	Quartz	0	0	200	100	20	220

Minerals in a sample were mixed until the additive mineral was distributed uniformly throughout the quartz volume. Next, 10 wt% (20 g) of oil was added to each sample. The same type of oil was used for all samples. This oil has the following properties at standard conditions: viscosity – 433 cP and density – 0.957 g/cm^3. Composition of the used oil is as follows: saturates – 31 wt%, aromatics 26 – wt%, resins – 15.7 wt%, asphaltenes – 27.3 wt%. Samples were mixed again until oil was distributed uniformly throughout the volume of the mineral mixtures.

Mineral mixtures saturated with oil were tightly packed in 6-in.-long and 1.5-in. in diameter Teflon tubes. Each sample was closed with 0.5-in.-long limestone plugs. The obtained sandpack was heated with fan to shrink Teflon sleeve and then it was placed in a rubber sleeve of a coreflooding setup for further tightening of the Teflon. 400°F and overburden pressure of 800

psi were applied to finalize the mixture compaction and shrinking of Teflon. The preparation process and the obtained sandpacks are shown in **Fig. 25**.

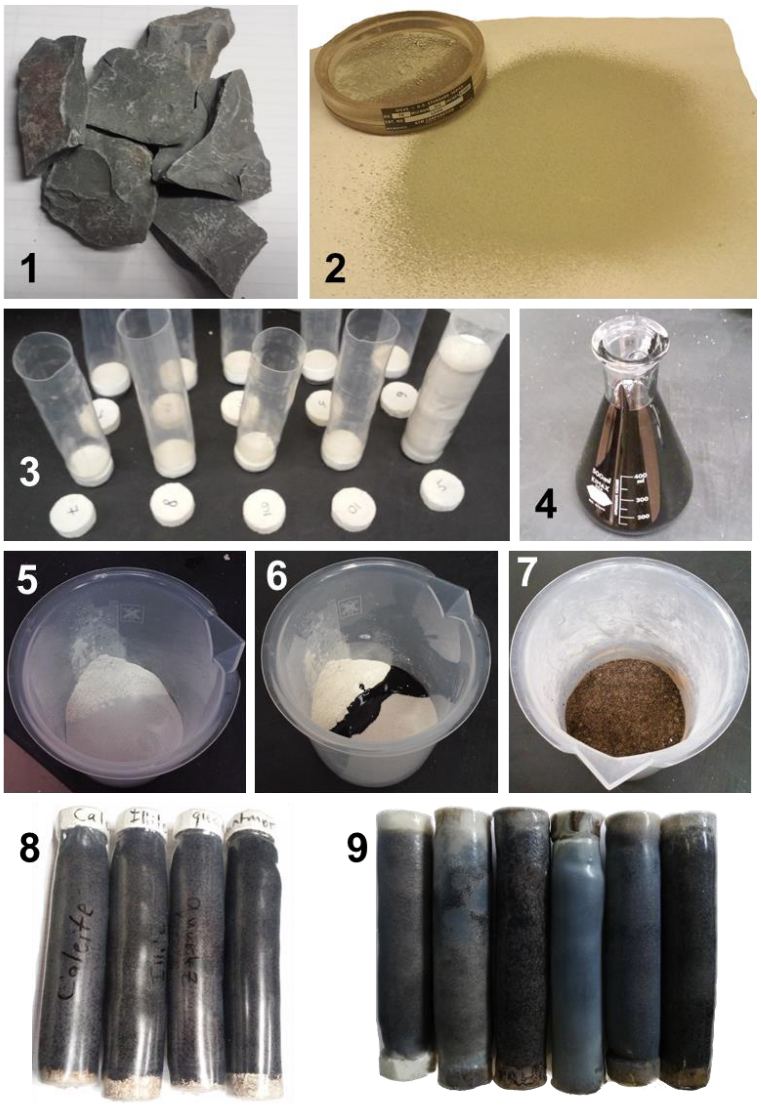

Figure 25 – Sandpack Preparation (1 – Initial Rock Samples; 2 – Crushed and Passed Through a Sieve Rock Samples; 3 – Teflon Pack and Limestone Plugs; 4 – Oil Sample; 5 – Mixture of Minerals; 6 – Mixture of Minerals with Oil Added; 7 – Oil and Minerals Mixed; 8 – Sandpacks Before Steam Injection; and 9 – Sandpacks After Steam Injection)

3.1.2 Steam Injection Experiments

The steam generator used in this study was assembled in-house. The schematics is shown in **Fig. 26**. It contains two heaters (120 V, 600 watts each) and can operate at pressures up to 3,000 psi. The controller system works with type K thermocouples to set the temperature on the heaters. Additional thermocouples were installed to monitor steam temperature at the outlet and in the insulated flowlines. The steam generator was connected to a regular coreflood setup. This configuration allows measurement of the permeability of a sandpack during the steam injection. During the steam treatment phase, deionized water (DI) was used as boiler feed water. The amount of injected steam was normalized based on the initial pore volume of each sandpack.

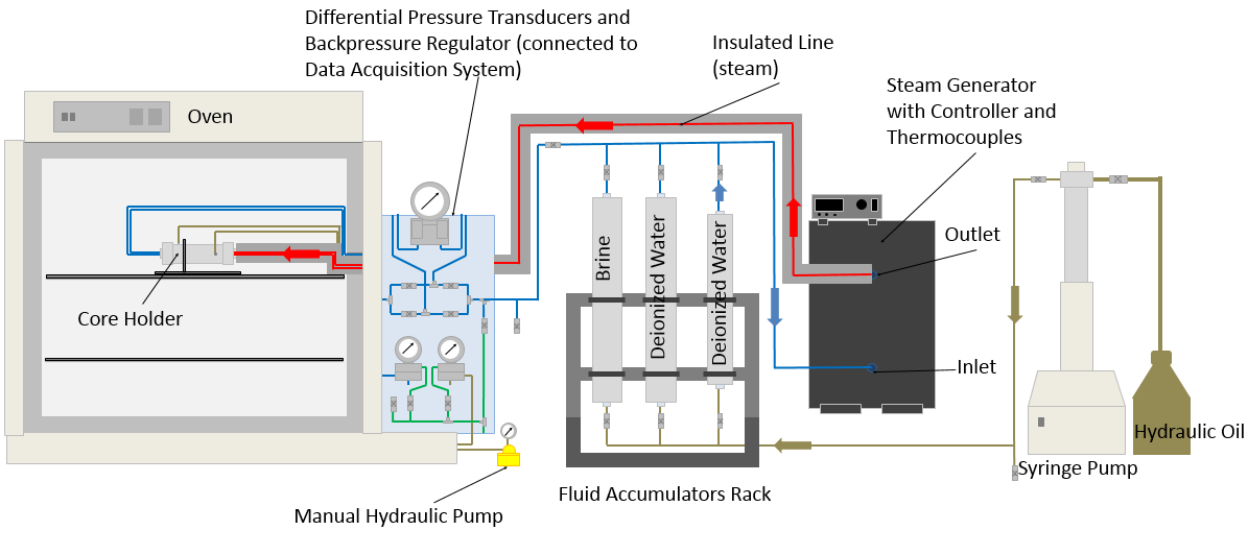

Figure 26 – Schematic of the Steamflooding Setup Used in the Study

Sandpacks were placed inside the core holder of the steamflooding setup. The overburden pressure was set at 800 psi, and the backpressure (outlet) was set at 450 psi. First, the oven was

turned on at 400°F but the steam generator was turned off. Once the temperature of the sandpack increased to 400°F then the steam generator heaters were turned on and steam was continuously generated and injected in the sandpack at a constant flow rate of 5 cm^3/min. Steam was generated from deionized water. The temperature on the heater was adjusted to keep the injected steam in superheated condition. Temperature adjustments depends on the changes in the injection pressure. Since the injection was conducted at a constant flow rate and constant outlet pressure then changes in pump injection pressure was constantly monitored. For example, if initial sandpack permeability was relatively high, then pressure drop across the sandpack was low and to inject constant flow of 5 cm^3/min pump pressure was only 500 psi, then the heater temperature would be set at only about 500°F. Once the operator observed that the injection pressure is increasing to 700 psi then the temperature was immediately set to 550°F. The temperature of the injected steam was monitored using thermocouples.

During the steam injection, hot liquid samples flowing out of the outlet of the sandpack were collected every 6 minutes. Liquid samples collected during the experiment contained aqueous and oil phases, and sometimes solid particles. After the injection of steam the heaters and the oven were turned off, and the system was cooled down for about 4 hours. Next, the sandpacks were extracted from the core holder.

3.1.3 Samples Analysis

The Teflon wrap was cut open and removed to extract the sandpack mixture for further analysis. Liquid samples are presented by mixtures of produced oil and water. Oil and aqueous phase were gravity separated and analyzed. pH was measured immediately after the steam injection experiments. Aqueous phase was diluted 250 times for chemical composition analysis

using ICP-EOS. For different minerals concentration of various elements were investigated: for calcite – Ca; for feldspar – K and Si; for kaolinite – Si and Al; for smectite – Ca, Si and Al; for illite – K, Si and Al; for quartz – Si. In cases when solids were observed in the collected liquid samples, they were separated, washed with xylene and DI, dried, and analyzed using SEM, XRF, and XRD.

To determine the oil recovery, aqueous and oil phases were separated. Oil recovered from the sandpack samples was collected in test tubes during the steam injection experiments. Mass of the oil in every test tube was determined using scale.

3.2 Results and Discussion

This section presents the results of the experiments and tests of the collected liquid (**Fig. 27**) and solid samples (**Fig. 28**).

Analysis of the produced from the sandpack outlet liquid samples is a powerful tool for identifying and interpretation of the processes that occurred inside of the sandpack during steam injection. Samples of produced mixture of oil and water for all the sandpacks are shown in **Fig. 27**. These samples were collected every 6 minutes and are shown in order. Most of the sandpacks exhibit similar progression of oil production: (1) no oil at the beginning, only aqueous phase is being produced; (2) amount of the produced oil increases; (3) decline in the oil production or plateau. **Fig. 27** is used for visualization of the amount of oil collected at each stage and comparison of these progressions for different sandpacks.

Recovered mixtures of the minerals were compared to the original mixtures. **Fig. 28** shows that sandpack mixtures after steam injection have lighter color and are less saturated with

oil. For example, for sandpacks #1, 3, 4, 5, and 6 – the color of saturated sandpack changed from black to brown; and for the sandpack #2 the color changed from black to a much lighter color.

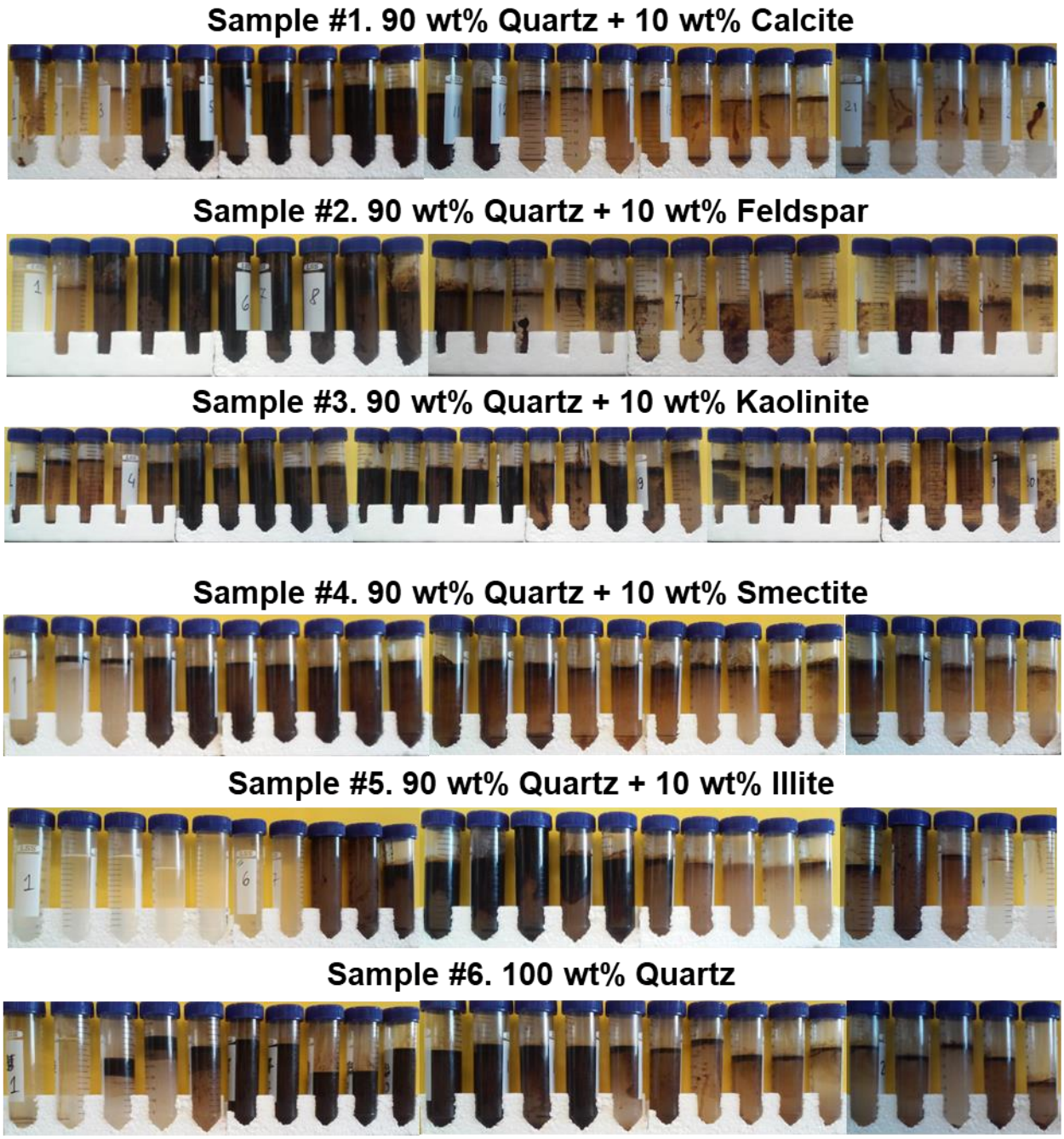

Figure 27 – Liquid Samples Collected for Sandpacks #1 to 6

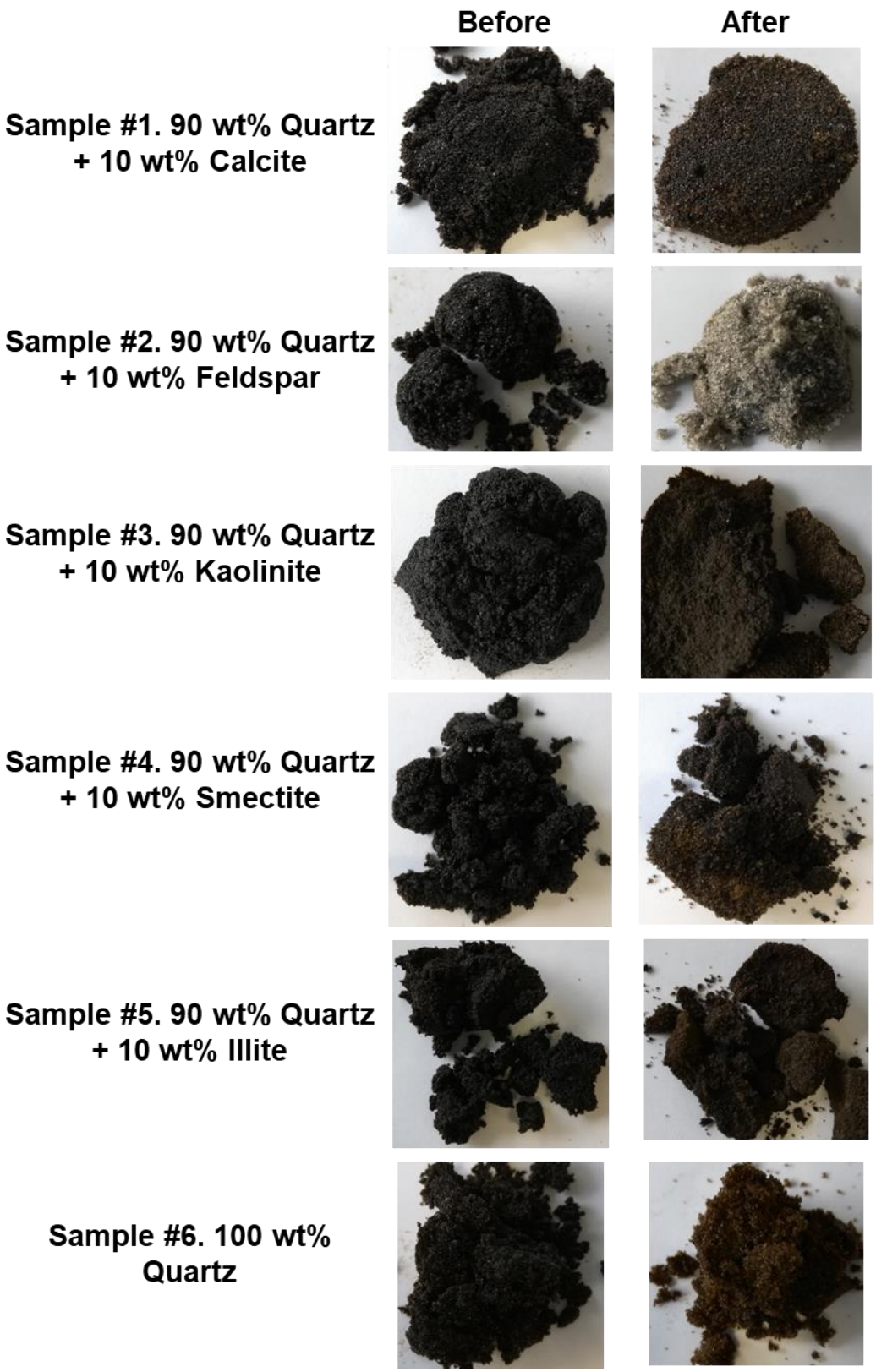

Figure 28 – Sandpack Mixtures Before and After Steam Injection Treatment

Change of the pressure drop across the sandpack during steam injection is shown in **Fig. 29** and **30**. It can be seen there that quartz sandpack maintains almost the same pressure drop with very minor growth over the time. Calcite sandpack shows more significant growth with some fluctuations during the injection. Feldspar sandpack experienced increase in pressure drop during injection of the first 12 PV and later stabilized at about 19 psi. These three sandpacks had high initial and final permeability. Kaolinite sandpack had slightly higher increase in pressure drawdown and stabilized at about 34 psi. Sandpacks of smectite and illite exhibited the most dramatic changes in the pressure drawdown stabilizing at about 150 and 410 psi, respectively. Increase in pressure drop in smectite sandpack happened during the injection of the first PV of steam, and for illite sandpack the pressure drop increase during injection of the fifth PV of steam.

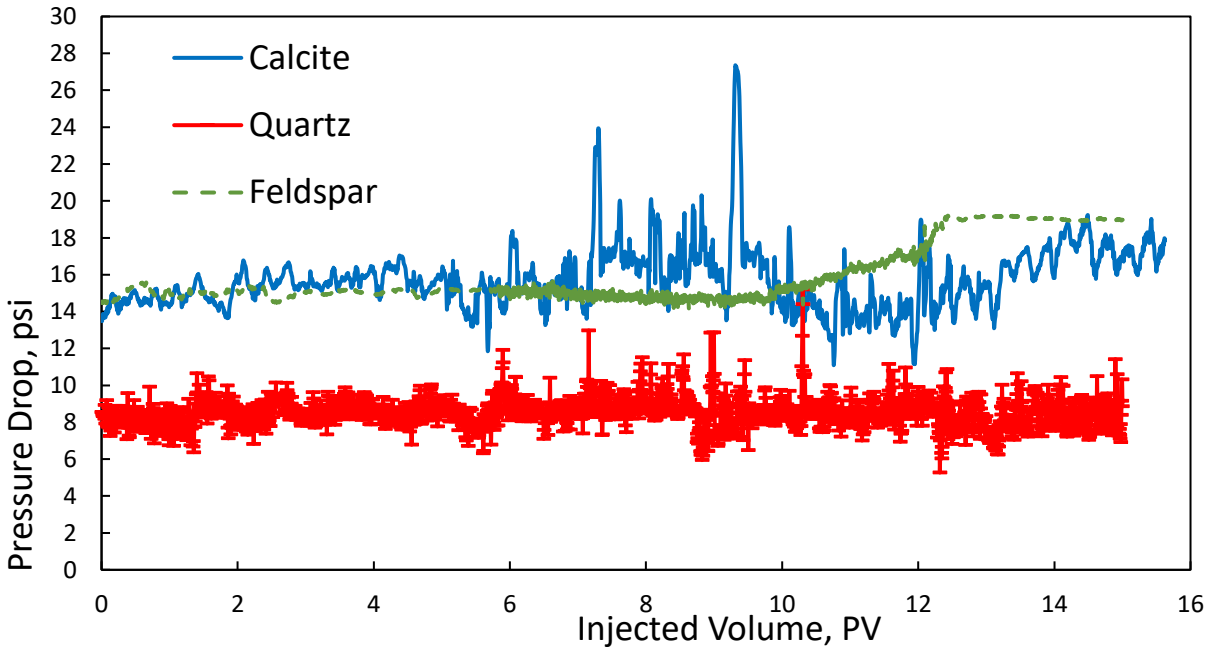

Figure 29 – Pressure Drop Across the Sandpacks #1 – 3

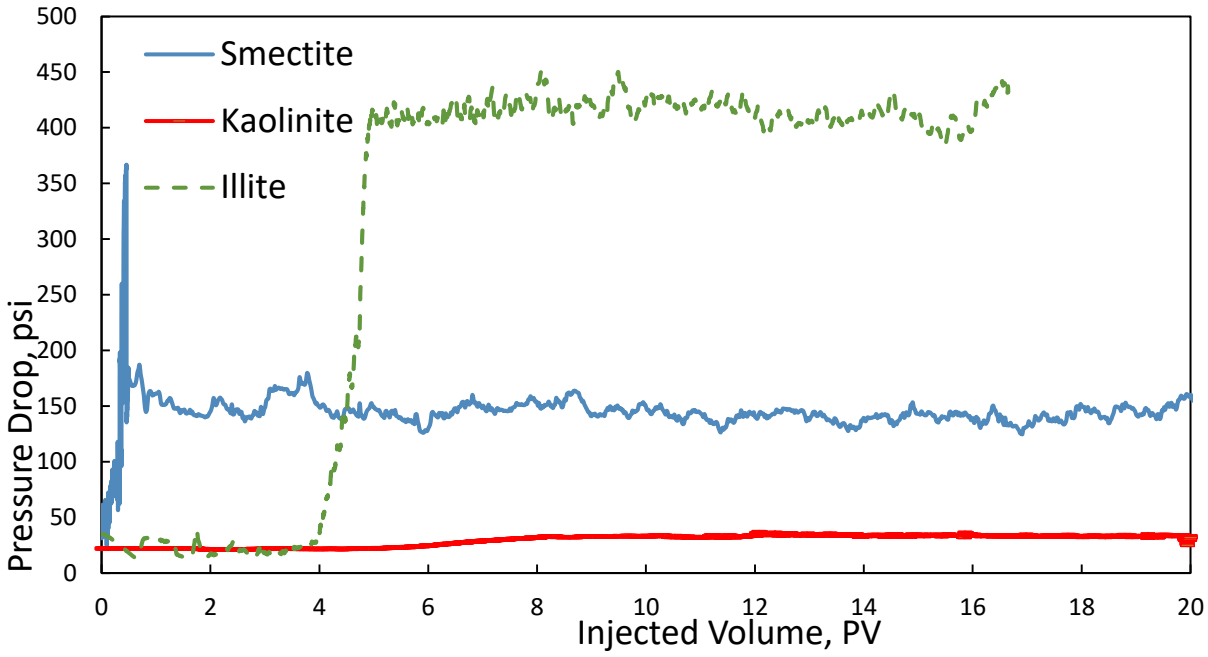

Figure 30 – Pressure Drop Across the Sandpacks #4 – 6

3.2.1 Oil Recovery

Cumulative oil recovery as a function of injected PV is presented in **Fig. 31**. Oil recovery is presented as a wt% of 20 g which was the original amount of oil added to each sandpack. During the experiment steam injection and production of liquid samples continued until no more oil was coming out from the outlet of the sandpack. For some samples, cumulative production curve becomes flat after injection of 15 PV, and for other samples production continues up to 21 PV. Vertical line was added to the **Fig. 31** at 15 PV for comparison of the recovery at 15 PV.

Based on the obtained results the sandpack samples can be roughly divided in two groups. Sandpacks that contain clay minerals (kaolinite, smectite, and illite) tend to have significantly smaller oil recovered than samples that do not contain clay minerals (sandpacks with calcite, feldspar and quartz). Sandpacks with clays also tend to reach flattening of the

cumulative oil production after injection of more pore volumes than samples without clay minerals. It is common for all the samples to have a slightly delayed production profile due to the design of the experimental setup. For many samples oil starts to appear in the produced water (condensated steam) after injection of 0.5 or 1 PV. This might not be the best representation of the timeline for a real reservoir performance, but the obtained trends and their position relative to each other provide insights into steam-minerals interaction and thermal oil recovery.

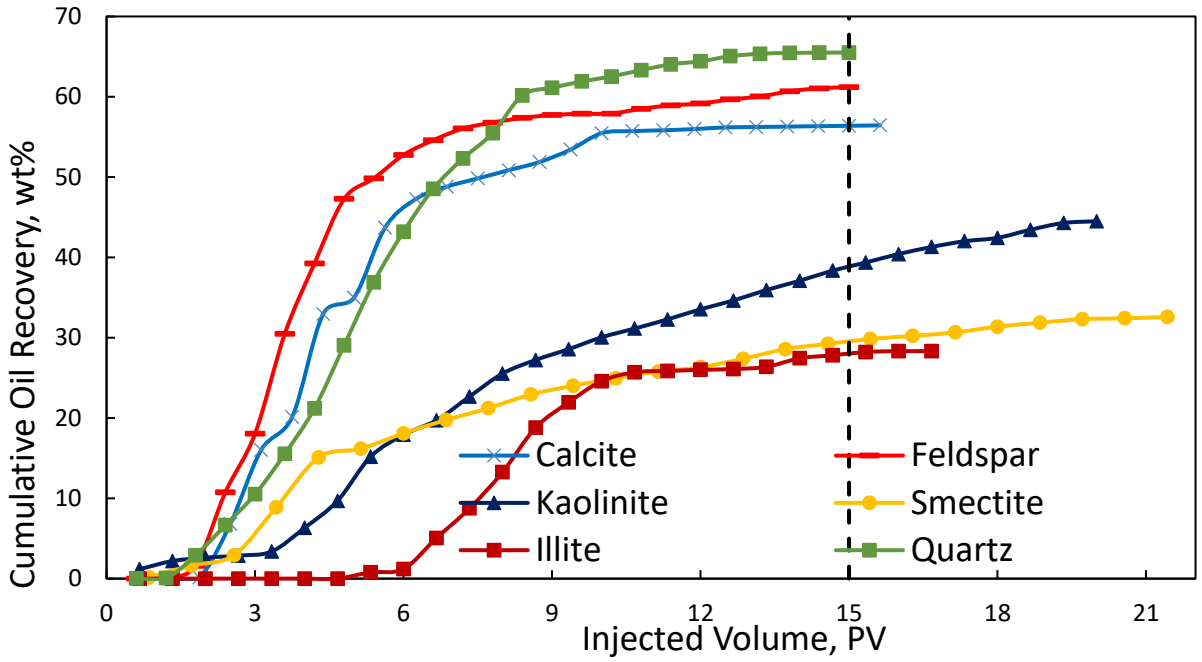

Figure 31 – Oil Recovery as a Function of Cumulative Injected Volume for the Sandpacks #1 – 6

It is important to underline that feldspar and calcite that were added to sandpacks have virtually the same particle size distribution as the used clay minerals (50-70 mesh size).

However, the sandpacks with calcite and feldspar tend to be similar in results to the clean quartz case. This means that not only the particles size, but the structure and reactive nature of clay minerals play significant role in the production from the sandpacks.

Sandpack with 100% of quartz was used as a baseline case. For this sample oil production starts at about 1 PV and grows fast until reaching 60 wt% oil recovery at about 8.4 PV. Then production slows down and reaches the final recovery of about 65 wt% at 15 PV. Interestingly, in the last plateau region production almost stopped – only about 1% was added to the recovery during the injection of the last 5 PV.

Sandpack with 90 wt% quartz and 10 wt% calcite exhibits similar performance, but oil production starts later (at about 2 PV) and it reaches the slowdown sooner (47 wt% recovery at about 6.3 PV). The cumulative production curve is not as smooth as the baseline case but it reaches similar result – 56 wt% recovery at 15 PV.

Sandpack with 90 wt% quartz and 10 wt% feldspar is the last sample in the group of sandpacks without clay minerals. This sample presents similar smooth pattern with delayed production (1 PV) but it produces slightly faster than the previous two cases. Within injection of 5.5 PV recovery reached more than 50 wt%. The plateau is located between calcite and quartz cases and the final oil recovery at 15 PV is 61 wt%.

Among sandpacks with clays, kaolinite sample has reached the highest oil recovery. This sandpack showed almost uniform oil recovery curve for 20 PV and reached the final recovery of 44.5 wt%. However, at 15 PV kaolinite-rich sandpack produced only 39 wt%.

Sandpack with 90 wt% quartz and 10 wt% smectite demonstrated even more prolonged production. It was producing oil for more than 21 PV and reached the final oil recovery of 33 wt%. The recovery at 15 PV was determined to be 29 wt%. Smectite-rich sandpack exhibited

fast growth in production between 2.5 and 4 PV of injected steam and was slowly declining after it.

The lowest oil recovery was registered for the sandpack with 90 wt% quartz and 10 wt% illite. The final oil recovery for this sample was found to be 28 wt% after almost 17 PV, and the recovery at 15 PV was about 28 wt%. Interestingly, illite sandpack almost did not have oil produced after almost 6 PV and then oil recovery accumulated up to 25 wt% during the injection of the next 4 PV.

3.2.2 Formation Damage Mechanisms

3.2.2.1 Baseline Case – Quartz

This sandpack was prepared as a baseline case. It consists of quartz and does not contain any additive minerals. This sandpack was the most unaltered and it demonstrated the least changes in petrophysical properties.

At normal conditions quartz is inert toward aqueous phase. However, at high temperatures steam is known to interact with quartz and cause quartz dissolution in condensated vapor phase. At pH, higher than 9 the solubility of both crystalline and amorphous silica is increasing significantly. The dominant formation damage mechanisms associated with quartz is dissolution and reprecipitation in regions with lower temperature. Sometimes rock softening in presence of steam also contributes to changes in petrophysical properties of sand.

For the given sandpack, quartz dissolution effect was found to be minimal. Concentration of Si^{4+} in the produced aqueous phase was insignificant and fluctuated around 10 ppm (**Fig. 32**). pH of these samples was slightly below 7 (**Fig. 33**). Both initial and final permeability of this

sandpack were high and did not have significant change during the steam injection – 195 and 187 mD, respectively.

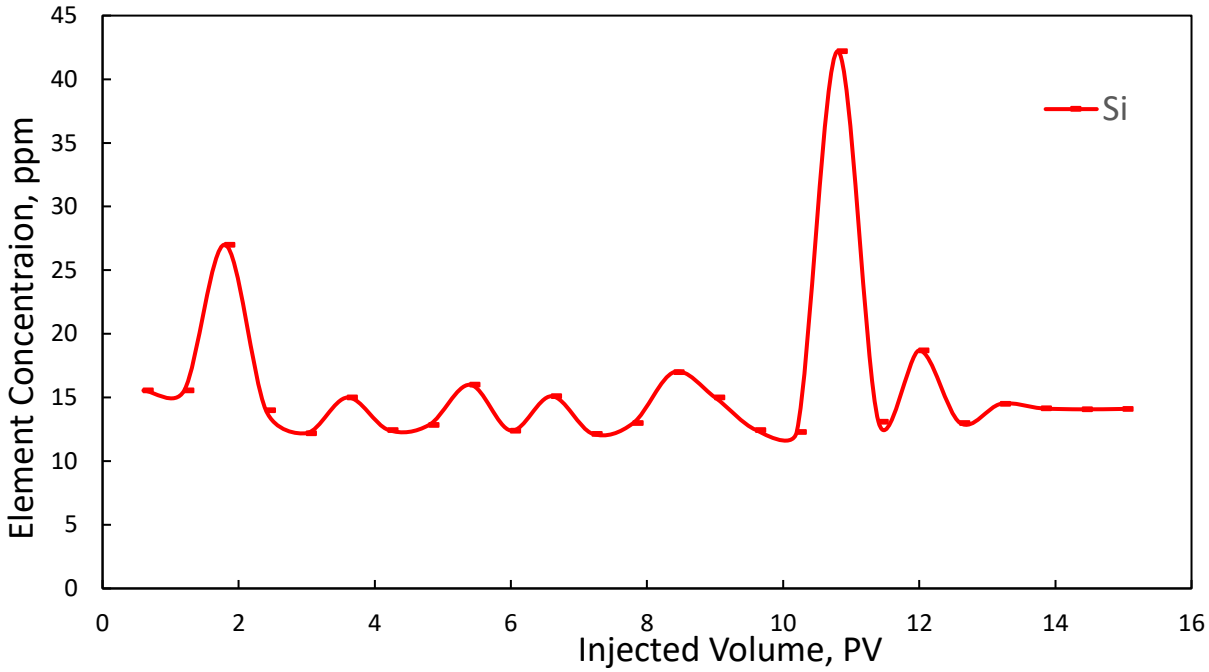

Figure 32 – Concentration of Si^{4+} in the Liquid Samples Collected During Injection of Steam into a Sandpack with Quartz

3.2.2.2 Calcite Case

Heating of calcium carbonate may lead to thermal decomposition which causes formation of calcium oxide. Dissolution of calcium oxide in water produces calcium hydroxide. Low solubility $Ca(OH)_2$ can precipitate in the sandpack.

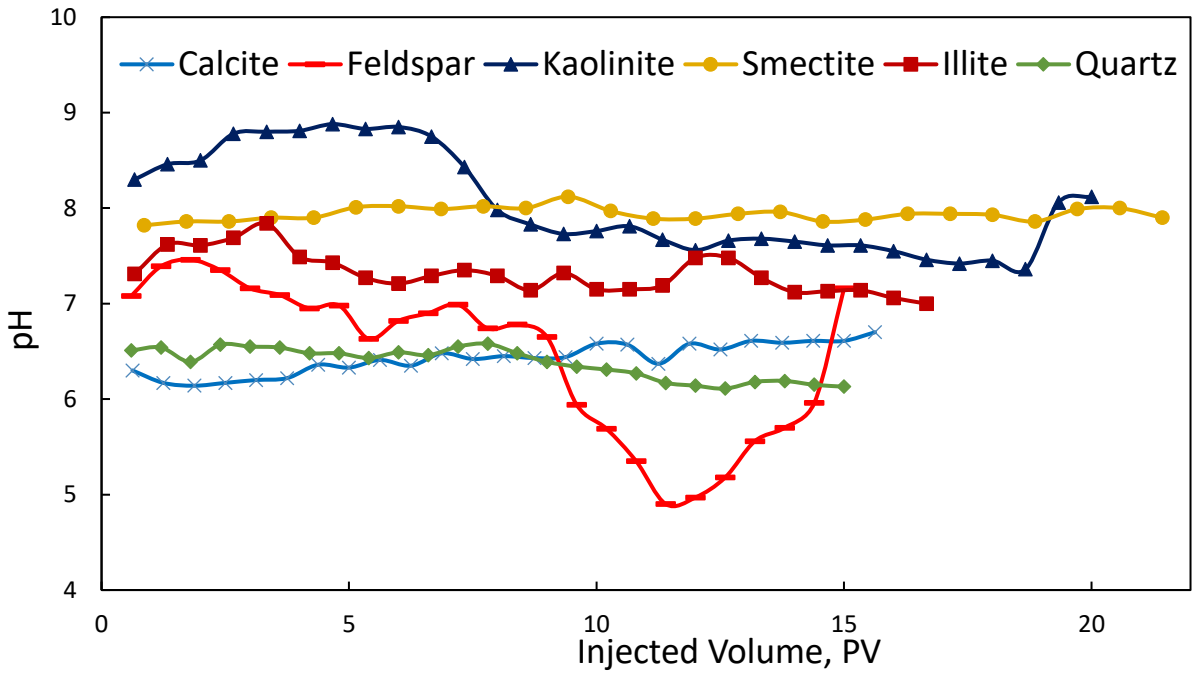

Figure 33 – pH of the Aqueous Phase of the Samples Collected During Injection of Steam the Sandpacks #1 to 6

Analysis of the collected aqueous phase showed that concentration of calcium ion declined with time (**Fig. 34**). This is an indication of precipitation of calcium-based material. It can be argued that presence of magnesite or dolomite may also lead to formation of magnesium hydroxide. Jain et al. (2015) reported steam-related precipitation mechanism for $Mg(OH)_2$ and $Sr(OH)_2$.

Precipitation of calcium hydroxide can be damaging for petrophysical properties of the sample. However, this effect was not very significant for the oil recovery in this study as it was discussed above. In comparison to baseline case and cases with high clay calcite-rich sandpack has relatively high oil recovery factor. Permeability of the sandpack showed a gradual decline

from 107 to about 93 mD. This means that discussed formation damage mechanism did not have dramatic effect on the result of the thermal recovery process. This can be explained by the fact that steam was generated from deionized water with neutral pH. pH of the produced aqueous phase slightly increased with time from about 7.4 to 7.9 (**Fig. 33**). High pH feed water would contribute hydroxyl ions (OH^-) which could have led to precipitation of more calcium hydroxide. Many divalent cations that may be present in the aqueous phase can form hydroxides with very low solubility. These precipitations can be much more detrimental to permeability of the sandpack. Another component that forms during thermal decomposition of calcium carbonate is acidic gas carbon dioxide. This product can dissolve in water and contribute to reduction of pH which would balance the precipitation. Reaction of calcite with steam and steam condensate in presence of formation fluids is a complex problem and further investigation is needed.

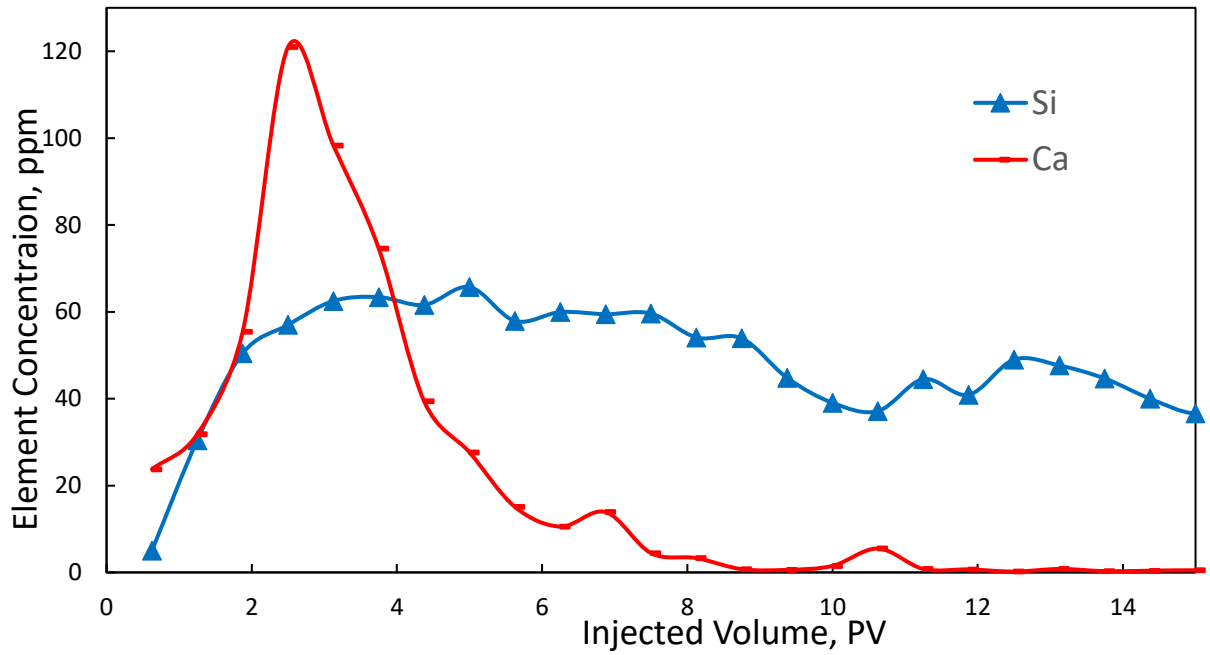

Figure 34 – Concentrations of Ca^{2+} and Si^{4+} in the Liquid Samples Collected During Injection of Steam into the Sandpack with Calcite

3.2.2.3 Feldspar Case

This sandpack was used to mimic quartz matrix mixed with fine non-clay aluminosilicate mineral particles. Numerous studies reported that feldspars have the potential to cause formation damage when subjected to elevated temperature. One of the dominant mechanisms is associated with fines release. Production of fines can be caused by mineral dissolution or structural breakdown.

ICP results (**Fig. 35**) supports this theory. Concentrations of both Si^{4+} and K^{+} have growing trends and reach significant values. Additionally, fine particles were present in the liquid samples produced from this sandpack (**Fig. 36**). They were separated by filtration, soaked and washed with toluene and DI to remove the organic matter, and analyzed with XRF and XRD.

Based on the 2 to 1 ratio of O^{2-} to Si^{4+} and broad diffused XRD peak – it can be concluded that this material is amorphous silica. Analysis has shown that these particles were found to migrate in both oil and aqueous phases. pH changes between 7.5 and 5. At the beginning it decreases and then it increases back to the original value.

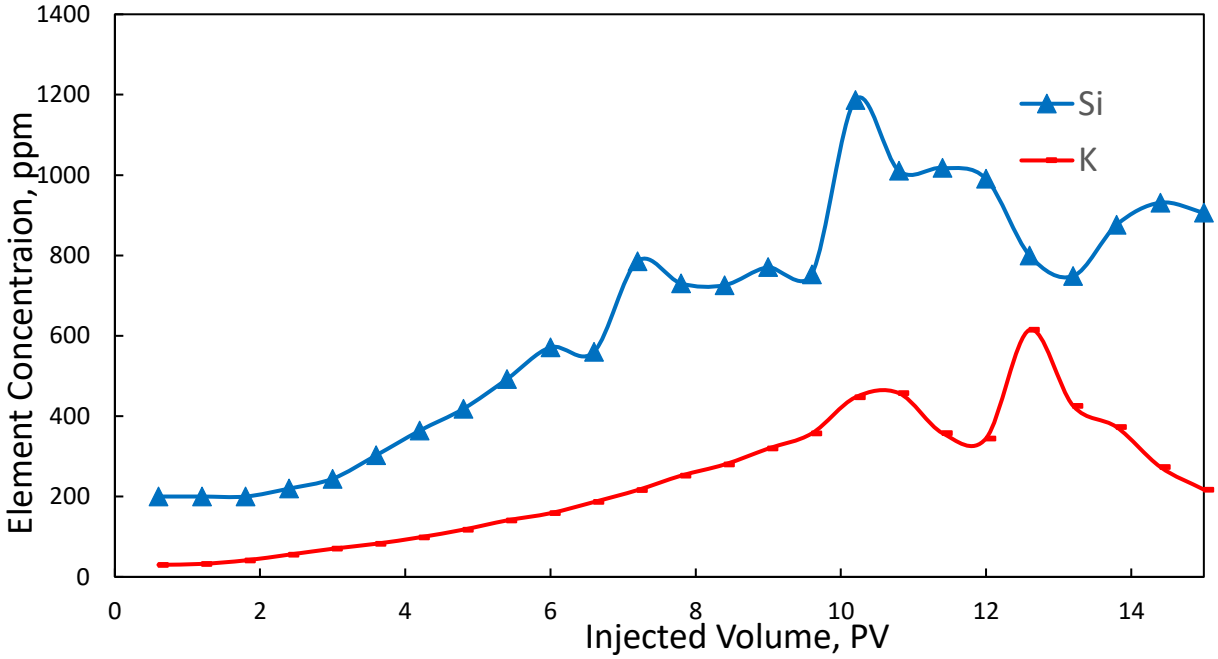

Figure 35 – Concentrations of K^{+} and Si^{4+} in the Liquid Samples Collected During Injection of Steam into the Sandpack with Feldspar

Permeability reduction (from 110 mD initially) was happening uniformly during injection of the 12 PV and then it remained at about 88 mD. Both initial and final permeabilities are relatively high for this sandpack and final oil recovery is very close to baseline case as discussed previously. Therefore, it can be concluded that fine aluminosilicate particles of potassium

feldspar, while having the effect on petrophysical properties of the sandpack, do not have critical damaging effect on oil recovery.

3.2.2.4 Kaolinite Case

This sandpack was used for investigation of steam effect on mixture of quartz and non-swelling clay mineral. Kaolinite is often associated with formation damage due to fines migration and plugging of pore throats. In changing conditions plate-like particles of kaolinite often detach from the matrix rock surface and move in the pore space. It may happen due to different mechanisms, such as wettability change, repulsion/attraction forces imbalance, clay dispersion, clay release due to excessive drag force, etc. Another damaging mechanism is alteration of kaolinite to other clay types, for example smectites.

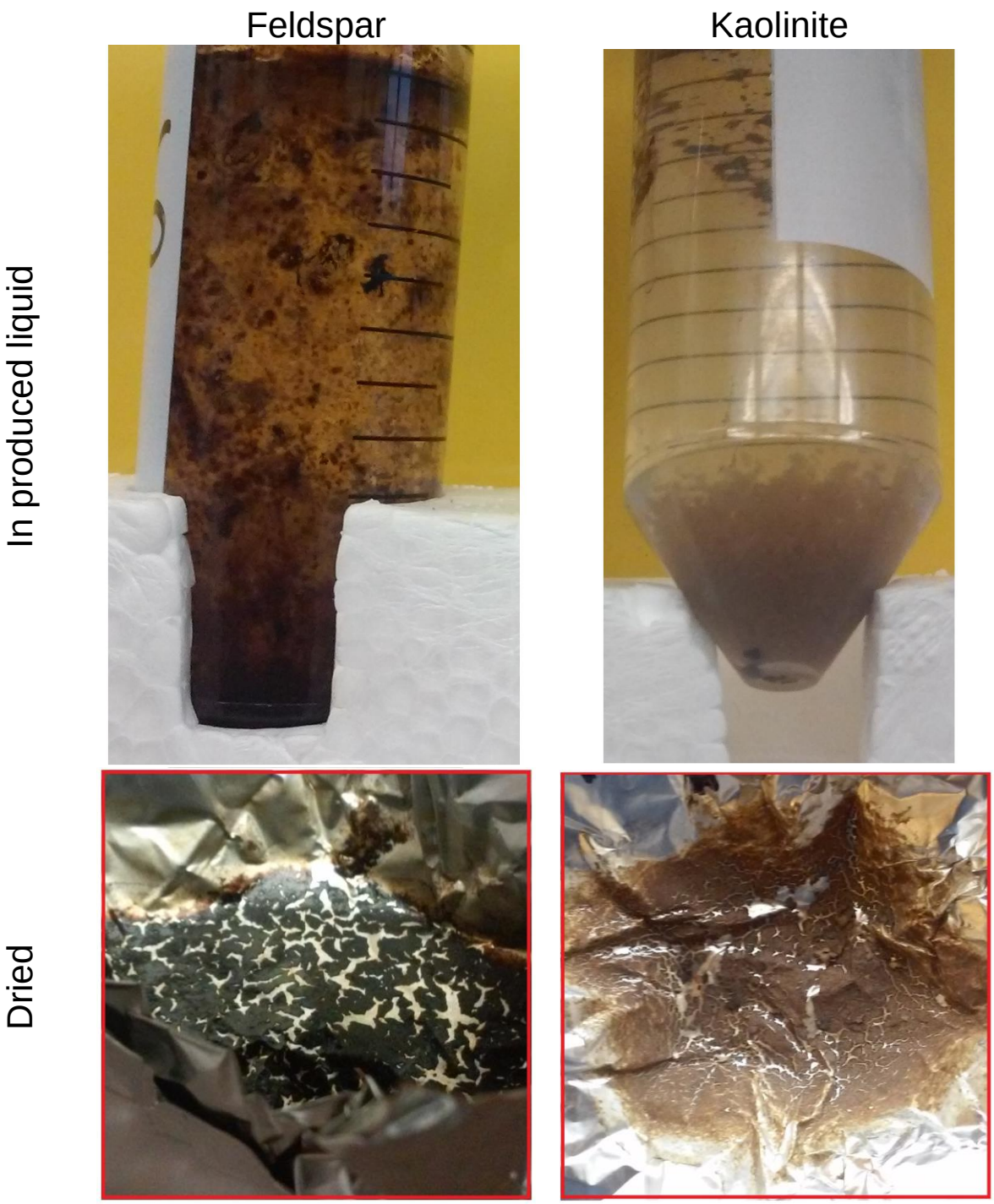

Figure 36 – Solid Materials Found in the Liquid Samples from Feldspar (left) and Kaolinite (Right) Sandpacks

ICP results detected significant growth of Si^{4+} concentration from 0 to almost 2,800 ppm (**Fig. 37**). Permeability reduction happens slowly from 74 to 49 mD during the injection of the first 8 PV and then stays at the same level of about 49 mD. Solid particles were found in the produced aqueous phase (**Fig. 36**).

It can be explained by kaolinite fines mobilization by steam and injected vapor condensate. In fresh aqueous phase the double layer extends away from the clay particles which may lead to the dispersion of clay particles. pH of the produced samples changed from 7.5 to 8.8. High pH contributes to deflocculation of kaolinite. XRD results showed that for this sandpack kaolinite did not alter to montmorillonite or other minerals.

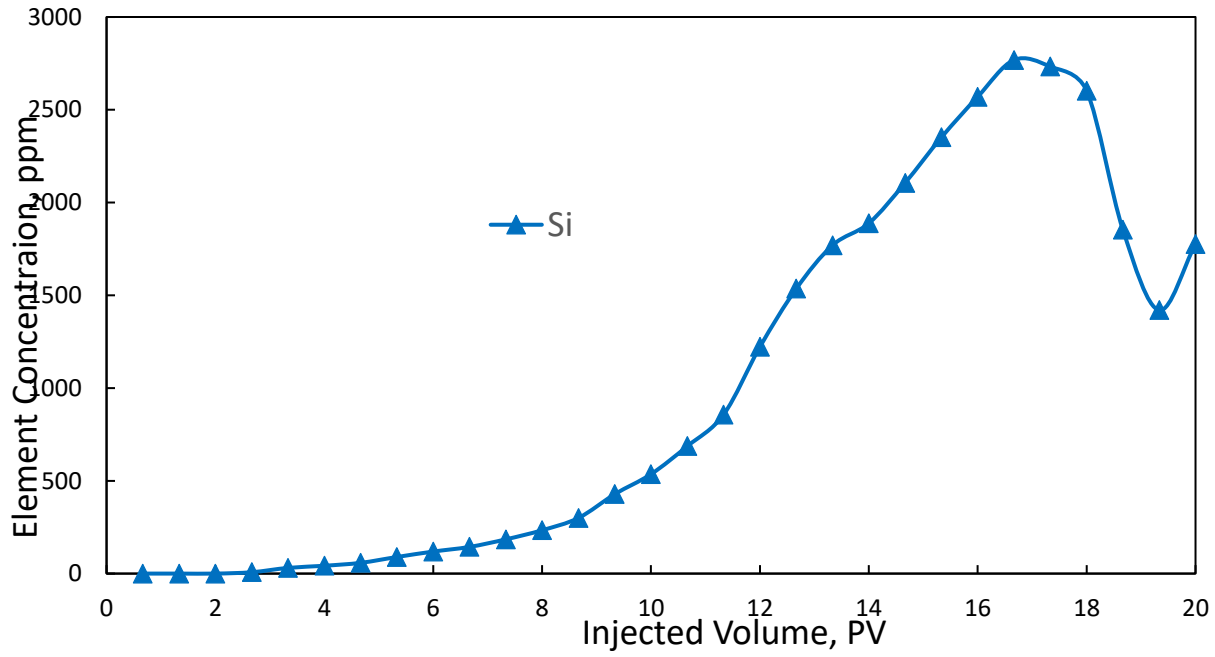

Figure 37 – Concentration of Si^{4+} in the Liquid Samples from the Sandpack with Kaolinite

These effects lead to the fact that for the given kaolinite-rich sandpack the oil recovery was significantly lower (39 wt%) than for the quartz baseline case (65 wt%).

3.2.2.5 Smectite Case

This sandpack was used for investigation of steam effect on mixture of quartz and swelling clay mineral. Montmorillonite is prone to swelling and dispersion when contacted by low-salinity water. At the same time, exposure of smectite to high temperature steam may lead to shrinking due to the loss of adsorbed and structural water. Reactive nature of both steam and montmorillonite may also lead to mineral reactions.

pH of these samples was found to stay at about 7.9. ICP analysis of the produced water showed fluctuation in Si^{4+} and Al^{3+} concentrations up to 300 ppm, while Ca^{2+} concertation remained almost constant at about 3 ppm (**Fig. 38**). This confirms slight mineral dissolution and clay structure damage caused by steam. At the same time permeability dropped from about 52 to 11 mD during injection of the first 0.5 PV. This quick reduction happened due to clay hydration swelling after exposure to steam and condensated aqueous phase. Swelling of smectites is associated with extensive growth and sealing or bridging of the pore throats. Analysis of the recovered sand mixture revealed that smectite stuck together and formed dense agglomerates in the first 2 inches of the sandpack. This is the zone where steam tend to condensate during the propagation at the beginning of the steam injection. These results mean that montmorillonite hydration effect dominated over the heating/dehydration effect of steam on the clay. This effect lead to reduced oil recovery from the smectite-rich sandpack. At 15 PV it has produced about 29 wt% of oil which is 10% less than kaolinite-rich sandpack.

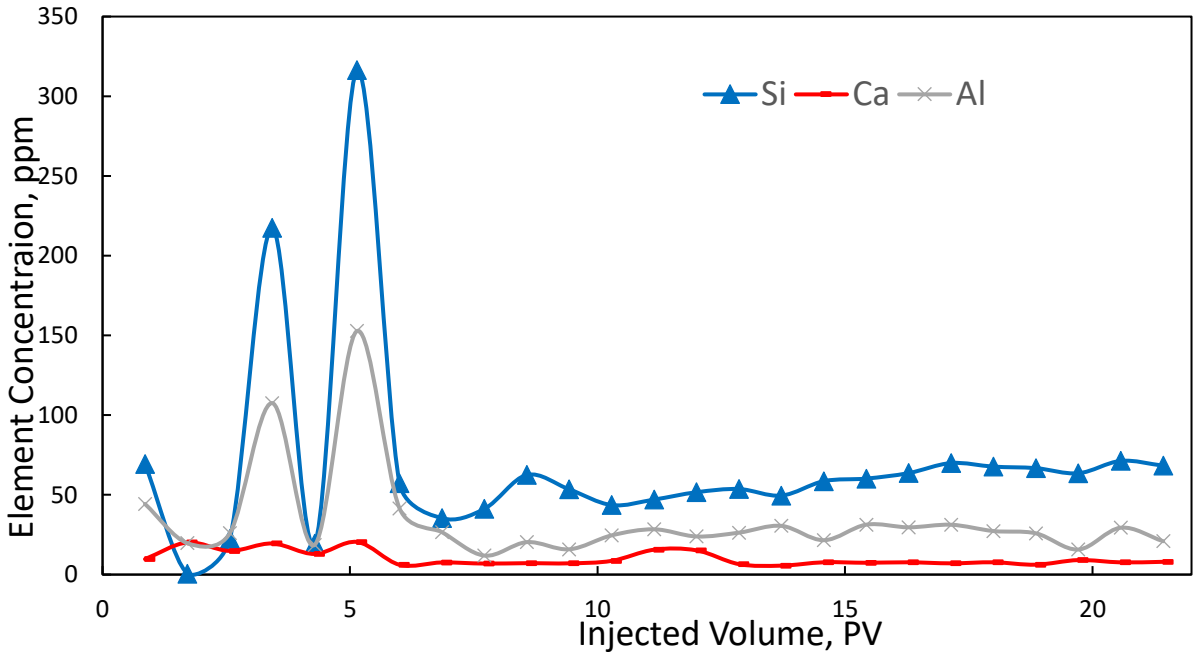

Figure 38 – Concentrations of Al^{3+}, Ca^{2+}, and Si^{4+} in the Liquid Samples from the Sandpack with Smectite

3.2.2.6 Illite Case

Illite is a clay mineral that is known for its high reactive area and needle-like morphology. There are many mechanisms that can lead to formation damage associated with illite. Fibrous illite may break during production, migrate and block pore throats.

Analysis of the chemical content of the produced aqueous phase revealed that concentration of Si^{4+} had a fast increase and drop at before injection of about 4 PV (**Fig. 39**). At the same time concentration of K^{+} started increasing after injection of about 5 PV and aluminum concentration remained at about same level for all the samples. This sharp decline in Si^{4+} concertation and continuous release of K^{+} mean that illite structure undergo some breakdown and dissolution and that some of the silicon-based material precipitated in the sandpack. There

were no solids found in the produced liquid samples. XRD and XRF analysis of the material collected from the sandpack revealed that this was amorphous silica (**Fig. 40**). XRD analysis of the sandpack did not reveal mineral alteration of illite into other crystalline material or minerals. pH values of these samples for the illite-rich sandpack fluctuate around 7.3.

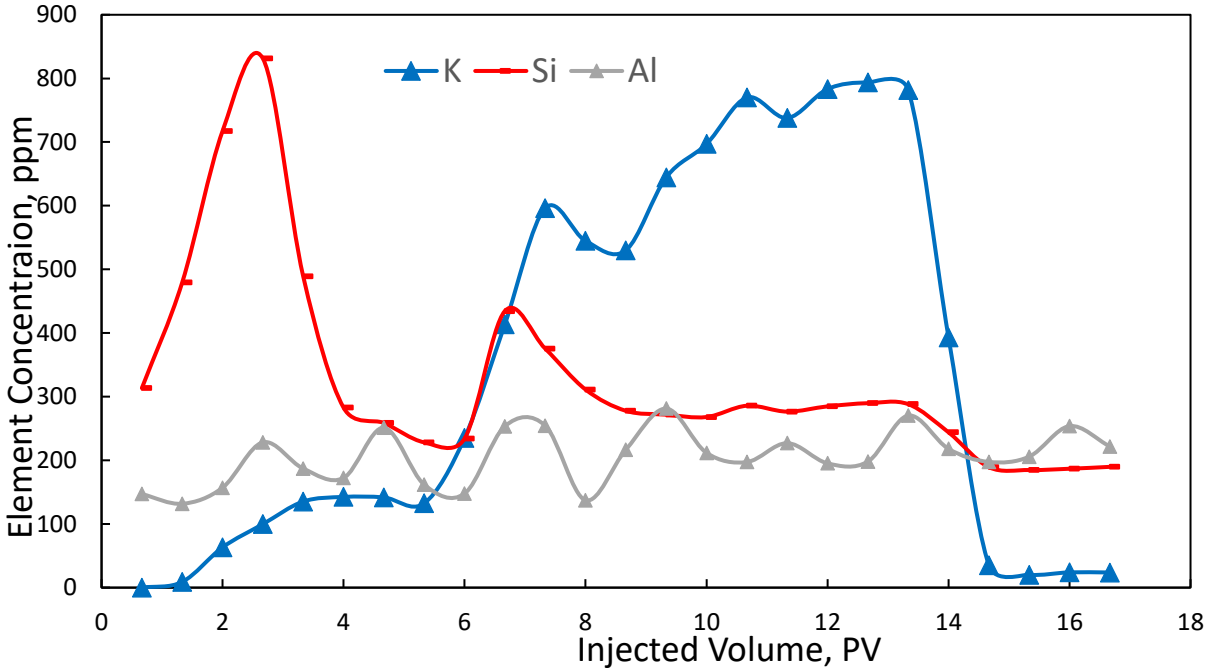

Figure 39 – Concentrations of Al^{3+}, K^{+}, and Si^{4+} in the Liquid Samples from the Sandpack with Illite

These effects had significant effect on petrophysical properties of the sandpack. Permeability decreased sharply from 47 to 4 mD during injection of the 5th PV. Also, illite-rich sandpack demonstrated the lowest oil recovery among all the sandpacks.

Figure 40 – Solid Precipitation Material Collected from the Sandpack with Illite

3.3 Conclusions

The following conclusions can be drawn from the results presented in this section:

1. Degree of interaction of steam with different minerals depends more on the nature of the mineral than on the particle size and reactive surface area. In this study, sandpacks with clay minerals demonstrated significantly lower oil recovery than sandpacks with non-clay minerals of the same particle size.

2. Aqueous phase samples produced from clay-rich sandpacks tend to have higher pH than samples produced from samples without clay minerals.

3. Sandpack with 100% quartz delivered 65 wt% final oil recovery after injection of 15 PV. Dissolution of quartz may happen during steam injection but it does not have significant effect on the reservoir permeability.

4. Sandpack with 90 wt% quartz and 10 wt% calcite managed to produce 56 wt% final oil recovery during injection of 15 PV. The most dominant formation damage mechanism for this sandpack is precipitation of Ca^{2+}-based material.

5. Sandpack with 90 wt% quartz and 10 wt% feldspar produced 61 wt% final oil recovery during injection of 15 PV. The main formation damage associated with structural breakdown and fines release. Fine particles of feldspar are transported in both organic and aqueous phases.

6. Sandpack with 90 wt% quartz and 10 wt% kaolinite had extended production up to 20 PV and the final oil recovery was found to be 39 wt%. At 15 PV, this sample produced about 15 wt% of oil. The main formation damage mechanism for kaolinite-rich sandpack is fines migration. It was also determined that kaolinite particles are mobilized and migrate within the aqueous phase.

7. Sandpack with 90 wt% quartz and 10 wt% smectite had shown extended oil production which reached about 32 wt% at 21 PV; and almost 16 wt% at 15 PV. In presence of steam smectite's hydration and swelling effects dominate the thermal dehydration and shrinking effects.

8. Sandpack with 90 wt% quartz and 10 wt% illite had shown the smallest delayed oil production which reached about 28 wt% after injection of 16 PV; and 28 wt% at 15 PV. The reason of the small oil production for this sandpack is precipitation of the amorphous silica inside the sandpack.

9. No mineral transformation was observed for any of the tested sandpacks.

Based on the obtained results and observations it is recommended to pay special attention to steam injection in clay-rich formations. Analysis of the aqueous phase (chemical content and pH) must be used to interpret interactions in steam-formation system. Coreflooding and analysis of the rock samples must be used in identification and characterization of the formation damage.

4. TREATMENT OF SCALE AND SOLUBILITY TESTS

This section presents experimental analysis of real samples of scale collected from injector wells and from ESP. These samples formed in the reservoir that is being produced using SAGD technique.

4.1 Solubility of Scale from Injection Wells

4.1.1 XRD Analysis

Scale samples collected from injector wells were analyzed using XRD to determine the mineralogical content. XRD results for sample #1 were collected for bulk sample (850-micron fraction, **Fig. 41**) and for crushed powder (300-micron fraction) sample (**Fig. 42**).

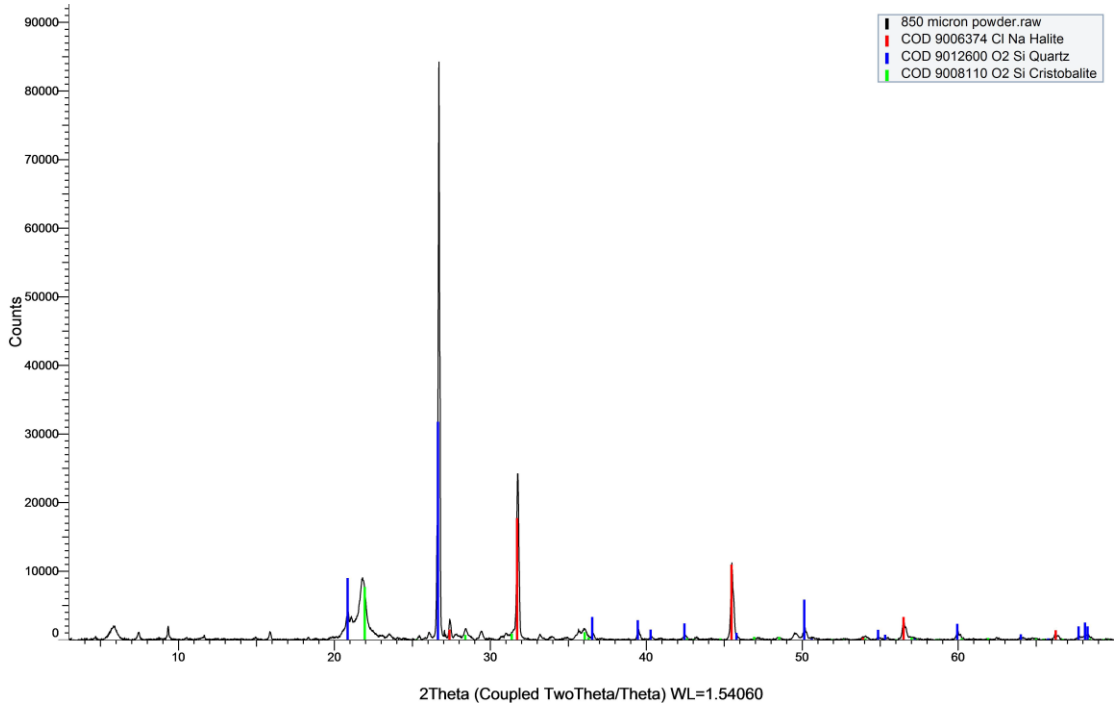

Figure 41 – XRD Result for Bulk Untreated Scale Sample

Bulk result identified presence of quartz, cristobalite, and halite. Analysis of the crushed sample allowed better precision and identified additionally the following minerals: calcite, mica, and muscovite.

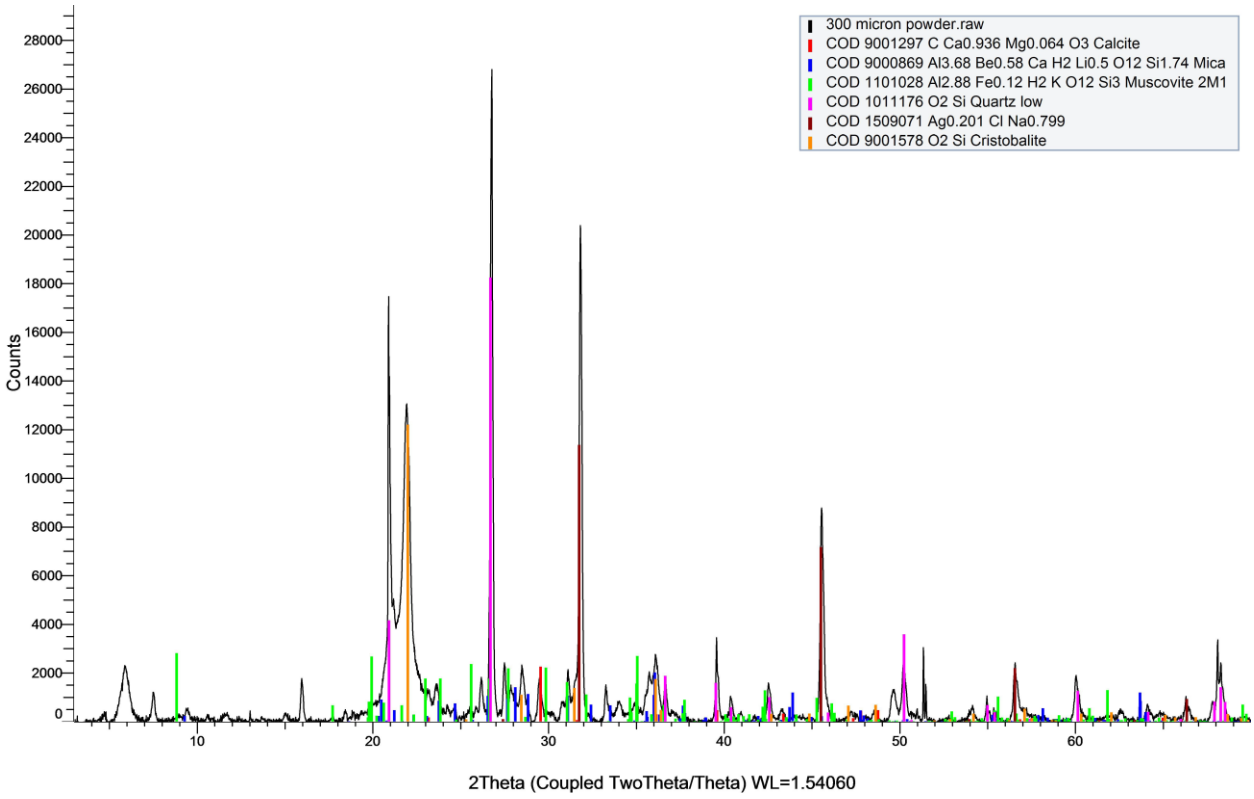

Figure 42 – XRD Result for Powdered Scale Sample

4.1.2 SEM Analysis

Scale samples collected from injector wells were analyzed using SEM to study the morphology and texture of the material, and to identify elemental composition of the scale. SEM

images and elemental composition of the 212-micron, 850-micron and scale chips samples are shown in **Figs. 43** – **47**.

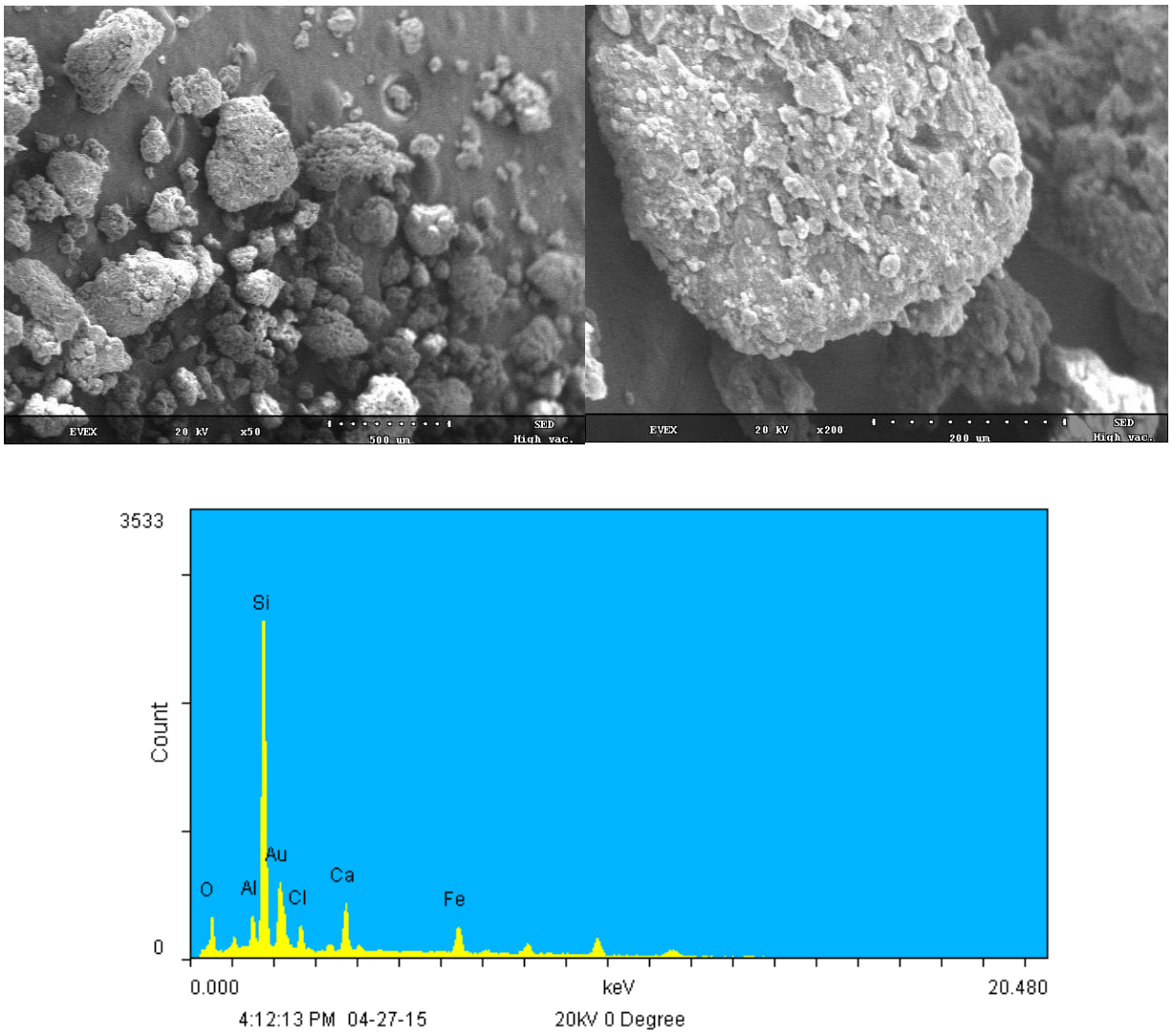

Figure 43 – SEM Results for 212-Micron Scale Sample

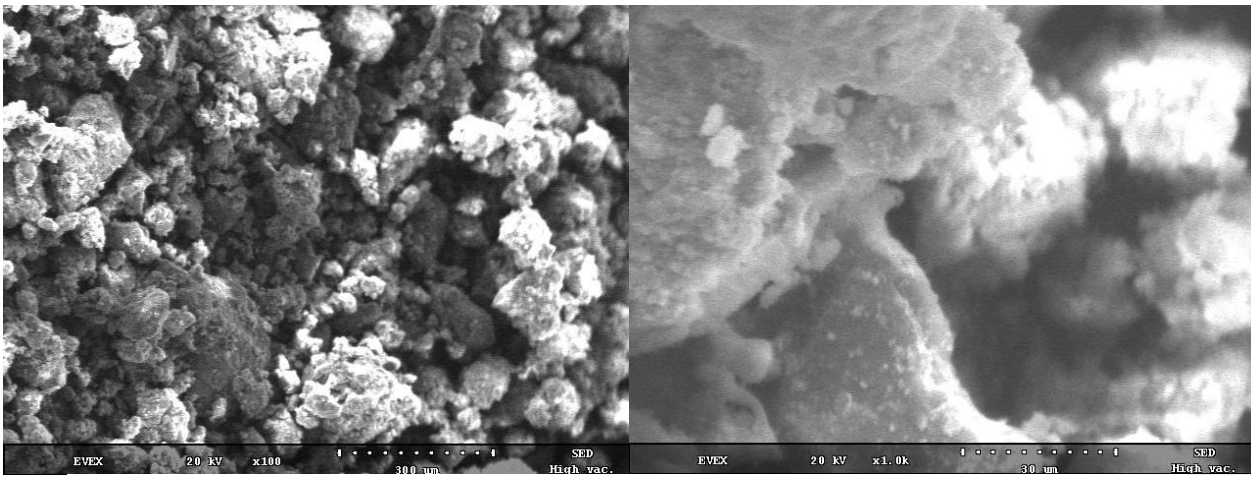

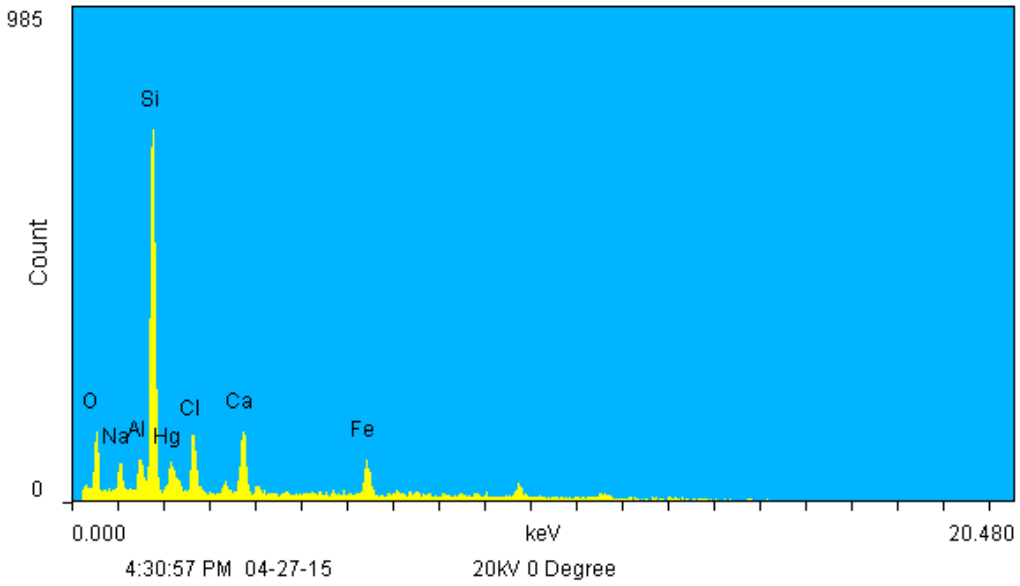

Figure 44 – SEM Results for 850-Micron Scale Sample

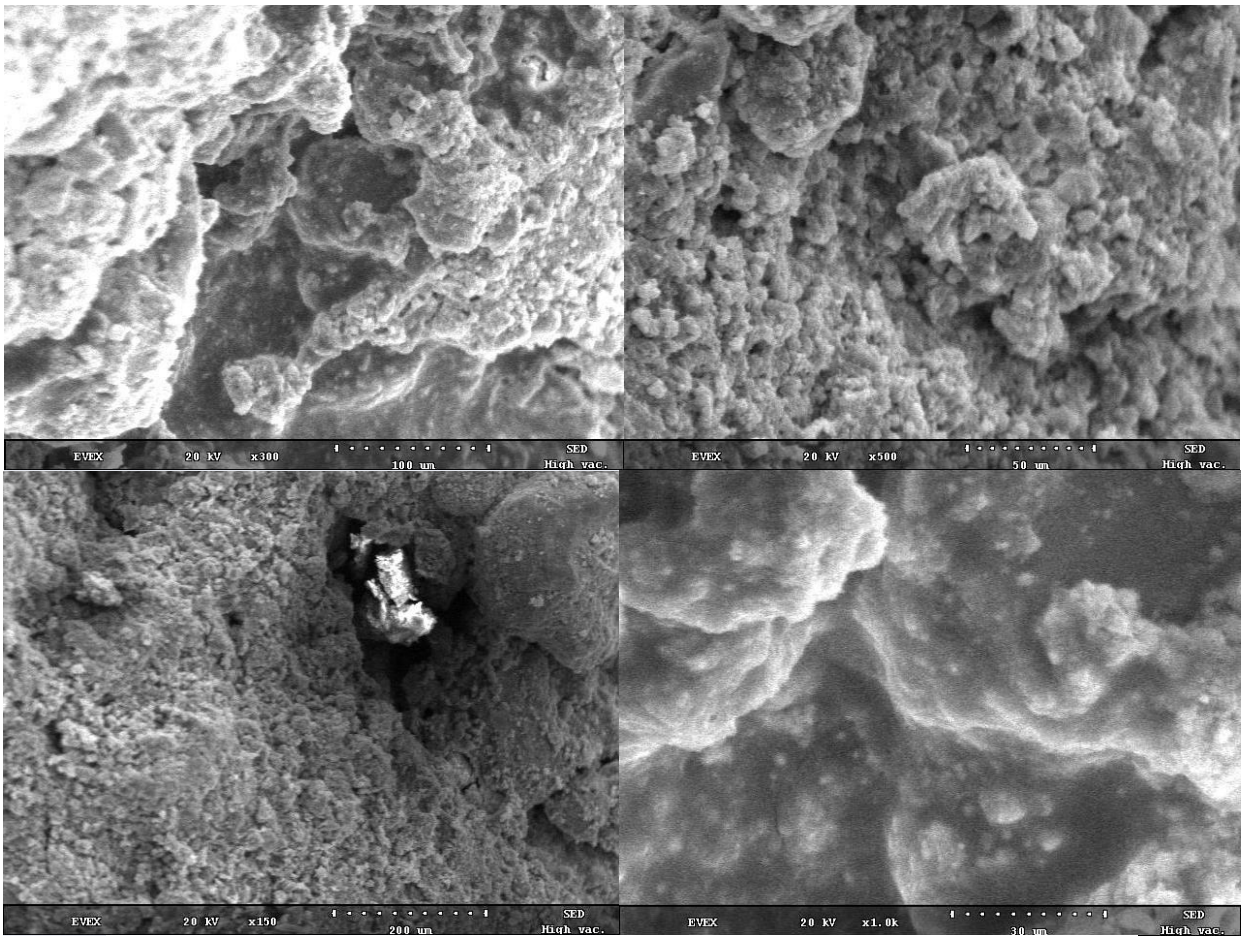

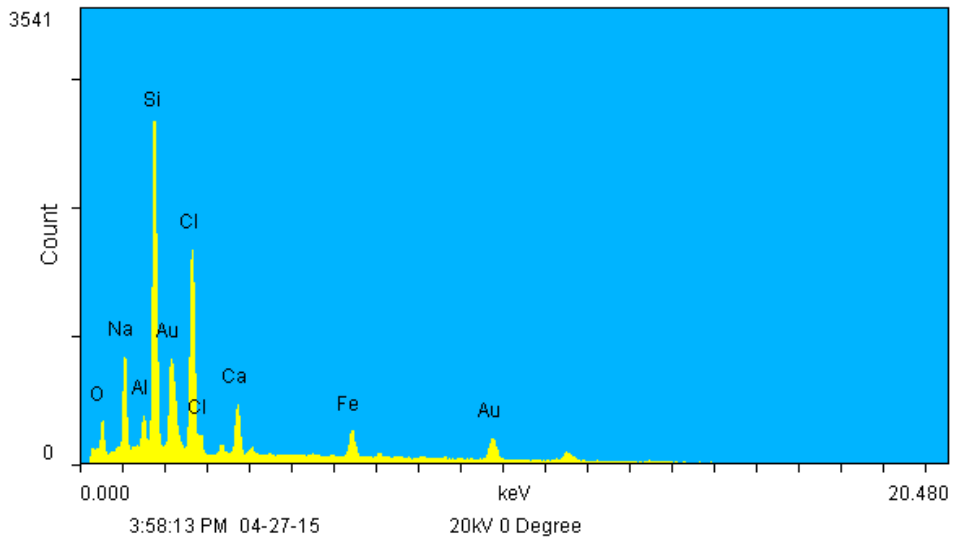

Figure 45 – SEM Results for Chip #1 Scale Sample

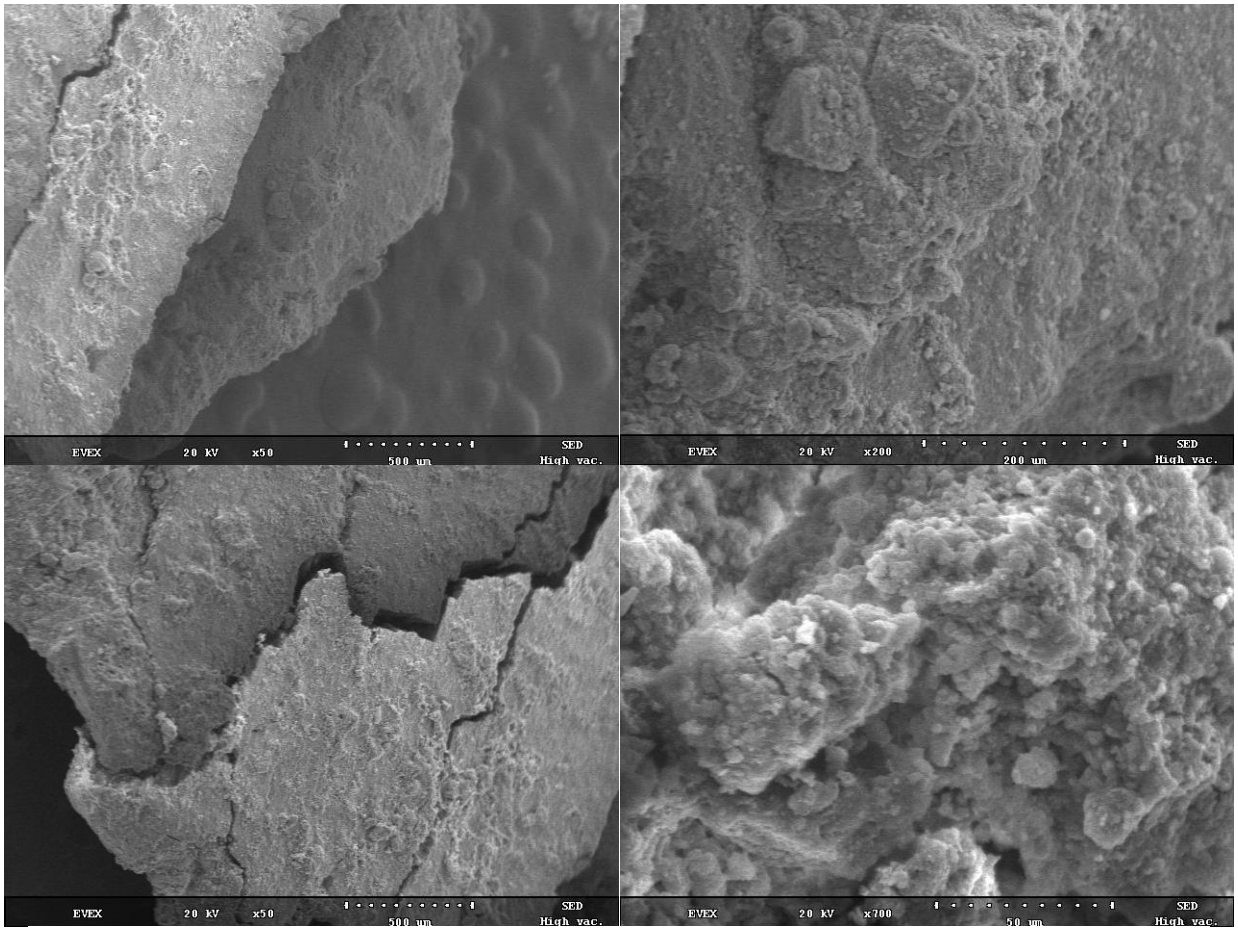

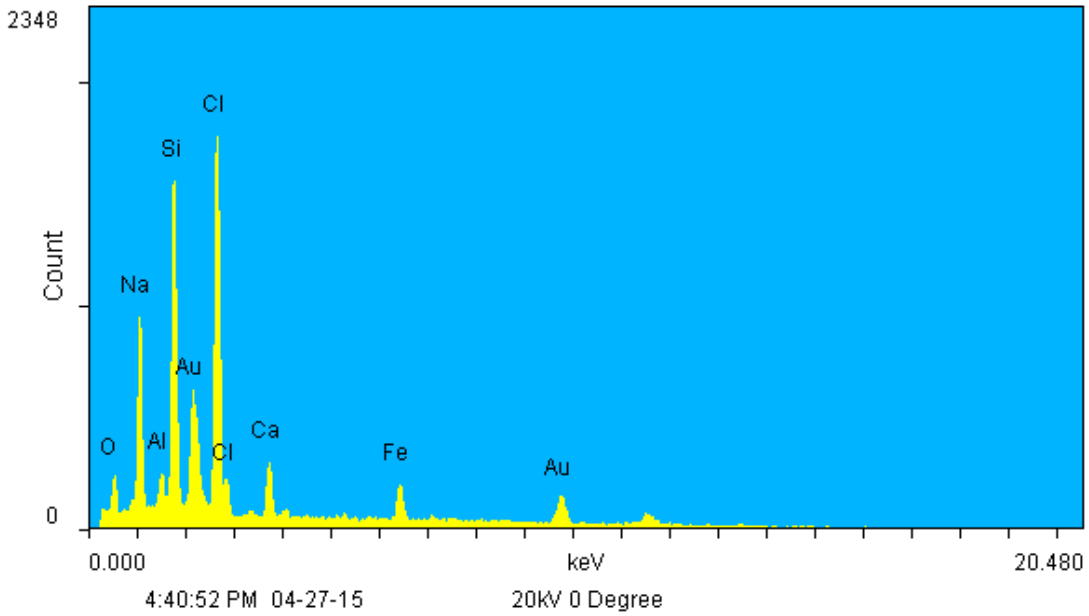

Figure 46 – SEM Results for Chip #2 Scale Sample

4.1.3 Standard Conditions Acid Solubility Tests

Two types of scale samples were tested for acid solubility at room conditions – powdered and uncrushed chip samples (**Fig. 47**). In both cases 1 gram of solid scale was added to 10 g of 15 wt% HCl, mixed and left for 30 minutes at static conditions. After the reaction undissolved scale was filtered, washed with DI, dried and solubility was measured using scale with four decimal place accuracy. Solubility of powdered samples was 23.96%, and chip samples – 13.05%. This difference can be explained due to higher reactive surface area of the powdered samples.

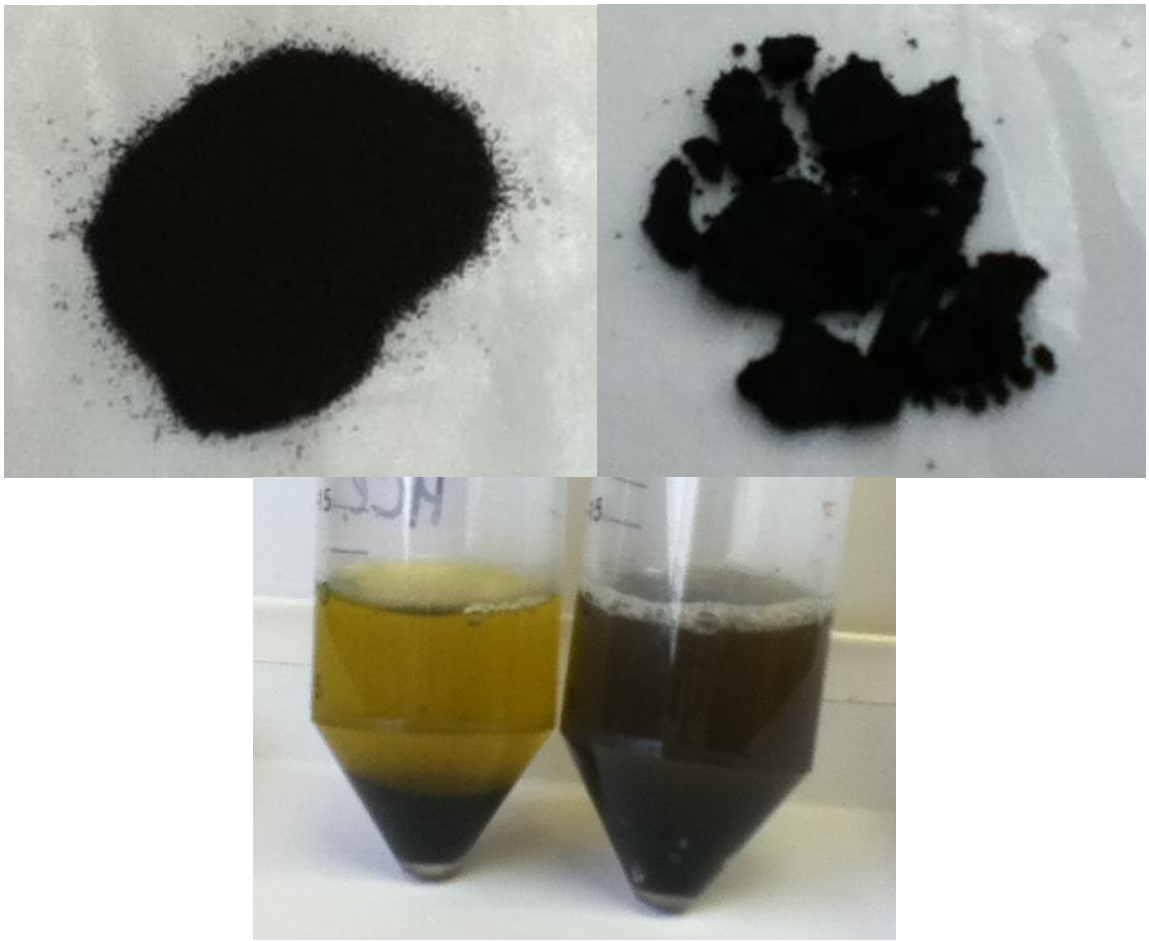

Figure 47 – Solubility Test at Room Conditions (Left – Powder Samples, Right -Chip Samples)

The same samples were also dissolved in regular mud acid (12/3 HCl/HF) and in chelating agent 50 wt% GLDA. The samples were mixed in ratio 10 to 1 (weight of acid to solids). Solubility in regular mud acid for powder sample was found to be 59.9% and for chip sample – 49.4%. Undissolved samples presented black material with some small visible grains. Solubility in GLDA for powder sample was found to be 5.1% and for chip sample – 4.6%.

4.1.4 HT/HP Mud Acid Solubility Tests

The same uncrushed scale sample from injector well was dissolved in regular mud acid at HT/HP conditions in ratio 1:10 solids to acid. The reaction cell was pressurized up to 300 psi and was heated to 200°F. The cell was rotated (dynamic solubility test) for 4 hours during the reaction. Average amount of dissolved scale for this experiment was 53.6 wt%. Unreacted sample presented black solids with organic material with no visible grains of quartz or other minerals (**Fig. 48**).

Figure 48 – HT/HP Mud Acid Solubility of the Scale Sample

4.1.5 Mud Acid Solubility Tests with Acetone Preflush

The same uncrushed scale sample from injector well was dissolved in regular mud acid at standard conditions with consequent acetone and 15 wt% HCl 2-stage preflush (**Fig. 49**). In this figure (1) shows the initial scale sample, (2) – scale soaked in acetone, (3) scale after the reaction with 15 wt% HCl, and (4) scale after the reaction with regular mud acid. The ratio 1:10 solids to fluid was used. Solubility of the sample in acetone was found to be 15.8%. Solubility of the remained sample in 15 wt% HCl was 4.6% of the unreacted weight. After the reaction sample was still not broken apart and presented chips and blocks. Finally, the solubility in the regular mud acid was found to be 57% of the unreacted weight. However, the remained undissolved sample was still consolidated.

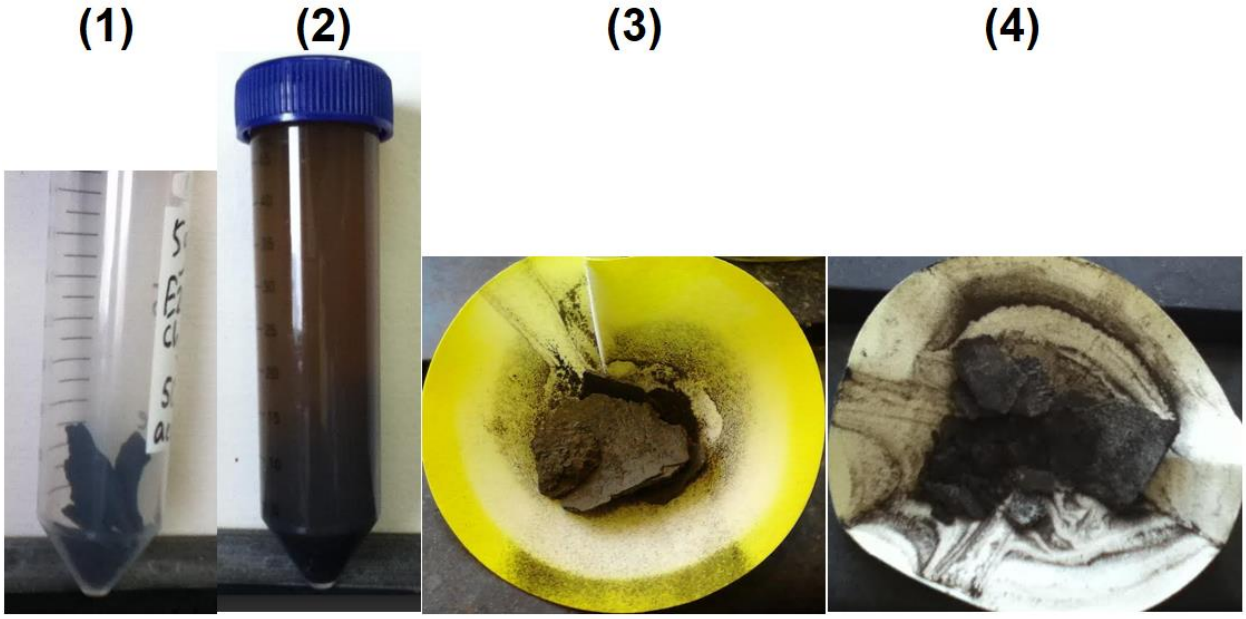

Figure 49 – Mud Acid Solubility Tests with Acetone Preflush

4.1.6 Mud Acid Solubility Tests with Xylene Preflush

Two scale samples were dissolved in xylene at room temperature to test xylene preflush effectiveness. Both samples were oil saturated and showed good solubility in xylene and both solutions became very dark after the mixing (**Fig. 50**). After the preflush samples were dried for solubility measurement. Next, samples were mixed with 15 wt% HCl. In Fig. 50 the top pictures present the first sample, and the bottom pictures present the second scale sample; and the number notes are following: (1) is the initial sample, (2) is sample soaked in xylene, (3) is sample after reaction with xylene; (4) is sample after reaction with 15 wt% HCl. Solubility of the first sample in xylene was 21.9% and in HCl – 16.9%. For the second sample, the solubility in xylene was only 2.5%, and in HCl – 6.9%. The second sample remained consolidated after the reactions.

In can be concluded that solubility in xylene depends on the consolidation and structure of the sample. Powdery samples react much better and consolidated samples are not very soluble.

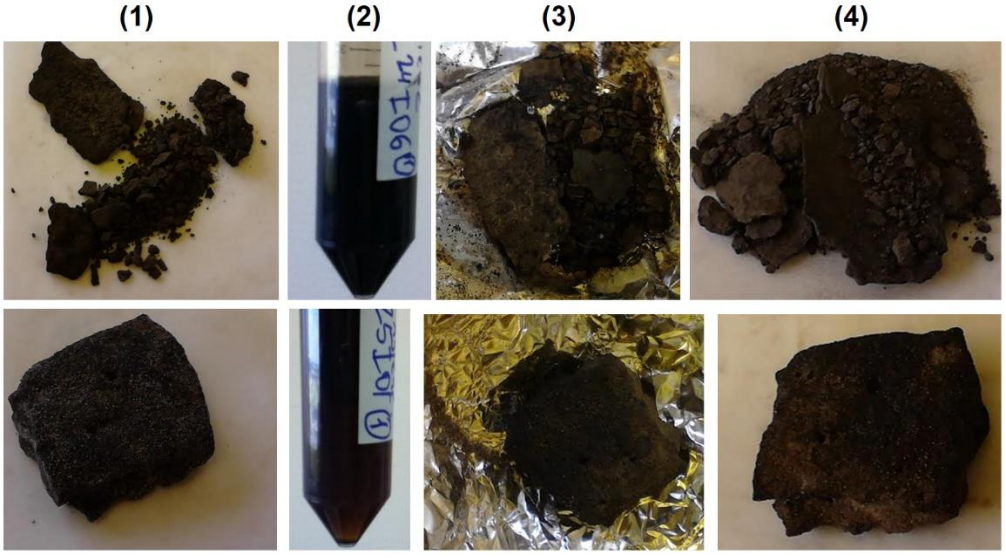

Figure 50 – Mud Acid Solubility Tests with Xylene Preflush

4.1.7 HT/HP Acid Treatments

Eleven samples of scale were collected from injector wells. These samples have different degree of consolidation, and saturation with organic matter. Texture and elemental analysis of the scale samples are presented in **Figs. 51** and **52**.

In **Fig. 53** all samples are shown before and after the reactions with xylene, acetone, 15 wt% HCl, and regular mud acid at standard and HT/HP conditions. Some samples are very layered, and others are conglomerated of sand-like particles cemented by organic matter. First, samples were washed with xylene in 1 to 10 solids to liquid ratio. Next samples were dried at 300^{o}F for 3 hours and solubility in xylene was determined. Then samples were washed with acetone in 1 to 10 solids to liquid ratio. Most of the samples remained consolidated after the two-stage preflush in organic solvents. The final stage of the preflush was reaction with 15 wt% HCl. After the preflush, samples were divided in two portions for reaction with regular mud acid. One portion was used for reaction at standard conditions and the other portion was used for reaction at HT/HP conditions.

HT/HP reactions were conducted in the special aging cells made of Hastelloy steel with Teflon liner inside (**Fig. 54**). The cells were pressurized up to 1000 psi using nitrogen and placed in the oven.

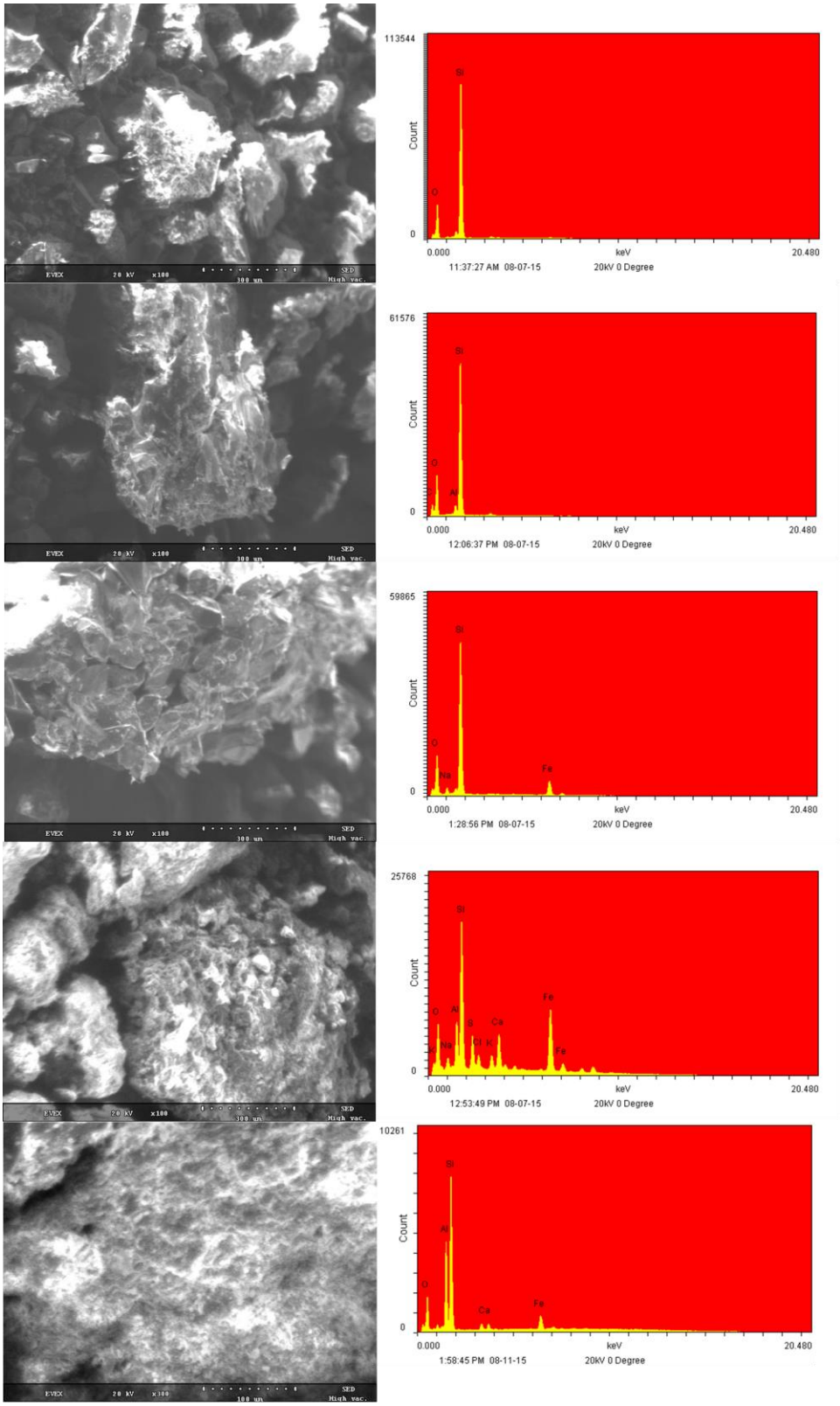

Figure 51 – SEM Results for Scale Samples # 1 – 5

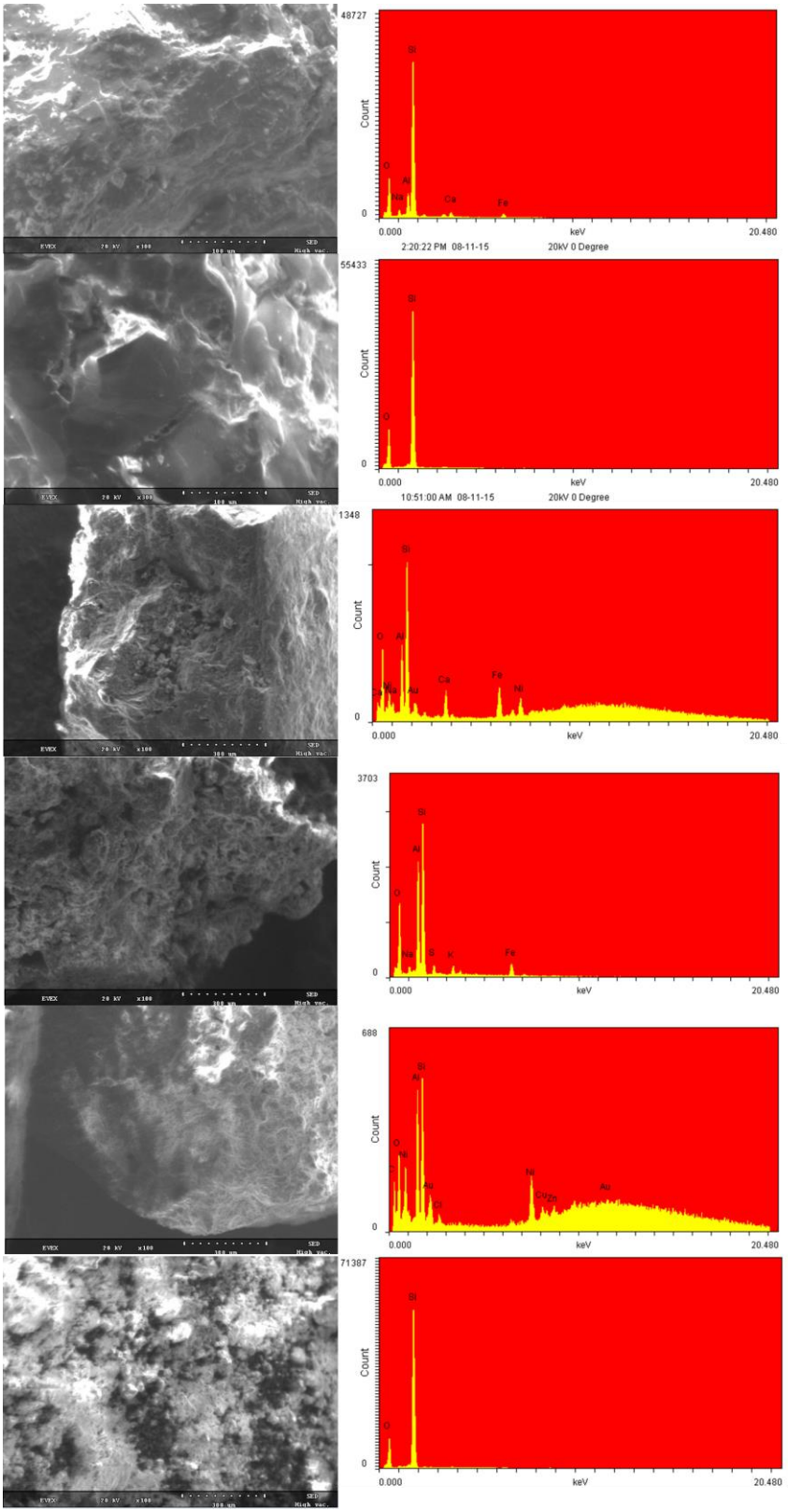

Figure 52 – SEM Results for Scale Samples # 6 – 11

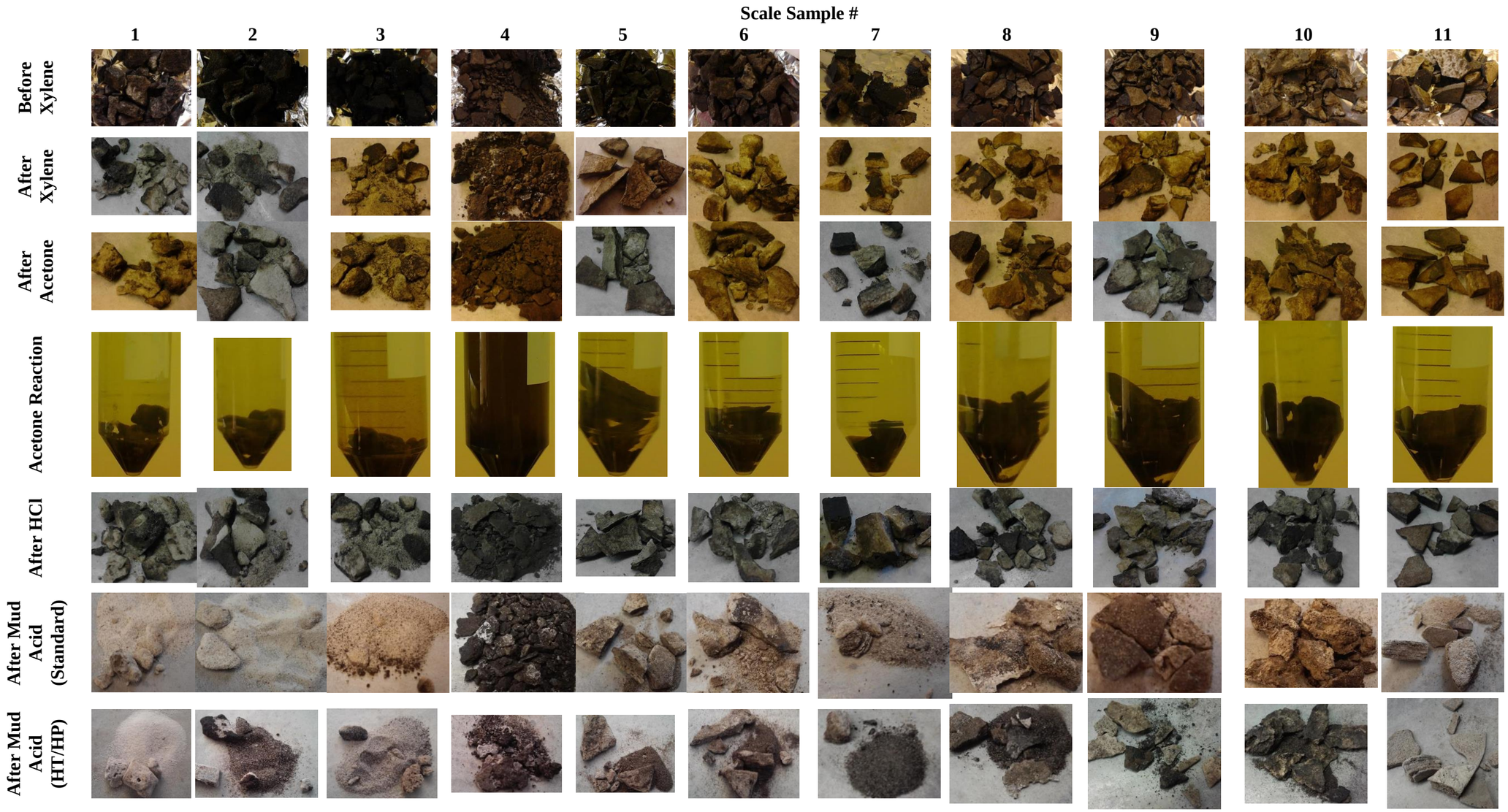

Figure 53. Scale Samples at Each Stage of the Treatment

Figure 54 – Setup for HT/HP Solubility Tests

Results of the solubility tests are presented in **Table 5**. Samples have very different morphology, color, and particles sizes. Some samples remained consolidated after all the reactions. Solubility of the samples is correlated with amount of organic matter and chemical composition of inorganic components of the scale.

Table 5: Results of the Solubility Tests for Scale from Wells

Scale Sample #	Solubility in Xylene, %	Solubility in Acetone, %	Solubility in HCl at Room Temperature, %	Solubility in Mud Acid at Room Temperature, %	Solubility in Mud Acid at HT/HP, %
1	5.60	0.00	1.91	18.29	16.80
2	5.80	0.42	2.13	20.00	18.10
3	16.30	0.71	4.31	24.51	28.80
4	21.40	3.30	15.75	39.77	71.30
5	6.60	0.43	2.80	34.82	38.50
6	4.40	0.42	2.31	30.12	35.80
7	4.90	0.00	2.04	39.42	41.30
8	4.40	0.62	2.31	26.87	30.40
9	5.70	0.42	20.55	43.07	56.50
10	2.80	0.21	1.65	34.50	38.60
11	3.20	0.00	0.41	31.58	25.00

4.2 Solubility of Scale from ESP

Solubility tests were performed for four scale samples collected from ESP. Samples were dissolved in xylene, 15 wt% HCl, and regular mud acid at standard conditions. Samples are shown in **Fig. 55**. Solubility results are shown in **Table 6**.

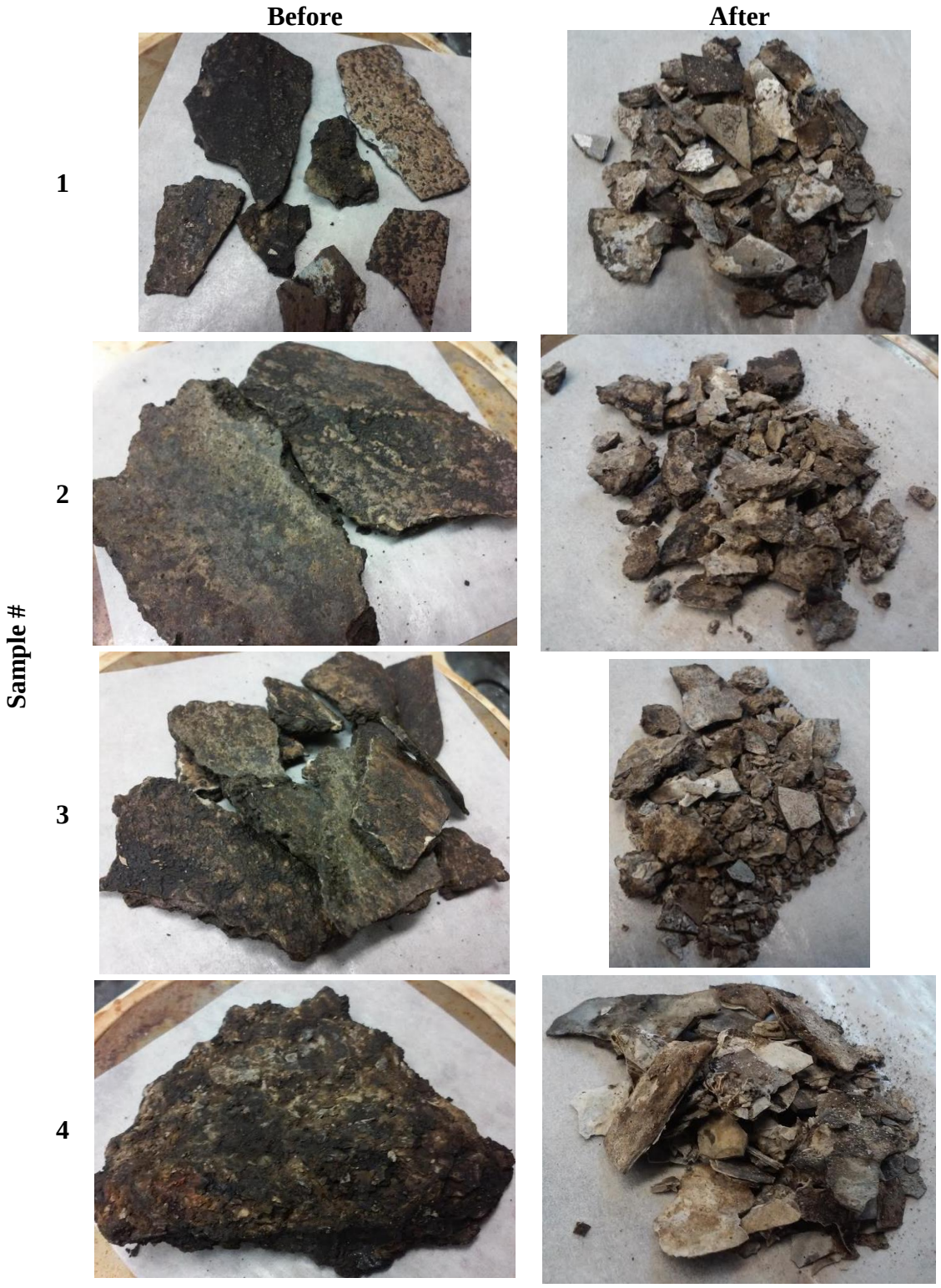

Figure 55 – ESP Scale Samples Before and After Solubility Tests

Table 6: Results of the Solubility Tests for ESP Scale Samples

Sample #	Solubility in xylene, wt.%	Solubility in 15wt% HCl, wt.%	Solubility in regular mud acid, wt.%	Cumulative solubility, wt.%
1	6.4	5.8	5.0	17.2
2	6.1	10.9	4.7	21.7
3	7.7	10.4	4.9	23.0
4	9.0	8.3	6.4	23.7

4.3 Conclusions

It can be concluded that real scale and blocking materials are very heterogeneous and consist of both organic and inorganic material. Based on the morphology of the scale it is clear that some of the materials were transported toward the deposition site and some have formed or precipitated at the site. It is crucial to ensure the contact of acid and scale in real conditions. Therefore, it is most effective to treat the damaging material with a preflush that can remove organic layers covering the scaling minerals. Removal of the cementing material of the scale often causes deconsolidation of the blocks and increases the reactive surface area, this normally improves overall solubility. All solubility tests are recommended to be conducted at reservoir conditions and in the presence of all additives that are normally used during the treatment.

5. SUMMARY AND CONCLUSIONS

In this chapter, results of the research work will be summarized, and conclusions will be formulated. Recommendations, potential improvements, and vision of the future work will be provided.

The objective of the first part of this research was to analyze the effect of steam on common sandstone minerals in the simplified system that excluded effect of oil phase. Steam injection experiments were used to investigate the changes in petrophysical properties of the sandpacks, and aging cells were used to clarify the mineral alterations. Obtained samples were characterized to determine the dominant formation damage mechanisms associated with steam-rock interaction. In this work special attention was paid to pore-filling clay minerals and their properties. Effective porosity and permeability changes associated with steam injection were determined for sandpacks of various mineralogical content.

Sandpacks with quartz and calcite represented the case of relatively clean sandstone. It was found that these sandpacks normally experience about 5% permeability reduction and 1-2% porosity reduction when contacted by steam. It was observed that most of the formation damage was associated with the slight redistribution of the rock matrix. For example, silica was dissolved in the hot part of the sandpack and precipitated once the solution was cooled during propagation in the sandpack.

Sandpacks with quartz, kaolinite, and carbonate minerals (calcite or dolomite) represented the sandstone reservoir with non-swelling clay minerals. It was observed that these sandpacks have lost 11-22% of the initial permeability and 2-7% of the initial porosity. Most of the formation damage associated with steam injection was shown to be caused by kaolinite fines migration. It

was also discovered that aging of these mixtures for 10 days at 400°F and 1,000 psi may lead to formation of swelling smectite clay (Ca montmorillonite). This can cause secondary formation damage mechanisms associated with clay swelling and dispersion. During the aging experiments it was found that mineralogy alteration was only possible when produced during the mineral reaction CO_2 can escape from the system. Mixtures with dolomite were determined to produce more montmorillonite than mixtures with calcite.

Mixtures of quartz with montmorillonite represented the sandstone with various amount of swelling clays. These sandpacks experienced the most dramatic changes in petrophysical properties. Exposure to steam injection led to high permeability reduction (77-84%) and moderate porosity reduction (7-8%). Formation damage was mainly caused by clay swelling, which lead to filling of pores with montmorillonite. It was observed that the microporous network that filled the pores does not affect porosity as much as it restricts the flow. Aging of montmorillonite-rich mixtures did not reveal mineral alterations but it allowed to visualize the morphological reorganization of montmorillonite and its pore bridging effect.

It is recommended to use real sandstone samples to calibrate the obtained results. Further study of the formation of the montmorillonite's microporous network is required to formulate the critical conditions and seriousness of smectite-steam interactions.

In the second part of this research, the effect of oil was taken into consideration. Moreover, oil recovery factors were determined as a function of injected pore volume (PV) of steam for sandpacks of different mineralogy.

Agreeing with the previous part of the work, it was concluded that the degree of interaction of steam with different minerals depends more on the nature of the mineral than on the particle size and reactive surface area. Thus, sandpacks with clay minerals demonstrated significantly

lower oil recovery than sandpacks with non-clay minerals of the same particle size. Sandpack with 100% quartz delivered high final oil recovery (65 wt%) after the injection of 15 PV. Permeability was not altered significantly during the thermal oil production from the baseline sandpack.

Addition of 10 wt% of calcite to quartz sandpack lead to slight reduction in final oil recovery (56 wt% after injection of 15 PV). Precipitation of Ca^{2+}-based material was observed in the recovered sandpacks.

For the sandpack with 90 wt% quartz and 10 wt% feldspar, oil production remained high, final oi recovery being about 61 wt% after injection of 15 PV. The identified formation damage was found to be associated with structural breakdown and fines release. It was determined that the fine particles of feldspar were transported in both organic and aqueous phases.

For the kaolinite sandpack oil production profile has extended up to 20 PV and the final oil recovery was found to be 39 wt%. However, at 15 PV, this sample produced only about 15 wt% of the initial oil in the sandpack. Kaolinite is known for being mobile and experiments showed that the dominant formation damage mechanism was fines migration. It was also determined that kaolinite particles are mostly mobilized and migrate within the aqueous phase formed when the steam condensated.

Sandpack with 90 wt% quartz and 10 wt% smectite had shown even more prolonged oil production which reached about 32 wt% at 21 PV; and almost 16 wt% at 15 PV. This is probably associated with oil retention in the microporous network that montmorillonite forms in presence of water. Effects of thermal dehydration and shrinking of smectite were found to be negligible for these experiments.

Illite-rich sandpack had shown the smallest oil production which reached about 28 wt% after injection of 16 PV; and 28 wt% at 15 PV. Clearly, the production was very delayed for this

case. The reason of the small oil production for this sandpack is precipitation of the amorphous silica inside the sandpack.

Finally, it was observed that aqueous phase produced from clay-rich sandpacks tend to have higher pH than samples produced from samples without clay minerals. Additionally, no mineral transformation was observed for any of the tested sandpacks. This can be explained by the fact that all the steam injection experiments lasted less than 10 hours, and this time is not long enough to form detectable amount of the altered minerals.

Based on the obtained results it is recommended to pay special attention to steam injection in clay-rich formations. Analysis of the aqueous phase (chemical content and pH) must be used to interpret interactions in steam-formation system. Aging, coreflooding and analysis of the rock samples must be used in identification and characterization of the formation damage.

REFERENCES

Al Shizawi, W., Al Zadjali, R., Mahajan, S. et al. 2018. Sand Production Assessment & Sand Control Selection for Steam Flood in South Oman. Presented at the SPE International Heavy Oil Conference and Exhibition, Kuwait City, Kuwait, 10-12 December. SPE-193777-MS. http://dx.doi:10.2118/193777-MS.

Al-Nakhli, A. R., Luai, A. S., Arukhe J. et al. 2016. In-Situ Steam Generation a New Technology Application for Heavy Oil Production. Presented at the SPE Heavy Oil Conference and Exhibition, Kuwait City, Kuwait, 6-8 December. SPE-184118-MS. http://dx.doi.org/10.2118/184118-MS.

Ameur, Z. O., Kudrashou, V. Y., Nasr-El-Din, H. A. et al. 2018. Stimulation of High-Temperature Steam-Assisted-Gravity-Drainage Production Wells Using a New Chelating Agent (GLDA) and Subsequent Geochemical Modeling Using PHREEQC. *SPE Prod & Oper* Preprint. SPE-173774-PA. http://dx.doi:10.2118/173774-PA.

Bayliss, P., Levinson, A. 1971. Low Temperature Hydrothermal Synthesis from Dolomite or Calcite, Quartz and Kaolinite. *Clays and Clay Minerals* **19** (2): 109-114. http://dx.doi.org/10.1346/ccmn.1971.0190207.

Bennion, D. B. 2002. An Overview of Formation Damage Mechanisms Causing a Reduction in the Productivity and Injectivity of Oil and Gas Producing Formations. *J Can Pet Technol* **41** (11). http://dx.doi.org/10.2118/02-11-DAS.

Bennion, D. B., Gupta, S., Gittins, S. et al. 2009. Protocols for Slotted Liner Design for Optimum SAGD Operation. *J Can Pet Technol* **48** (11): 21-26. http://dx.doi.org/10.2118/130441-PA.

Bennion, D. B., Thomas, F. B., and Sheppard, D. A. 1992. Formation Damage Due to Mineral Alteration and Wettability Changes during Hot Water and Steam Injection in Clay-Bearing

Sandstone Reservoirs. Presented at the SPE Formation Damage Control Symposium. Lafayette, Louisiana, 26-27 February. SPE-23783-MS. http://dx.doi.org/10.2523/23783-MS.

Bonorino, F. G. 1959. Hydrothermal Alteration in the Front Range Mineral Belt, Colorado. *Geological Society of America Bulletin* **70** (1): 53. http://dx.doi.org/10.1130/0016-7606(1959)70[53:haitfr]2.0.co;2.

Boon, J. A., Hamilton, T., Holloway, L. et al. 1983. Reaction between Rock Matrix and Injected Fluids in Cold Lake Oil Sand — Potential for Formation Damage. *J Can Pet Technol* **22** (04): http://dx.doi.org/10.2118/83-04-03.

Bowen, N. L., Tuttle, O. F. 1949. The system MgO—SiO_2—H_2O. *GSA Bulletin* **60** (3): 439-460. http://dx.doi.org/10.1130/0016-7606(1949)60[439:TSM]2.0.CO;2.

Bundy, W. M. 1958. *Wall-Rock Alteration in the Cochiti Mining District, New Mexico*. New Mexico, State Bureau of Mines and Mineral Resources, Bulletin 59, 71 p.

Butler, R. M., McNab, G. S., Lo, H. Y. 1981. Theoretical Studies on the Gravity Drainage of Heavy Oil During In-situ Steam Heating. *The Canadian Journal of Chemical Engineering* **59** (4): 455-460. http://dx.doi.org/10.1002/cjce.5450590407.

Cao, N., Almojtaba, M., Babadagli, T. 2017. Wettability Alteration of Heavy-Oil-Bitumen-Containing Carbonates by Use of Solvents, High-pH Solutions, and Nano/Ionic Liquids. *SPE Res Eval & Eng* **20** (02): 363-371. http://dx.doi.org/10.2118/183646-PA.

Castro, L. U. 2001. Demulsification Treatment and Removal of In-Situ Emulsion in Heavy-Oil Reservoirs. Presented at the SPE Western Regional Meeting, Bakersfield, California, 26-30 March. SPE-68852-MS. http://dx.doi.org/10.2523/68852-MS.

Crawford, B., Searles, K., Hsu, S. Y. et al. 2006. Plastic Compaction in Diatomite: In-Situ Stress versus Temperature Effects. Presented at the 41st U.S. Symposium on Rock Mechanics (USRMS), Golden, Colorado, 17-21 June. ARMA-06-1122. http://dx.doi.org/ARMA-06-1122.

Day, J. J., Huitt, J. L. 1967. Laboratory Study of Rock Softening and Means of Prevention during Steam or Hot Water Injection. *J Pet Technol* **19** (05): 703-711. http://dx.doi.org/10.2118/1561-PA.

Duanzong, C., Jin, Q., and Xu, R. 2000. Research on Packing Materials for Sand Control in Steam Injection Wells. Presented at the International Oil and Gas Conference and Exhibition in China. Beijing, China, 7-10 November. SPE-64734-MS. http://dx.doi.org/10.2523/64734-MS.

El-Saleh, M. M., and Ali, S. M. F. 1968. A Theoretical and Experimental Study of Steam Drive. Presented at the Fall Meeting of the Society of Petroleum Engineers of AIME, Houston, Texas, 29 September-2 October. SPE-2234-MS. http://dx.doi.org/10.2523/2234-MS.

Garrels, R. M. 1984. Montmorillonite/Illite Stability Diagrams. *Clays and Clay Minerals* **32** (3): 161-166. http://dx.doi.org/10.1346/ccmn.1984.0320301.

Gunter, W. D., Zhou, Z., Perkins, E. H. 1994. Modeling Formation Damage Caused by Kaolinite from 25 to 300 Degrees Centigrade in the Oil Sand Reservoirs of Alberta. *SPE Advanced Technology Series* **2** (02): 206-213. http://dx.doi.org/10.2118/23786-PA.

Harvey, R. D., Vitaliano, C. J. 1964. Wall-Rock Alteration in the Goldfield District, Nevada. *The Journal of Geology* **72** (5): 564-579. http://dx.doi.org/10.1086/627014.

Hawkins, D. B., Roy, R. 1963. Experimental Hydrothermal Studies on Rock Alteration and Clay Mineral Formation. *Geochimica et Cosmochimica Acta* **27** (10): 1047-1054. https://dx.doi.org/10.1016/0016-7037(63)90065-6.

Hebner, B. A., Bird, G. W., & Longstaffe, F. J. 1986. Fluid/Pore-Mineral Transformations During Simulated Steam Injection: Implications for Reduced Permeability Damage. *J Can Pet Technol* **25** (5). PETSOC-86-05-09. http://dx.doi:10.2118/86-05-09.

Howard, F. A. 1923. Method of Operating Oil Wells. US Patent No. 1473348A.

Huang, W. L., Longo, J. M. 1994. Experimental Studies of Silicate-Carbonate Reactions—I. Applications to Diagenesis. *Applied Geochemistry* **9** (5): 501-522. http://dx.doi.org/10.1016/0883-2927(94)90013-2.

Huang, W. L., Longo, J. M. 1994. Experimental Studies of Silicate-Carbonate Reactions—II. Applications to Steam Flooding of Oil Sands. *Applied Geochemistry* **9** (5): 523-532. http://dx.doi.org/10.1016/0883-2927(94)90014-0.

Hui, Q., Zhenghua, Y., Yunfeng, L. et al. 2006. Water–Rock Interaction during the Process of Steam Stimulation Exploitation of Viscous Crude Oil in Liaohe Shuguang Oil Field, Liaoning, China. *Environmental Geology* **50** (2): 229-236. http://dx.doi.org/10.1007/s00254-006-0203-7.

Hutcheon, I., Oldershaw, A., Ghent, E. D. 1980. Diagenesis of Cretaceous Sandstones of the Kootenay Formation at Elk Valley (southeastern British Columbia) and Mt Allan (southwestern Alberta). *Geochimica et Cosmochimica Acta* **44** (10): 1425-1435. http://dx.doi.org/10.1016/0016-7037(80)90108-8.

Iler, R. K. 1979. *The Chemistry of Silica: Solubility, Polymerization, Colloid and Surface Properties and Biochemistry of Silica*, second edition. New York, N. Y.: A Wiley Interscience.

Jain, A. K., Ahmed, K., Ferdous, H. et al. 2016. An Experimental Investigation of Steam Induced Permeability Changes in Clay Bearing Formation of North Kuwait. Presented at the SPE EOR Conference at Oil and Gas West Asia, Muscat, Oman, 21-23 March. SPE-179762-MS. http://dx.doi.org/10.2118/179762-MS.

Jain, A. K., Ahmed, K., Ortiz-Volcan, J. L. 2015. Water Analysis - A Key Tool for Reservoir Monitoring Under Cyclic Steam Stimulation. Presented at the SPE Kuwait Oil and Gas Show and Conference, Mishref, Kuwait, 11-14 October. SPE-175287-MS. http://dx.doi:10.2118/175287-MS.

Kar, T., & Hascakir, B. 2016. The Interaction of Asphaltenes with Solvents Water and Clays During Bitumen Extraction through Solvent-Steam Injection. Presented at the SPE Heavy Oil Conference and Exhibition, Kuwait City, Kuwait, 6-8 December. SPE-184081-MS. http://dx.doi:10.2118/184081-MS.

Kar, T., & Hascakir, B. 2017. Impact of Clay type on SAGD Performance Part I: Microscopic Scale Analysis of Clay-SARA Interactions in Produced Oil. Presented at the SPE Latin America and Caribbean Petroleum Engineering Conference, Buenos Aires, Argentina, 17-19 May. SPE-185533-MS. http://dx.doi:10.2118/185533-MS.

Kar, T., Mukhametshina, A., Unal, Y. et al. 2015. The Effect of Clay Type on Steam-Assisted-Gravity-Drainage Performance. Society of Petroleum Engineers. *J Can Pet Technol* **54** (6). SPE-173795-PA. http://dx.doi:10.2118/173795-PA.

Keith, D. C., Harrison, W. J., Wendlandt, R. F. et al. 1998. Mineralogical Responses of Siliciclastic Carbonate-Cemented Reservoirs to Steamflood Enhanced Oil Recovery. *Applied Geochemistry* **13** (4): 491-507. https://dx.doi.org/10.1016/S0883-2927(97)00082-6.

Keith, M. L., Schairer, J. F. 1952. The Stability Field of Sapphirine in the System MgO-Al_2O_3-SiO_2. *The Journal of Geology* **60** (2): 181-186. http://dx.doi.org/30061252.

Khaledi, R., Reza, M. H., Boone, T. J. et al. 2018. Azeotropic Heated Vapour Extraction- A New Thermal-Solvent Assisted Gravity Drainage Recovery Process. Presented at the SPE Canada Heavy Oil Technical Conference, Calgary, Alberta, Canada, 13-14 March. SPE-189755-MS. http://dx.doi.org/10.2118/189755-MS.

Khansari, Z., and Gates, I. 2015. Reactive Steam Assisted Gravity Drainage Oil Sands Recovery Process. Presented at the SPE Canada Heavy Oil Technical Conference, Calgary, Alberta, Canada, 9-11 June. SPE-174428-MS. http://dx.doi.org/10.2118/174428-MS.

Kirk, J. S., Bird, G. W., Longstaffe, F. J. 1987. Laboratory study of the effects of steam-condensate flooding in the Clearwater Formation; high temperature flow experiments. *Bulletin of Canadian Petroleum Geology* **35** (1): 34-47. http://dx.doi.org/10.1016/0016108-8.

Koh, C. J., Dagenais, P. C., Larson, D. C. et al. 1996. Permeability Damage in Diatomite Due to in-Situ Silica Dissolution/Precipitation. Presented at the SPE/DOE Improved Oil Recovery Symposium, Tulsa, Oklahoma, 21-24 April. SPE-35394-MS. http://dx.doi.org/10.2523/35394-MS.

Kubacki, W., Boon, J., Bird, G. et al. 1984. Effect of Mineral Transformation on Porosity and Permeability of Dolomite Rock during In-Situ Recovery of Bitumen. A Preliminary Study. *Bulletin of Canadian Petroleum Geology* **32** (3): 281-288. http://dx.doi.org/10.20060/2017.34.2704.

Kudrashou, V. Y., and Nasr-El-Din, H. A. 2019a. Formation Damage and Compatibility Issues Associated with Use of Corrosion Inhibitors in Well Acidizing - A Review. Presented at the SPE/ICoTA Coiled Tubing and Well Intervention Conference and Exhibition, The Woodlands, 26-27 March. SPE-194301-MS. http://dx.doi:10.2118/194301-MS.

Kudrashou, V. Y., and Nasr-El-Din, H. A. 2019b. Formation Damage Associated with Mineral Alteration and Formation of Swelling Clays Caused by Steam Injection in Sandpacks. *SPE Res Eval & Eng* Preprint. SPE-195700-PA. https://dx.doi.org/10.2118/195700-PA.

Kumar, A., Noh, M., Pope, G. A. et al. 2004. Reservoir Simulation of CO_2 Storage in Deep Saline Aquifers. Presented at the SPE/DOE Symposium on Improved Oil Recovery, Tulsa, Oklahoma, 17-21 April. SPE-89343-MS. http://dx.doi.org/10.2118/89343-MS.

Lefebvre, R., Hutcheon, I. 1986. Mineral Reactions in Quartzose Rocks during Thermal Recovery of Heavy Oil, Lloydminster, Saskatchewan, Canada. *Applied Geochemistry* **1** (3): 395-405. http://dx.doi.org/10.1016/0883-2927(86)90024-7.

Levinson, A. A., Day, J. J. 1968. Low Temperature Hydrothermal Synthesis of Montmorillonite, Ammonium-Micas and Ammonium-Zeolites. *Earth and Planetary Science Letters* **5** (Supplement C): 52-54. https://dx.doi.org/10.1016/S0012-821X(68)80011-1.

Levinson, A. A., Vian, R. W. 1966. The Hydrothermal Synthesis of Montmorillonite Group Minerals from Kaolinite, Quartz and Various Carbonates. *Am. Mineral.* **51**: 495-498. https://dx.doi.org/10.1016/S0012-821X(68)80011-1.

Li, B., & Wong, R. 2015. Effect of Heating in Steam-Based-Oil-Recovery Process on Deformation of Shale: A Compositional Thermal Strain Model. *J Can Pet Technol* **54** (1). SPE-165393-PA. http://dx.doi:10.2118/165393-PA.

Mahmoudi, M., Fattahpour, V., Nouri, A. et al. 2017. An Experimental Evaluation of Pore Plugging and Permeability Reduction Near SAGD Sand Control Liners. Presented at the SPE Canada Heavy Oil Technical Conference, Calgary, Alberta, Canada, 15-16 February. SPE-184999-MS. http://dx.doi.org/10.2118/184999-MS.

Marx, J. W., and Langenheim, R. H. 1959. Reservoir Heating by Hot Fluid Injection. Society of Petroleum Engineers General Proceedings. SPE-1266-G. http://dx.doi.org/1266-G.

Matvienko, A. A., Chizhik, S. A., Sidel'nikov, A. A. 2013. A new kinetic model of calcite thermal decomposition. Pleiades Publishing Ltd. *Doklady Physical Chemistry* **451** (2). http://dx.doi.org/10.1134/s001250161308006x.

Mishra, P. K., Ahmad, K., & Al Khandari, J. 2018. Spatial Distribution of Clay Minerals in the Neogene Sediments of North Kuwait and its Impact on Thermal Production. Presented at the SPE International Heavy Oil Conference and Exhibition, Kuwait City, Kuwait, 10-12 December. SPE-193711-MS. http://dx.doi:10.2118/193711-MS.

Mohnot, S. M., Bae, J. H. 1989. A Study of Mineral/Alkali Reactions-Part 2. *SPE Res Eng* **4** (03): 381-390. http://dx.doi:10.2118/13576-PA.

Mohnot, S. M., Bae, J. H., Foley, W. L. 1987. A Study of Mineral/Alkali Reactions. *SPE Res Eng* **2** (04): 653-663. http://dx.doi:10.2118/13032-PA.

Montgomery, W., Sephton, M., Watson, J. et al. 2014. The Effects of Minerals on Heavy Oil and Bitumen Chemistry When Recovered Using Steam-Assisted Methods. Presented at the SPE Heavy Oil Conference-Canada. Calgary, Alberta, Canada, 10-12 June. SPE-170035-MS. http://dx.doi.org/10.2118/170035-MS.

Moore, C. H. 2001. Computer Simulation of Formation Damage Resulting from Thermal Recovery. Presented at the Proceedings of SPE International Thermal Operations and Heavy

Oil Symposium. Porlamar, Margarita Island, Venezuela, 12-14 March. SPE-69716-MS. http://dx.doi.org/10.2523/69716-MS.

Morey, G. W., and Fenner, C. N. 1917. The Ternary System H_2O-K_2SiO_3-SiO_2. *Journal of the American Chemical Society* **39** (6): 1173-1229. http://dx.doi:10.1021/ja02251a008.

Morey, G. W., and Niggli, P. 1913. The Hydrothermal Formation of Silicates, A Review. *Journal of the American Chemical Society* **35** (9): 1086-1130. http://dx.doi:10.1021/ja02198a600.

Nabzar, L., Aguilera, M. E., Rajoub, Y. 2005. Experimental Study on Asphaltene-Induced Formation Damage. Presented at the SPE International Symposium on Oilfield Chemistry, The Woodlands, Texas, 2-4 February. SPE-93062-MS. http://dx.doi.org/10.2523/93062-MS.

Nadeau, P. H. 1998. An Experimental Study of the Effects of Diagenetic Clay Minerals on Reservoir Sands. *Clays and Clay Minerals* **46** (1): 18-26. http://dx.doi:10.1346/ccmn.1998.0460103.

Nengkoda, A. 2012. The Role of Calcite in CO_2 Increase 25% during Cyclic Steam Injection in Sandstone Heavy Oil Reservoir: Case Study. Presented at the SPE International Production and Operations Conference & Exhibition. Doha, Qatar, 14-16 May. SPE-157632-MS. http://dx.doi.org/10.2118/157632-MS.

Nghiem, L., Shrivastava, V., Kohse, B. et al. 2009. Simulation of Trapping Processes for CO_2 Storage in Saline Aquifers. Presented at the Canadian International Petroleum Conference. Calgary, Alberta, 16-18 June. PETSOC-2009-156. http://dx.doi.org/10.2118/2009-156.

Okoye, C. U., Onuba, N. L., Ghalambor, A. et al. 1992. An Experimental Investigation of Formation Damage in Heavy Oil Reservoir during Steam Injection. Presented at the SPE

Formation Damage Control Symposium, Lafayette, Louisiana, 26-27 February. SPE-23781-MS. http://dx.doi.org/10.2118/23781-MS.

Oldershaw, A., Hutcheon, I., and Nahnybida, C. 1981. The Effects of In-Situ Steam Injection on Cold Lake Oil Sands. *Bulletin of Canadian Petroleum Geology* **29** (4): 447-478. http://dx.doi:029/029004/0447

Reed, M. G. 1980. Gravel Pack and Formation Sandstone Dissolution during Steam Injection. *J Petr Technol* **32** (06): 941-949. http://dx.doi.org/10.2118/8424-PA.

Regis, A. J., Sand, L. B., Calmon, C. et al. 1960. Phase Studies in the Portion of the Soda-Alumina-Silica-Water System Producing Zeolites. *The Journal of Physical Chemistry* **64** (10): 1567-1571. http://dx.doi.org/10.1021/j100839a057.

Rieke, H. 1972. Mineralogy of Montmorillonite under Elevated Temperature and Pressure. Presented at the Abnormal Subsurface Pressure Symposium, Baton Rouge, Louisiana, 15-16 May. SPE-3852-MS. http://dx.doi.org/10.2523/3852-MS.

Romanova, U. G., Ma, T. 2013. An Investigation on the Plugging Mechanisms in a Slotted Liner from the Steam Assisted Gravity Operations. Presented at the SPE European Formation Damage Conference & Exhibition, Noordwijk, The Netherlands, 5-7 June. SPE-165111-MS. http://dx.doi.org/10.2118/165111-MS.

Romanova, U. G., Ma, T., Piwowar, M. et al. 2015. Thermal Formation Damage and Relative Permeability of Oil Sands of the Lower Cretaceous Formations in Western Canada. Presented at the SPE Canada Heavy Oil Technical Conference, Calgary, Alberta, Canada, 9-11 June, SPE-174449-MS. http://dx.doi.org/10.2118/174449-MS.

Romanova, U. G., Michel, D., Strom, R. et al. 2017. Understanding Sand Control for Thermal Heavy Oil and Bitumen Production Operations. Presented at the SPE Thermal Well Integrity

and Design Symposium, Banff, Alberta, Canada, 28-30 November. SPE-188155-MS. http://dx.doi.org/10.2118/188155-MS.

Roy, D. M., and Roy, R. 1955. Synthesis and Stability of Minerals in the System MgO-Al_2O_3-SiO_2-H_2O. *Am Mineral* **40**: 147-178. http://dx.doi:AM40/147.

Roy, R., and Tuttle, O. F. 1956. Investigations under Hydrothermal Conditions. *Physics and Chemistry of the Earth* **1** (Supplement C): 138-180. https://dx.doi.org/10.1016/0079-1946(56)90008-8.

Schembre, J. M., Tang, G., Kovscek, A. R. 2006. Interrelationship of Temperature and Wettability on the Relative Permeability of Heavy Oil in Diatomaceous Rocks. *SPE Res Eval & Eng* **9** (03): 239-250. http://dx.doi.org/10.2118/93831-PA.

Schoen, R., and White, D. E. 1965. Hydrothermal alteration in GS-3 and GS-4 drill holes, Main Terrace, Steamboat Springs, Nevada. *Economic Geology* **60** (7): 1411-1421. http://dx.doi.org/10.2113/gsecongeo.60.7.1411.

Schutjens, P. M., Hanssen, T. H., Hettema, M. H. et al. 2004. Compaction-Induced Porosity/Permeability Reduction in Sandstone Reservoirs: Data and Model for Elasticity-Dominated Deformation. *SPE Res Eval & Eng* **7** (03): 202-216. http://dx.doi.org/10.2118/88441-PA.

Smyth, F. H., and Adams, L. H. 1923. The System, Calcium Oxide-Carbon Dioxide. *Journal of the American Chemical Society* **45** (5): 1167-1184. http://dx.doi.org/10.1021/ja01658a009.

Somerton, W. H., and Boozer, G. D. 1960. Thermal Characteristics of Porous Rocks at Elevated Temperatures. *J Pet Technol* **12** (06): 77-81. http://dx.doi.org/10.2118/1372-G.

Somerton, W. H., and Selim, M. A. 1961. Additional Thermal Data for Porous Rocks--Thermal Expansion and Heat of Reaction. *SPE J.* **1** (04): 249-253. http://dx.doi.org/10.2118/1613-G.

Steiner, A. 1968. Clay Minerals in Hydrothermally Altered Rocks at Wairakei, New Zealand. *Clays and Clay Minerals* **16** (3): 193-213. http://dx.doi.org/10.1346/ccmn.1968.0160302.

Subagjo, W. W., Pratitis M. A., and Fajrin, A. 2017. Thermal decomposition of dolomite under CO_2-air atmosphere. AIP Conference Proceedings. http://dx.doi.org/10.1063/1.4974427.

Sudo, T., Hayashi, H., and Shimoda, S. 1962. Mineralogical problems of intermediate clay minerals. *Clays and Clay Minerals* **9**: 378-392. https://dx.doi.org/10.1016/B978-1-4831-9842-2.50028-6.

Sztukowski, D. M., and Yarranton, H. W. 2005. Oilfield solids and water-in-oil emulsion stability. *Journal of Colloid and Interface Science* **285** (2): 821-833. http://dx.doi.org/10.1016/j.jcis.2004.12.029.

Tang, G. Q., Inouye, A., Lowry, D. et al. 2011. Recovery Mechanism of Steam Injection in Heavy Oil Carbonate Reservoir. Presented at the SPE Western North American Region Meeting, Anchorage, Alaska, USA, 7-11 May. SPE-144524-MS. http://dx.doi.org/10.2118/144524-MS.

Tang, G. Q., Inouye, T. A., Lee, V. et al. 2012. Investigation of Recovery Mechanism of Steam Injection in Heavy Oil Carbonate Reservoir and Mineral Dissolution. Presented at the SPE Western Regional Meeting, Bakersfield, California, USA, 21-23 March. SPE-153812-MS. http://dx.doi.org/10.2118/153812-MS.

Tooker, E. W. 1955. Altered Wall Rocks Along Vein Deposits in the Central City-Idaho Springs Region, Colorado. *Clays and Clay Minerals* **4** (1): 348-361. http://dx.doi.org/10.1346/ccmn.1955.0040139.

Watkins, D. R., Kalfayan, L. J., & Blaser, S. M. 1987. Cyclic Steam Stimulation in a Tight Clay-Rich Reservoir. Presented at the SPE California Regional Meeting, Ventura, California, 8-10 April. SPE-16336-MS. http://dx.doi:10.2118/16336-MS.

Watkins, D. R., Kalfayan, L. J., Watanabe, D. J. et al. 1986. Reducing Gravel Pack and Formation Dissolution during Steam Injection. *SPE Prod Eng* **1** (06): 471-477. http://dx.doi.org/10.2118/13660-PA.

Williamson, H., Babaganov, A., Romanova, U. G. 2016. Unlocking Potential of The Lower Grand Rapids Formation, Western Canada: The Role of Sand Control and Operational Practices in SAGD Performance. Presented at the SPE Canada Heavy Oil Technical Conference, Calgary, Alberta, Canada, 7-9 June. SPE-180700-MS. http://dx.doi.org/10.2118/180700-MS.

Xiao, Y., Jones, G. D. 2006. Reactive Transport Modeling of Carbonate and Siliciclastic Diagenesis and Reservoir Quality Prediction. Proc., Abu Dhabi International Petroleum Exhibition and Conference, Abu Dhabi, UAE, 5-8 November. SPE-101669-MS. http://dx.doi.org/10.2118/101669-MS.

Yakubov, M. R., Amerkhanov, M. I., Khisamov, R. S. et al. 2017. World experience of solvents injection for extraction of heavy oil and solvent-based processes potential in TATNEFT PJSC heavy oil fields (Russian). *Oil Industry Journal* **2017** (02): 78-81. http://dx.doi.org/OIJ-2017-02-078-081-RU.

Yongbin, W., Xingmin, L., Wanjun, H. et al. 2017. Numerical Simulation of Electrical-Heating Assisted SAGD in Heterogeneous Heavy Oil Reservoirs. Presented at the SPE Reservoir Characterization and Simulation Conference and Exhibition, Abu Dhabi, UAE, 8-10 May. SPE-186023-MS. http://dx.doi.org/10.2118/186023-MS.

Zen, E. 1959. Clay Mineral-Carbonate Relations in Sedimentary Rocks. *American Journal of Science* **257** (1): 29-43. http://dx.doi.org/10.2475/ajs.257.1.29.